8-2005

Evaluation of Seal Integrity of Flexible Food Polytrays by Destructive and Non-Destructive Techniques

Kshitish A. Patankar
University of Tennessee - Knoxville

To the Graduate Council:

I am submitting herewith a thesis written by Kshitish A. Patankar entitled "Evaluation of Seal Integrity of Flexible Food Polytrays by Destructive and Non-Destructive Techniques." I have examined the final electronic copy of this thesis for form and content and recommend that it be accepted in partial fulfillment of the requirements for the degree of Master of Science, with a major in Polymer Engineering.

Kevin M. Kit, Major Professor

We have read this thesis and recommend its acceptance:

Marion G. Hansen, Roberto S. Benson

Accepted for the Council:
Carolyn R. Hodges

Vice Provost and Dean of the Graduate School

(Original signatures are on file with official student records.)

To the Graduate Council:

I am submitting herewith a thesis written by Kshitish A. Patankar entitled "Evaluation of Seal Integrity of Flexible Food Polytrays by Destructive and Non-Destructive Techniques". I have examined the final electronic copy of this thesis for form and content and recommend that it be accepted in partial fulfillment of the requirements for the degree of Master of Science, with a major in Polymer Engineering.

Kevin M. Kit

Major Professor

We have read this thesis
and recommend its acceptance:

Marion G. Hansen

Roberto S. Benson

Accepted for the Council:

Anne Mayhew

Vice Chancellor and
Dean of Graduate Students

(Original signatures are on file with official student records.)

Evaluation of Seal Integrity of Flexible Food Polytrays by Destructive and Non-Destructive Techniques

A Thesis Presented for the Masters of Science Degree

The University of Tennessee, Knoxville

Kshitish Patankar

August 2005

This thesis is dedicated to the following:

My Parents

Anil Patankar and Anagha Patankar

My Brother

Anish Patankar

My Granny

Usha Patankar

My Professors

&

My Friends

Acknowledgements:

The author would like to sincerely thank and extend his gratitude to Dr. Kevin M. Kit for his continuous support and knowledge for this project over the past two years. He would also like to thank Dr. Marion G. Hansen and Dr. Roberto Benson, his committee advisors, for their encouragement and help throughout his tenure at the University of Tennessee, Knoxville in Materials Science and Engineering.

The author thanks Doug Fielden and the machine shop for all of their hard work, Van Brantley in TANDEC for help with film testing, Bill Barlow for all of his help on this project, Sherry Liu for her help with the FTIR spectroscopy, Greg Jones and Dr. Dunlap for all the help with SEM and COMSOL support group for their help with FEMLAB® simulations.

The author would like to thank Fengxio Lin and Bing Yang for all their help with Infrared thermography.

Abstract:

The companies which supply military ration packages (MRP) have been suffering significant loss due to high rejection rate (more than 20 %) by the military. The standards set by the military, as far as acceptance of packages is concerned, are very high and conservative. The means employed are also based mostly on visual observation. The aim of the project is to quantitatively device test which reduce the high rejections the companies are incurring. Thus the drive behind this project is to determine the extent to which certain defects affect the seal strength of food trays.

Earlier work on this project was used as a guideline to decide the parameters for an optimized test. A package which develops a significant leak under a pressure of 20 psi is considered a defective package irrespective whether it has any visual defects. With the current laboratory set-up, leaks as low as 4-5 cc/minute were identified. The food packages with different defects namely; short seals, entrapped matter, blisters and air bubbles, tunneling, and wrinkles from Stegner and Wornick Co were tested destructively and non-destructively.

A destructive burst test was used to test the burst pressures and the leak developed in trays. A computer interface was designed using National Instrument Labview® program which could automatically detect the leak through the seal and measure the pressure in the package while simultaneously increasing the pressure in step mode. Based on the results from the burst test, a systematic study of the burst pressures that different types of defective packages withstood and the correlation with the seal width was carried out. It was found that non-defective trays from both Stegner and Wornick performed equally well averaging 34.2 and 34.4 psi respectively. Blisters and entrapped matter seemed to drastically reduce the average burst pressure for Stegner trays, while Wornick trays with these defects did not show a substantial reduction in the burst pressure. Stegner trays with blisters in their seals sustained the average burst pressure of 23 psi, while those from Wornick performed better than their counterparts sustaining 35 psi. Short seal trays

from Wornick were found to perform better than non-defective trays sustaining 37.7 psi, while those from Stegner sustained 28.3 psi. Although burst test gives the quantitative measure of seal strength, it cannot be implemented on the production line to test 100% of the production packages.

The stress condition developed in the package as a result of burst test was simulated using a finite element analysis program Femlab®. Simulations were performed to better understand the visual presentation of stresses in the package; especially across the seal. Three-dimensional simulations although more effective; needed the coupling equations between the acrylic plate of a burst chamber and lid of a package. Two-dimensional simulations were performed with varying distances between acrylic plate and lid at constant boundary conditions gave exponential increase in the stress across the seal.

Non-destructive techniques such as ultrasonic C-scan inspection and infrared thermography were examined as techniques which could be installed in-line to detect the defects in the seal and reduce the defective packages reaching the consumer. Pulse-echo technique was used for ultrasonic inspection. Only packages with tunneling defects were tested. The presence of tunneling could be seen on the images. But the presence of small diameter channels like 50.8 microns could not be seen at all. So after some experiments the technique was not found of high utility and lacked the reproducibility. The infrared thermography on the other hand showed promise as a useful utility. Polytrays with many kinds of defects were examined using infrared camera. A 100W lamp was used to heat the packages. Differential heat loss across the defect was recorded by the camera.

The results from burst tests were complimented using characterization techniques such as scanning electron microscopy (SEM). The SEM data was also complimented by FTIR/ATR spectroscopy technique to analyze as to which layer was undergoing delamination during the burst. Delamination was seen to occur between PP/PET layers for the trays which burst. Crazing was seen as the failure mechanism for PP.

Table of Content:

List of Tables:

List of Figures:

Chapter 1: Introduction

1.1 Background:

The US military has been suffering huge losses on their supply of food ration packages due to sealing defects. Since food supply is probably one of the most critical factors for any army on the battlefield; heavy rejection of food trays has been a major concern for the military. The food trays are inspected visually on the site of production by the USDA inspectors. Trays with defects are never shipped to the military. The current standards are set to the highest level to ensure quality food product is delivered to the military in the field. Therefore the development and standardization of seal integrity tests will be a major tool to understand the seal quality and reduce the losses. Various destructive and non-destructive tests will be evaluated and their feasibility will be tested in this project. Various types of defects in the seal will be identified and qualitatively classified. Based on those defects; the suggested test or tests could be standardized. Such modified test(s) will then be useful to reduce the losses without having to modify the tray or lid material currently in use.

A military group ration package (MRP) consists of a tray and a lid. The tray is composed of five layers, polypropylene (PP)/recycled PP/ethylene-vinyl alcohol (EVOH) copolymer/recycled PP/PP. The lid-stock is made from a four-layered laminated film; cast polypropylene/aluminum/nylon/polyester which is thermally bonded to the tray under pressure and vacuum. Such trays are designed to preserve food for a period up to 18 months at 80°C. This demanding requirement dictates the use of materials with excellent gas barrier properties such as ethylene-vinyl alcohol copolymers and aluminum. A schematic of the polymer package can be seen in Figure 1.1.

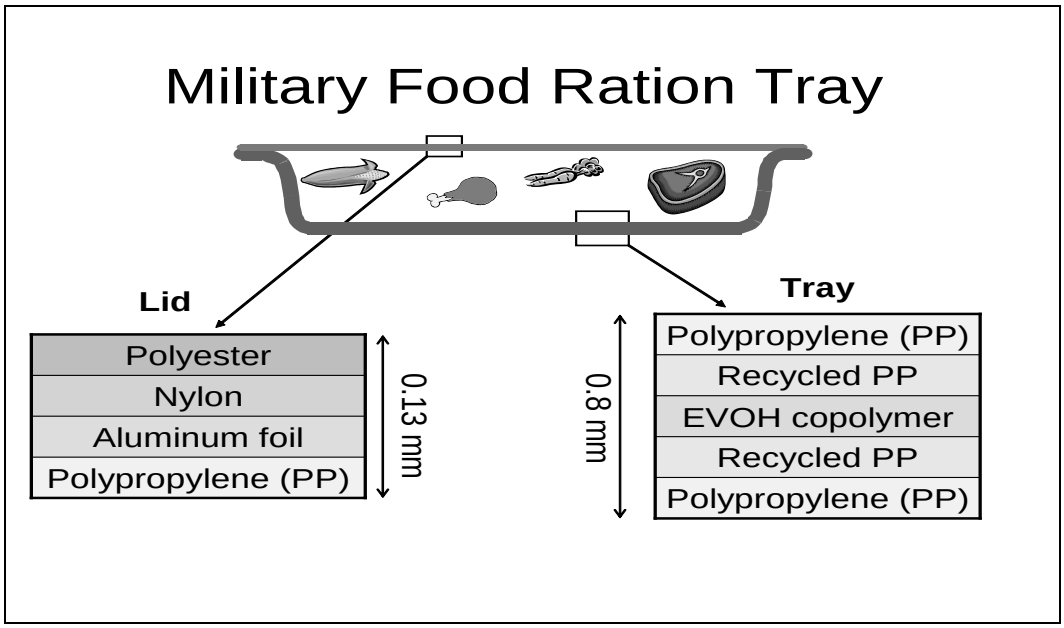

Figure 1.1: Schematic drawing of polytray showing the materials used in both the lid-stock (film) and the tray.

Packaging lid-stocks and trays are almost always composed of multiple laminated or co-extruded polymer films. A laminate performs much better to meet the stringent requirements of high barrier properties and better moisture resistance as compared to a single layer of polymer film [1]. At the same time, the rigidity and mechanical strength of the food package cannot be compromised. PP provides good moisture barrier properties maintaining high impact properties and excellent sealability. Aluminum provides excellent gas and moisture barrier properties; while nylon provides good puncture resistance in the lid [2].

The food ration packaging is a continuous process in which the plastic trays (approximately 31.2 cm x 26 cm) are filled with uncooked food one at a time then heat-sealed with the tetra-layered film, or lid-stock under a heated, vacuum press. One polytray is successfully produced every 3-4 seconds. The heated press creates a thermal seal between the bottom layer of the lid stock (PP) and the top of the tray (PP). No adhesive is used in the process. The polytrays, especially the sealing area, are visually

inspected as they come off the production line. The polytrays are then loaded into racks and are placed in a retort, where a steam bath maintained at 123.8ºC (255ºF) cooks and sanitizes the food for 3-4 hours. The polytrays are once again visually inspected after the retort process because of the high possibility of defect development during the retort process. The polytrays are then wiped dry and packaged in sets of four in cardboard boxes ready for shipping.

1.2 Objective:

The objective of this project is to determine the extent to which certain defects affect seal strength of food trays. Destructive and non-destructive tests will be performed on the polymeric food polytrays. Destructive burst test will be performed on non defective food trays from two different companies; Stegner and Wornick Co. These results will provide a quantitative basis on which all further tests and seals will be assessed. Food trays from these two companies with naturally occurring and artificially created defects will then be tested and results compared with those of non defective polytrays. Statistical data will then be presented showing various defects and corresponding burst pressure and the seal width. Although these destructive tests are effective in the determination of seal quality, 100% of packages can not be inspected by these methods. The stress conditions present in the package as a result of burst test will be simulated using finite element analysis program such as Femlab®.

Post failure characterization techniques such as SEM and FTIR/ATR provide very valuable information about the mode of failure. These techniques will be used to examine the seal of the burst package and useful facts regarding the failure and delamination will then be discussed. Non-destructive techniques such as ultrasonic B and C-scans and infrared thermographic imaging could provide useful tools to examine the packages. Almost 100% of packages could be tested using these techniques and thus defective packages reaching the consumer could be avoided. Feasibility of these techniques will be considered.

Chapter 2: Literature Review

2.1 Packaging Films:

In most food applications a single layer plastic film is not adequate and does not meet stringent requirements of barrier properties, adequate strength and reasonable cost. These requirements could be met by using a multilayer laminate, coating or manufacturing co-extruded films. Laminates consist of two or more plastic layers bonded together with an adhesive or a tie-layer; which is a low melting plastic film. Aluminum foils are often used in laminates to improve stiffness and barrier properties [3]. Coextrusion is a process by which several layers of plastic films are extruded simultaneously with tie layers to facilitate the bonding between adjacent layers. The layers do not mingle but remain separate and form discrete separation lines. Coextrusion has been widely used industrially because it offers some unique advantages. Some of them have been listed below: enhanced barrier properties, stiffness to improve machinability of films, providing heat-sealable layer, providing metallizable surface, making opaque or colored films.

Most coextruded films are based on polyolefins owing to easy processability and low cost. Low density and linear low density polyethylene (LDPE and LLDPE respectively) are used for their toughness and easy sealability. LDPE and LLDPE cannot provide high barrier properties. In such cases, high barrier materials like ethylene- vinyl alcohol random copolymer (EVOH) or chlorinated polymer films like polyvinylidene chloride (PVDC), or aluminum coated films are used extensively [2, 4]. Some examples of coextruded structures used in food packaging industry are LLDPE/tie layer/ EVOH/ tie layer/ LDPE for wine and fruit juices, nylon/ ethylene- vinyl acetate for frozen food, polyamide/ LDPE for processed meat, high density polyethylene (HDPE)/ EVOH/ HDPE for ketchup and sauces [1, 4]. It is important to review the important mechanical and barrier properties of plastic films used in food packaging applications.

1. Impact Strength: This implies to the resistance film offers to rupture of catastrophic failure when it is subjected to stress. Impact strength of films is measured by a dart impact test [5].

2. Tensile Strength: It refers to resistance film offers to breaking by a slowly applied stress over a certain time period. Orientation significantly improves tensile strength in plastic films as compared to their unoriented counterparts.

3. Tear Strength: There are two ways this property is measured in plastic films, from a notched tear or from a smooth edge. Some polymers have good unnotched tear resistance but poor notched tear strength.

4. Flexural Modulus: This refers to stiffness of a plastic film. Higher flexural modulus can be imparted by orientation or adding fillers. Stiff films are easier to manage on machines as well.

5. Water Vapor Transmission Rate (WVTR): This property of a plastic film is very important for packaging moisture sensitive food. Chlorinated films have an inherently low WVTR. Oriented and highly crystalline films also have low WVTR. It decreases with increasing film thickness and increases with both temperature and relative humidity.

6. Oxygen Permeability (OPV): This property is important for packaging oxygen-sensitive food. OPV can depend on humidity for moisture sensitive polymers such as polyamides and ethylene-vinyl alcohol copolymers [3].

2.2 Fracture and Failure in Polymer:

Mechanical properties and mode of fracture depend heavily on temperature and strain rate. At low temperature, polymers often fail in a brittle manner where load increases linearly with increasing elongation up to the breaking point. At high temperatures, polymers often yield where load falls before failure due to yielding and necking processes.

2.2.1 Brittle Fracture of Polymers:

The starting point for discussion of brittle failure in polymers is Griffith's theory of linear elastic fracture mechanics. The theory is based on two ideas; firstly, rupture produces a new surface area and energy required in this process is balanced by a decrease in elastically stored energy; and secondly, elastically stored energy is not distributed uniformly throughout the specimen but is concentrated in the neighborhood of small cracks. This can be mathematically represented as:

$$\frac{dW}{dc} - \frac{dU}{dc} \geq \gamma \frac{dA}{dc}$$

where the crack growth will be associated with an amount of work dW being done on the system and a change dU in the elastically stored energy. The difference gives the energy available for formation of new surfaces. The surface free energy per unit area of surface is give by γ and dA is the associated increment of surface. Berry later suggested that a largest contribution to the surface energy of glassy polymers come from viscous flow process [6]. Berry also proposed that the large surface energy term arises from work required to align polymer chains ahead of a crack. Thus crack growth leaves a thin, highly oriented polymer film on the surface. This is termed as craze and formation of craze taken place under plain strain condition. The fracture toughness of glassy polymers depends on two parameters; crack opening distance (δ_t) and the craze stress (σ_c). The product of these two is referred to as critical strain energy release rate (G_{IC}). Since both crazing and shear yielding are dependant on temperature and strain rate, one will be favored over the other for some conditions and vice versa for some other conditions [7].

Craze Criteria:

Crazing criteria is given by Sternstein's equation [8]. For a planar stress condition ($\sigma_3 = 0$),

$$\sigma_b = |\sigma_1 - \sigma_2| = A + \frac{B}{I_1}$$

where A and B are temperature dependant constants and I_1 is the first stress invariant given by $I_1 = \sigma_1 + \sigma_2$.

2.2.2 Yield Behavior of Polymers:

As stated in the previous section, temperature and strain rate play a crucial role in determining whether a polymer undergoes crazing or yielding. Some polymers show necking while some are brittle and fail catastrophically. The other class of polymers like rubber extends uniformly and ruptures in the end. The important point is that a polymer can show all these transitions based on the test conditions. The most characteristic feature of yielding is the formation of neck. In such cases the plastic deformation is concentrated in a small region of specimen. The nature of plastic deformation depends on the applied stress and geometry of specimen.

The characteristics of necking can be explained using load-extension curve. On the initial elongation of specimen, homogenous deformation occurs and load increases approximately linearly with increase in elongation (AB in Figure 2.1). At point B, the specimen thins in cross-section, which marks the formation of a neck. Further elongation is marked with a reduction in load. Line CD is marked with a propagation of neck along the specimen. The necking process is accompanied by non-uniform distribution of stress and strain along the length of the specimen. As the cross-sectional area of specimen decreases with increasing extension, the true stress keeps on increasing even when the apparent stress remains constant or even decreases. The true stress $\sigma = P/ A$, where A is the actual cross-sectional area at any time. Comparison of engineering and true elongation – stress curve is shown in Figure 2.2. True stress-strain curve of a necking polymer is shown in Figure 2.3.

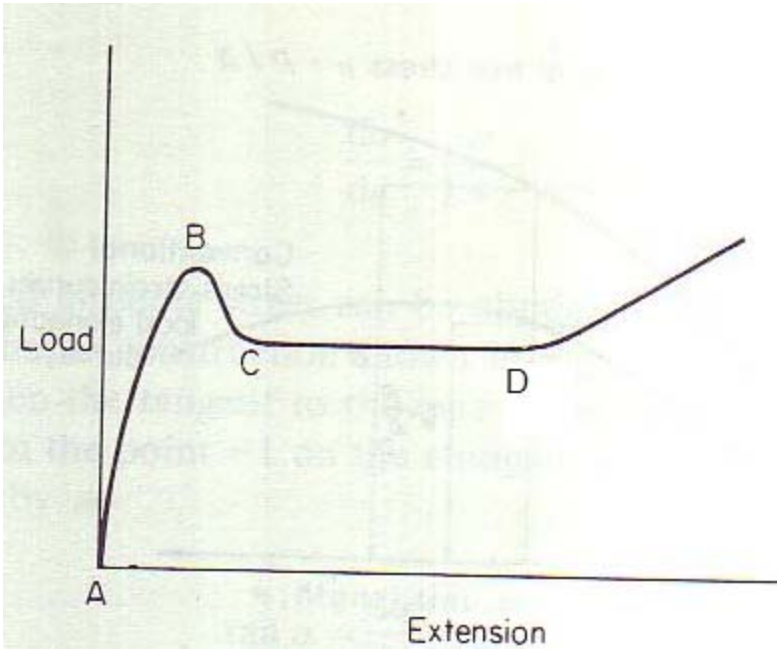

Figure 2.1: Load-extension curve for a cold drawing polymer.

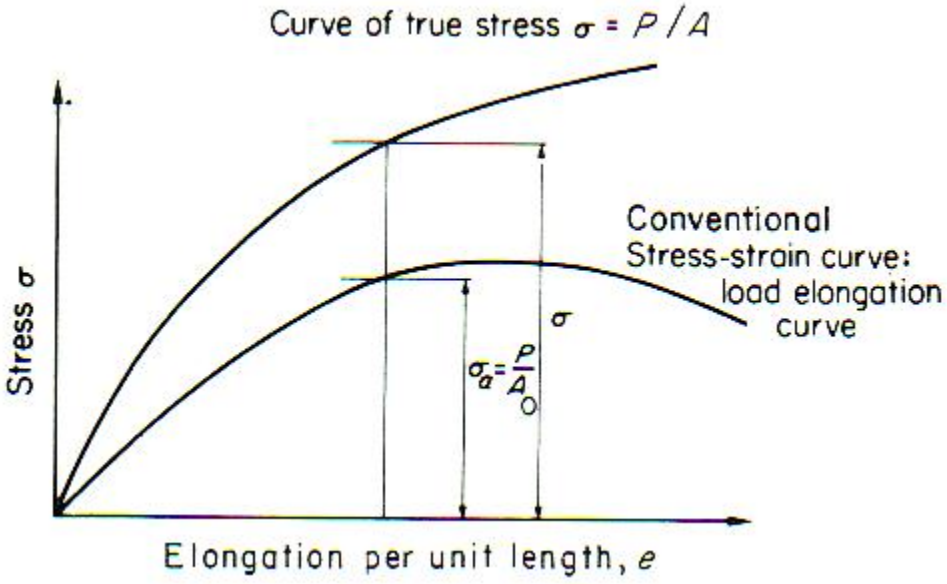

Figure 2.2: Comparison of engineering and true stress- elongation curve.

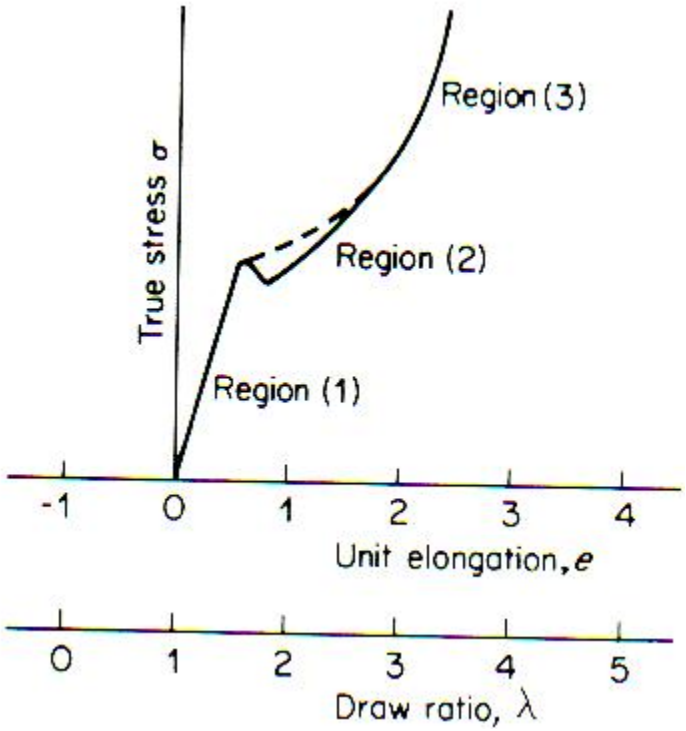

Figure 2.3: True stress-strain curve of a cold-drawing polymer.

It can be seen that stress rises in a linear manner with strain initially (Region 1). At the yield point true stress falls and then rises less steeply with strain. (Region 2). Finally at larger elongation slope of stress-strain curve increases again, the effect referred to as 'strain-hardening' (Region 3) [7]. The natural draw ratio is defined as ratio of the length of cold-drawn region to the length of the same material before it was stretched. Natural draw ratio is not constant for a given polymer, but changes with experimental conditions [9].

At this point it is important to mention yield stress and yield stress criteria. Yield stress can be defined as the minimum stress at which permanent strain is produced even when stress is removed.

Von Mises Yield Criteria:

Octahedral stress (τ_{oct}) is given as

$\tau_{oct} = \frac{1}{3}((\sigma_1 - \sigma_2)^2 + (\sigma_2 - \sigma_3)^2 + (\sigma_3 - \sigma_1)^2)$ where σ_1, σ_2 and σ_3 are principle normal stresses. Von Mises criteria states that yielding occurs if,

$\frac{3}{\sqrt{2}} \tau oct \geq \sigma y$ where σ_y is the uniaxial yield strength [4].

It would be really worthwhile to make a mention of adherence and fracture mechanics approach. The rupture between two solids occurs by propagation of crack in which bonds are broken. The surface energy required to break these bonds is given by 2γ per unit of surface area where γ represents the surface energy of the material. The work to break these bonds is given by Dupre energy of adhesion:

$w = \gamma_1 + \gamma_2 - \gamma_{12}$ where γ_1 and γ_2 represent the surface energies and γ_{12} the interfacial energy.

The separation of two solids always takes place by progressive reduction in the area until complete separation is achieved. Consider the system of two elastic solids in contact over the area A. This area of contact is allowed to vary at a fixed load P or at fixed displacement δ. Thus the state of the system depends mainly on two sets of variables; P and A or δ and A. The energy of the system U = U (S, δ, A) is a function of extensive variables entropy S, δ, and A. The first differential of the energy is given by:

dU = TdS + Pdδ + (G-w) dA; where G describes the variation of elastic energy with A at constant δ; which also describes the strain energy release rate. Equilibrium at fixed temperature and fixed load conditions (dT = 0, dP = 0) is given by:

G = w

If G is not equal to w; then the area of contact will change spontaneously so as to decrease the thermodynamic potential.

1. If G < w; then A increases and crack recedes.
2. If G > w; then A decreases and crack propagates[10].

The quantity GdA is the mechanical energy released when the crack propagates by dA. The breaking of interfacial bonds requires the energy equal to wdA. The quantity G-w is the crack extension force, which is zero at equilibrium[10]. At this point, it is important to mention the stress-concentration factor near the crack tips. Consider a plate containing an elliptical hole. Let a and b represent the half major and minor axes respectively. Let σ_{max} and σ_a be the maximum stress at the end of the major axis and the applied stress normal to the major axis respectively. The relationship between the σ_{max} and σ_a is given by:

$\frac{\sigma_{max}}{\sigma_a} = 1 + \frac{2a}{b}$. The Figure 2.4 shows the stress concentration near the end of crack tips in the elliptical hole in a plate.

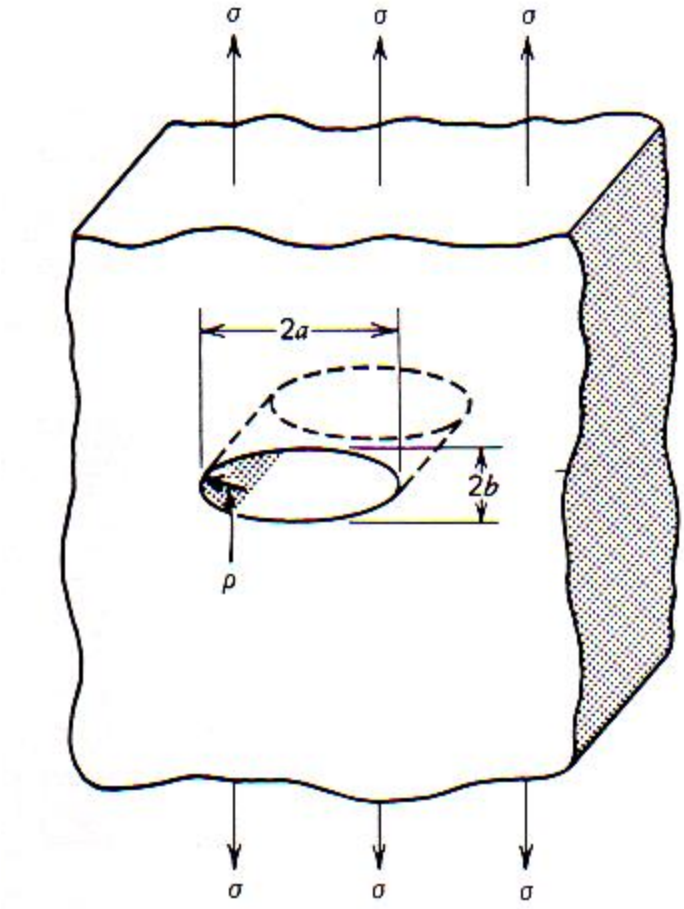

Figure 2.4: Elliptical hole in infinitely large plate producing stress concentration of 1 + 2a/b[11].

Since the radius of curvature r at the end of the ellipse is given by b^2/a, the maximum stress at the end of major axis is given by:

$$\sigma_{max} = \sigma a(1 + 2\sqrt{a/r})$$

In most cases a >>r, thus

$$\sigma_{max} = 2\sigma_a\sqrt{a/r}$$

The term $2\sqrt{a/r}$ represents the stress concentration factor k, and describes the crack geometry on the local crack-tip stress level [11].

2.3 Ultrasonic Inspection:

Polytrays with channel defects in their seals will be examined under this project. The objective will be to specify the minimum channel defect size that could be detected with the system. Feasibility of ultrasonic inspection will later be discussed. The C-scan with the pulse-echo technique will be utilized in which the polytrays are submerged into water and scanned with varying frequency acoustic transducers. This review only deals with some basic principles and applications of non-destructive ultrasonic testing. The theory behind the applications involving mathematics has not been dealt with in this review.

The ultrasonic method is based on transmission of waves of mechanical energy at frequencies higher than 20 kHz. Such short wavelengths ensure rectilinear propagation of waves. Most current applications use pulse-echo technique even though through-transmission is still in use [12]. Most of the ultrasonic applications are associated with

flaw detection in metals. However the technique has been used to some extent in plastic, rubber and laminate industry.

2.3.1 Pulse-Echo Technique:

In this technique, an ultrasonic beam is produced by mechanical pulses, which in turn are produced by electrical impulses, a phenomenon known as 'piezoelectric effect'. The mechanical waves penetrate into the object under test. These waves travel through the object and then reflected back. They are then received as an echo. The receiver probe converts this energy into electrical pulses. Any flaw in the path of waves reflects some part of energy. The amplitude, form and duration of a reflected signal provide information about size and nature of the flaw.

2.3.2 Through-Transmission Technique:

The waves pass between transmitter and receiver, placed on opposite sides of an object under test. Acoustic energy collected by the receiver is then compared with a standard. When the ultrasonic beam encounters a defect, the monitor gives audible warning. The amplitude of signal is displayed on the screen. The advantage of transmission method over pulse-echo technique is that it avoids the formation of standing waves [12]. The ultrasonic inspection technique has been successfully utilized by Pascall et.al. [13]. Pascall et.al were successful in assessing seal quality of heat seal in polymeric trays. They could determine the optimum sealing temperature (204°C) based on ultrasonic analysis. Channel leaks greater than 20μm were identified using ultrasonic testing. Pilar Llull et.al [14] used ultrasonic imaging to evaluate moisture content and textural properties of Sobrassada from Mallorca (a raw cured pork product). Z Ayhan et.al used high frequency non-contact ultrasonic technique in pulse-echo mode to evaluate the use of this technique in the defect detection in the seal-area of semi-rigid cups and polymeric trays [15].

2.4 Thermographic Inspection:

The technique of inspecting the samples for flaws or defects has been extensively used with mechanical components. Infrared thermography is a powerful non- contact diagnostic tool that monitors the thermal energy difference across the defect in a sample under investigation. Any body above absolute zero radiates thermal energy in the form of invisible infrared radiations. The infrared part of electromagnetic spectrum spans from 0.7 to 2000 microns, however radiations in the range of 0.7 to 20 microns are used for practical purposes [16]. Thermography is an infrared imaging technique that utilizes a camera to monitor variations in infrared radiation. The following treatise from physics would be useful to understand the principles on which the parameters measuring the IR radiations depend upon. Stefan- Boltzman's law states that total thermal energy flux radiated by a body of thermal emissivity ε is directly proportional to the fourth power of absolute temperature of the body. Thus it can be seen that even a small change in temperature can bring about a substantial change in the heat flux radiated by the body. The infrared camera is sensitive enough to record a very small temperature difference. When an electromagnetic radiation interacts with a surface, following events may occur. The surface may reflect, absorb or transmit the energy. The relation, in accordance with conservation on energy, is given by:

$A + R + T = 1$ where A, R and T stand for absorbed, reflected and transmitted part of energy respectively. In case of 'black body' A = E. For a perfectly black body, E =1, i.e. all energy is absorbed and reemitted. E is referred to as emissivity. Several factors affect emissivity. Apart from material type, surface condition, temperature and wavelength may change emissivity of the material [17]. Accurate thermographic inspection is only possible with objects with high emissivity. This is the fundamental limitation of thermography. Generally, it is not recommended to make temperature measurements of surfaces with emissivity less than 0.50 [17]. A Al-Habaibeh et.al [18] have discussed an approach that uses an online infrared system to assess the heat distribution within the container seal to maintain the integrity of the process. Figure 2.5 shows a schematics describing a complete sealing and monitoring system.

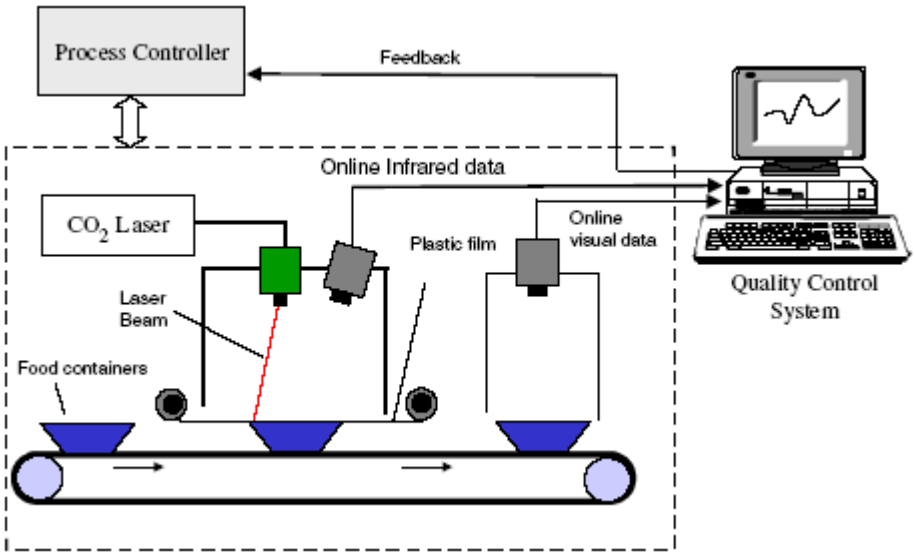

Figure 2.5: A schematic diagram showing a complete sealing and monitoring system[18].

This is probably one of the most economical ways to implement the infrared monitoring system on the industrial scale. A 50 W RF excited carbon dioxide laser with a wavelength of 10.6 microns was used to seal the lid to food containers under the work. The infrared camera analyzes the heat distribution in scanned trays during the sealing process. The system then compares the data with the data from the expected normal sealing process. If the data matches, then tray is moved to the visual image processing system for seal integrity confirmation [18]. Figure 2.6 shows the experimental set-up and Figure 2.7 shows good and defective seal image respectively.

Traditionally, the food packaging industry has been using adhesives or tie layers to bond the lid to the container. Laser welding of polymer films to the container substrate would be another option worth consideration. Brown et.al [19] discussed the design of a suitable test apparatus for laser- welding thin films to heavier substrates like food containers. They found that with a precise machine design, a seal of high mechanical strength and integrity would be possible. Not only does the process avoid any possible contact between the sealing plate and a container, as the process is completely non-contact one; but it offers a possibility of higher sealing speeds. Jones et.al successfully utilized laser welding at speeds of 50 m/min [20]. Such welds were found to have adequate weld strength and high peel strength. J.P Coelho et.al [21] studied the welding of white and transparent thin films of polypropylene and polyethylene of low and high density and thickness of 10-100 microns at high speeds of 20 m/min using carbon dioxide laser.

2.4.1 Infrared Cameras:

An infrared camera is a device that forms an image using infrared radiation, similar to common cameras that form images using visible lights. Images from infrared cameras tend to be monochromatic as the sensors in the cameras are designed to respond only to a particular band of infrared wavelengths.

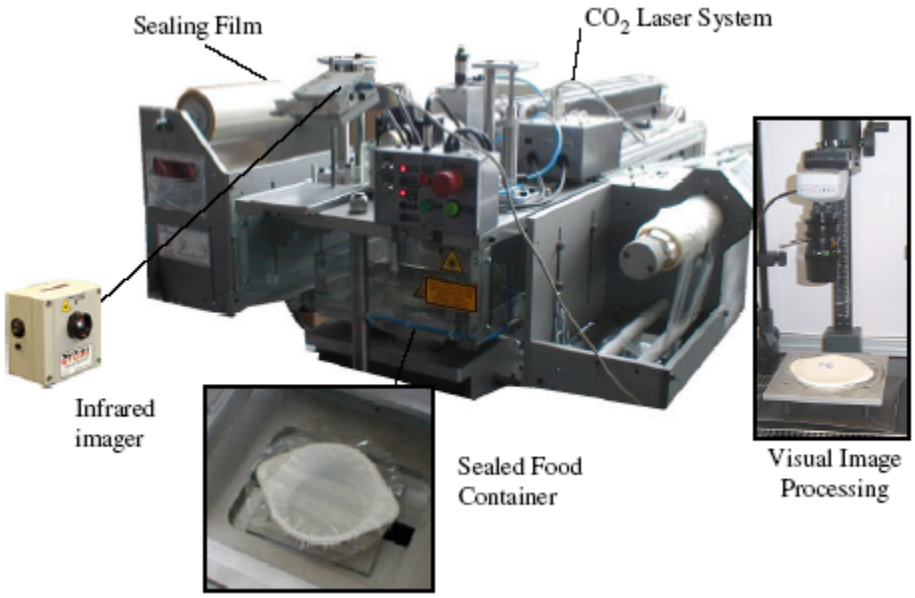

Figure 2.6: Experimental set-up showing infrared camera, optical camera, laser system and sealing film roll [18].

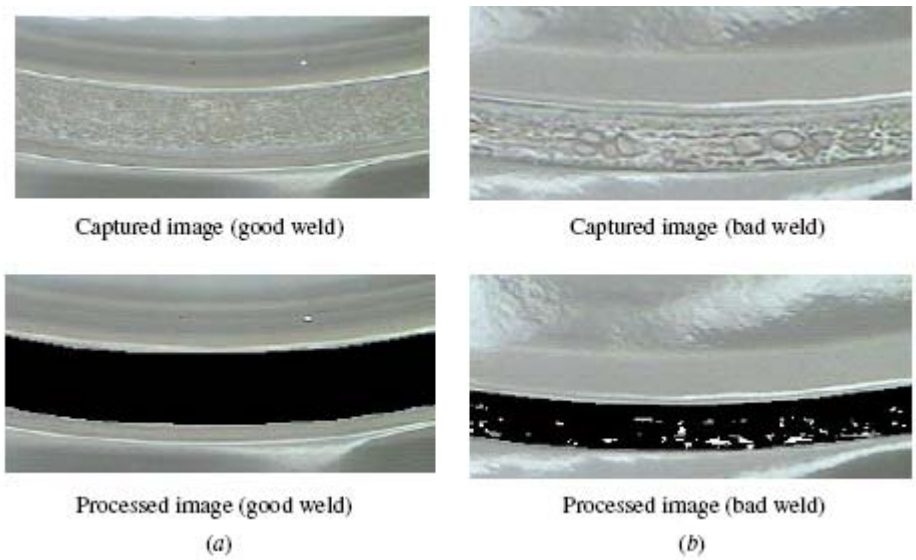

Figure 2.7: The captured and processed images of good (a) and defective (b) seals [18].

Infrared cameras are categorized into two types:

1. Cooled Infrared Detectors: This type of detectors are contained in a vacuum-sealed case and cryogenically cooled. Cooling greatly enhances the sensitivity of a camera. The cooled infrared detectors are expensive and the vacuum casing is difficult to fabricate. The system consumes a lot of power and takes time to get to the operating temperatures. The cooling assembly makes the cameras bulky, but the quality of images is much better than uncooled detectors. Indium antimonide, indium arsenide, lead sulfide, lead selenide are some of the materials used for such detectors [22].

2. Uncooled Infrared Detectors: This type of detectors operates at room temperatures. Modern uncooled detectors use sensors which change the electrical properties of the material when heated by infrared radiation. These changes are then compared to the properties at the operating conditions of the sensor. Uncooled cameras are not bulky and not very expensive. However, they have low resolution and poor quality relative to cooled detectors. Most of the current uncooled detectors are based on pyroelectric materials or microbolometer technology [22]. The essential difference between the cooled and uncooled detectors is the extent to which they reduce the level of noise in the system. There are different types of "noise" namely; electronic (likely to occur in imaging system of infrared detector), optical (random fluctuations in the incident radiation), heating, and environmental (electromagnetic interference) noise [44].

Thermal Detectors:

In thermal detectors, the incident radiation heats the surface. The heating changes the intrinsic property of the material; such as electrical conductivity, which in turn changes the output signal. The characteristic of such type of detectors is that the output radiation does not depend on the incident wavelength. Different types of thermal detectors are

bolometers, thermopiles, pneumatic, pyroelectric and liquid crystals. For bolometers the heating affects the electrical conductivity. Typically bolometers have slow response time. Thermopiles generate the voltage difference upon heating following thermoelectrical Thomson effect. Thermopiles are constructed from many thermocouples connected either in parallel or series. Serial connection improves the signal level. The major problems are the need of contact for measurement and the limited number of measurement points. Pneumatic detectors work on the pressure variation due to expansion of gas. Certain crystals change the electrical polarity of the surface by a change in temperature. A change in detector temperature generates a transient change in the surface charges, thus generating a momentary current to be read by the output. Liquid crystals (cholesterol esters) change the orientation upon change in temperature and reflect colored light. They are not expensive, quite sensitive (0.01°C) to slight thermal variations, and have the capability of surface measurement [23].

Photonic Detectors:

Unlike the thermal detectors, in the photonic detectors the signal is generated by the excitation generated by the incident photons. These detectors can be of two types: photoemissive and quantum. In photoemissive detectors, the output signal comes from the current generated from the action of incident photon on photocathode. The electro flow is maintained from cathode to anode by applying a static polarization. Thus, the electrons generated are accelerated and multiplied by internal plates called dynodes. Multiplication factors of 10^5-10^7 can be obtained by using 10-stage tubes. Quantum detectors are solid-state detectors in which photon interactions either change electrical conductivity (photoconductor) or generate voltage (photoelectric). The response time with quantum detectors is typically small. They are compact, robust, and reliable. With photoconductive detectors, the external current is required; while photoelectric detectors do not need the polarized to give signal. Common materials used in photoelectric are Si, InAs, InSb etc [23]. The detector used in the project falls under the category of photoelectric detector.

2.5 Adhesion:

An adhesive is defined as any material which causes one body to stick to another. This is probably the most important perspective of any food packaging application. The adhesion of polypropylene tie-layers is the primary concern during this project and the seal strength entirely depends on the adhesion between polypropylene layers from the lid and tray. The adhesion can be categorized into three main types namely; chemical, diffusive, and mechanical.

2.5.1 Chemical Adhesion:

To understand the way adhesive works, it is important to recognize chemical forces namely; ionic, covalent and metallic and physical Van der Waals forces. The latter are the weak forces originated from fields associated with polarized covalent bonds. Van der Waals forces are generally classified into three types namely; Debye forces, Keesom forces, and London forces [24]. Debye forces are associated with interaction of a permanent dipole with a bond system which can be polarized. London forces are associated with polarization of one molecule by another due to oscillation of electron clouds. Keesom forces originate from the interaction of two permanent dipoles [24]. Thus polar or Keesom and dispersion or London forces are mainly responsible for the strength of an adhesive. In other words, higher the polar group density, stronger is the adhesive force.

Apart from abundance of polar groups present in the molecules, adhesive is required to have a sufficiently high molecular weight. A low molecular weight compound fails to perform as a good adhesive because of the lack of cohesive strength. Practically an ideal molecular weight range for adhesive is a trade-off between ease of application and freedom from stresses, and loss of cohesive strength [24].

2.5.2 Diffusion Theory:

The **diffusion theory** originated from the work of Voyutskii [25]. If two polymers come in contact with each other above the glass transition temperature, the long chain segments may interdiffuse. This would take place across the boundary of two layers, i.e. interface. Eventually interface would cease to exist and there would be a continuum. This phenomenon can only take place if two polymers are thermodynamically compatible. This idea was supported with the aid of mathematical equations by Vaselin [26]. It was shown that for autohesion of a polymer to itself, the peeling force was directly proportional to the rate of separation, to the fourth root of the time for which the surface had been in contact and inversely proportional to the two-thirds root of molecular weight. Campion [27] considered the free volume within the structure of polymers. He extended the previous concepts by correlating autohesion properties with the cross-sectional area of free spaces which enabled diffusion. Figure 2.8 shows the schematic sketch showing the process of interdiffusion.

2.5.2 Mechanical Interlocking Theory:

Mechanical Interlocking is probably the oldest and simplest explanation for adhesion. The idea is adhesion depends on the surface roughness and mechanical interlocking of adhesive with this roughness. Various examples have been cited in the literature [29, 30]. Packham [31] worked on the adhesion of molten polyethylene to aluminum and showed a direct relation between the size and surface density of the pores in hexagonal aluminum cell structure and adhesive bond strength measured by peeling. Electron micrographs of the polymer surfaces which had been separated from the aluminum surface made it clear that adhesion was influenced by the pores which in turn supported the theory of mechanical interlocking. Figure 2.9 shows schematic sketch of the process of mechanical interlocking between the substrate and adhesive.

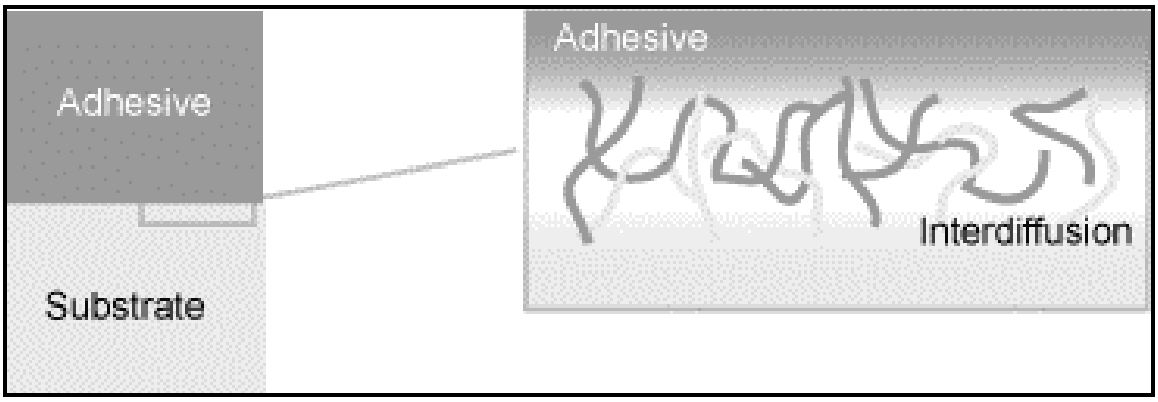

Figure 2.8: Schematic sketch showing the process of interdiffusion of polymeric chains above the Glass transition temperature [28].

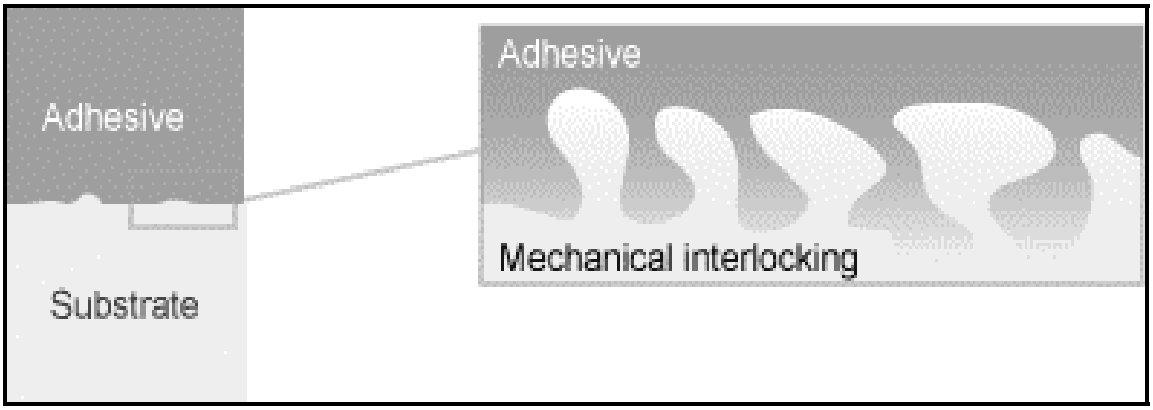

Figure 2.9: The schematic drawing showing the process of mechanical interlocking [28].

2.5.3 Other Theories:

Other theories have been put forward to explain specific drawbacks of the theory based on interaction of molecular forces. Electrical double-layer theory is amongst them [32]. This theory assumes that an electrical double-layer is set up between two dissimilar surfaces when they come into contact with each other. This theory is too specific to be generally applicable [24, 32, 33]. Another theory is based on relative surface tensions of two surfaces. The condition for strong adhesion is that either material will spread on the other [22]. None of the theories can successfully explain all the facts about adhesion, but a theory of interaction of molecular forces with stress on polymer diffusion would probably provide a good insight into this topic.

2.5.4 Hot-Melt Adhesives:

Hot-melt adhesives are being used extensively in the packaging industry. Hot melt adhesives give instantaneous adhesion to practically any surface. This makes bonding to highly impervious substrates possible. Efficiently used hot melt adhesive can greatly reduce the downtime and cleaning time of a laminator with little maintenance. Hot melt adhesives are thermoplastic, amorphous and softening over a wide range of temperature. The functional cycle of all hot melt adhesives is quite simple and reversible and can be represented like below [34]:

Solid + heat ⟶ Liquid ⟶ Applicator ⟶ Cooling and Solidified film

Hot melt adhesives work best when the applied film is sufficiently hot and liquid to adequately wet the surface. The performance of hot melt depends on following factors: mass of adhesive applied per unit area and application temperature. Higher the film thickness, greater is the heat retained in the film [34]. The strength of an adhesive bond depends on surface characteristics as well. Surface porosity, thermal properties and moisture content may play crucial may heavily influence the bonding process. Therefore

if one or both the surfaces are impervious, the surface energy of adhesive melt should be lower than that of surfaces being bonded.

2.6 Finite Element Analysis:

In continuum analysis, primary dependant variables (e.g. pressure, displacement etc.) posses infinitely many values as they are the functions of each generic point in the body. Therefore, such a continuum problem has infinitely many degrees of freedom. In order that such a problem is solved numerically, the problem should have finite number of degrees of freedom. Approximate solutions generated using the finite element method (FEM) are based on following steps:

1. The governing differential equations are put into a "weak" or integral form. This form is not only closer to the physical aspects of the problem but is desirable from mathematical point of view.
2. The continuum problem is replaced by an approximate problem [35].

Such a construction is based on the creation of a mesh that approximates the domain Ω. This process can be represented by:

$\Omega = \sum_{e=1}^{NE} \Omega^e$ where Ω^e represents finite number of non-overlapping sub-domains or elements and NE represents total number of elements. Every element Ω^e is characterized by the following quantities:

1. The geometry of Ω^e.
2. The set of degrees of freedom defined on Ωe.
3. The basis polynomial for the interpolation functions.

Thus the primary dependant variable can be approximated as follows:

$\overset{*}{\phi} = \sum_{m=1}^{NDOF} \phi_m N_m$ where φ_m denoted the nodal values of primary dependant variable. N_m represents the interpolation function. NDOF denoted the number of degrees of freedom for φ within the element [35].

The finite element analysis software Femlab® 3.0 was used to simulate the stresses the food tray might experience in practice. "Structural mechanics" with 2D-plane stress module was utilized. Femlab® 3.0 bases the interpolation equation on the equilibrium equations expressed in global stress components. Using a compact notation, the relationship can be written as:

$-\nabla \cdot \sigma = F$ where σ is the stress tensor.

Static analysis was done on the problem under consideration. The stress-strain relationship for linear conditions can be stated as:

$\sigma = D\varepsilon$ where σ and ε represent stress and strain tensors respectively. D represents the elasticity matrix. The strain-displacement tensor is represented by a strain matrix consisting of 6 terms, both shear and normal strain components. In static analysis substitution of stress-strain and strain-displacement relationship into static equilibrium equation produces Navier's equation of equilibrium expressed in displacement.

$-\nabla \cdot (c\nabla u) = F$ where u denotes the displacement under equilibrium conditions and F is the force acting on a body [36].

There have been some references cited in the literature which deal with finite element analysis in flexible food packaging. Simulation of migration of a food constituent from a multilayer laminate was performed and analyzed by Roduit et.al.[37].

An analytical solution to the migration problem was obtained by assuming that migration followed a diffusive process (Fick's law). The diffusion was assumed to be temperature dependant. Reed et al. [38] have reported the finite element simulations of the drop impact test for molded thermoplastic container holding liquid . They analyzed the experimental data from the drop impact testing of water-filled blow molded drums. It was found that the impact test follows the solid body dynamics equations. The loads and loading conditions were used as an input for finite element simulation. Travesin et al. [39] used finite element analysis to evaluate the performance of metal food container with special note on the geometric variations. Wang [40] evaluated the structural capability of a food container and made accurate assessment of axial load and paneling performance of cans. He discussed the effect of design parameters on the structure performance of containers. An algorithm developed by Wang [40] generated the optimal design of metal containers that would meet the structural requirement with least material consumption.

Chapter 3: Experimental Procedure

3.1 Introduction:

Food trays from two different companies; Stegner and Wornick, both located in Cincinnati, OH, were tested. The consignments from these companies contained the food trays with defects in the seal. Some of the defects were artificial (section 4.4.1); whereas the others were naturally occurring as the consequence of the process. Some of the packages were defect- free to enable us to compare the results with the defective ones. The packages were received in two different consignments, and were filled with different media. Both the consignments came from Stegner and Wornick and the author was not present at the time the packages were made in–line.

3.1.1 Consignment 1:

This consignment of 24 packages came from Wornick food products, Cincinnati, OH on July 14, 2004. The food trays were inspected visually and then categorized according to defects in them. The consignment had 13 defective and 11 non-defective food trays. All the packages had been filled with blueberry desert. The results of burst test on these packages and discussion will follow in the next section.

3.1.2: Consignment 2:

The author made a trip to Cincinnati, OH to pick up the packages manufactured by Stegner Food Products and Wornick. The food trays were visually inspected first and categorized according to defects in seal area. The military inspection guide [41] was followed throughout the classification process as a reference. Table 3.1 and 3.2 show the classification of the food trays:

Table 3.1 Categorization of defective and non-defective food trays from Stegner Co.

Defect	**Number of Trays**
Non-Defective	19
Delamination	11
Entrapped Matter	9
Blisters/ Air Bubbles	28
Damaged Trays	3
Tunneling	8
Short Seal	8
Total	**86**

Table 3.2 Categorization of defective and non-defective food trays from Wornick Co.

Defect	**Number of Trays**
Non-Defective	25
Short Seal	22
Entrapped Matter/ Moisture/ Air Bubbles	6
Multiple Defects (Short Seal + Wrinkles + Moisture)	8
Total	**61**

The non-defective packages were the first to be tested; while categorizing the defective packages. Following details were noted during categorization:

1. Food Material inside the tray
2. The dimensions of the defect; i.e. length of the short seal, the diameter of the air bubble, the width of the short seal,
3. The non-defective seal width
4. A rough sketch of the defective side of the seal

Some of the rough sketches of the defects are presented in Figure 3.1. It shows four different types of defects namely; short seal, uneven seal, entrapped matter and air bubble in the seal. According to inspection guide, the seal width less than 5/16'' will be scored a short seal [21]. Entrapped matter or void in the seal will be scored a defective seal. The dimensions of the defect and defect-free seal width will be noted. Pictures of the defects were taken in order to properly document the defects. Figures 3.2 and 3.3 show blister and tunneling defects in the seal of the package respectively.

Figure 3.4 is the schematic sketch of a short seal package received from Wornick Food Products with dimension of the short seal and length of the short seal. The sketch shows the approximate dimensions of the tray. The side of the tray in which the hole is drilled is referred with number 1 and other sides are referred accordingly in clockwise manner. In this particular case, the length and width of the short seal are 7''and ¼'' respectively. Seal width across the corner is also noted in order to accurately categorize the tray.

3.2 Mechanical (Destructive) Testing:

Even though non-destructive testing is by far preferred over destructive testing, as it evaluates the properties without destructing the package; destructive technique is the one which lets us evaluate the seal integrity directly.

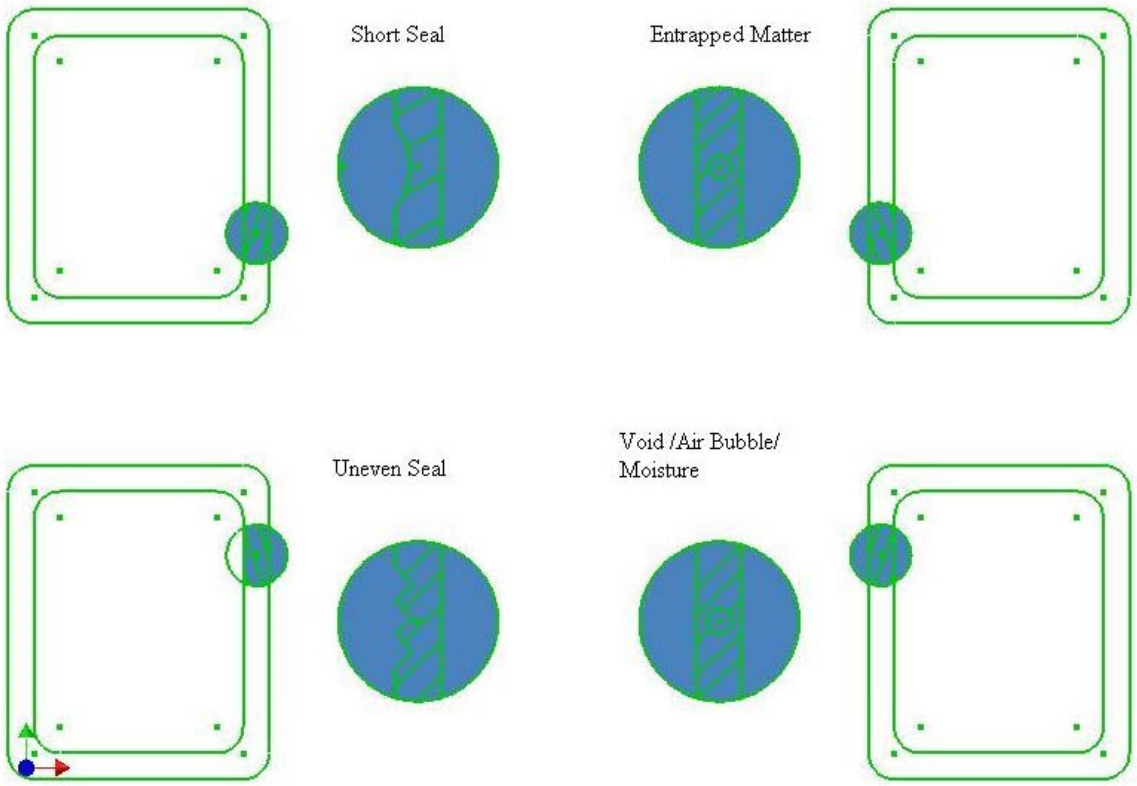

Figure 3.1: The schematic drawing of some of the defects in the seal.

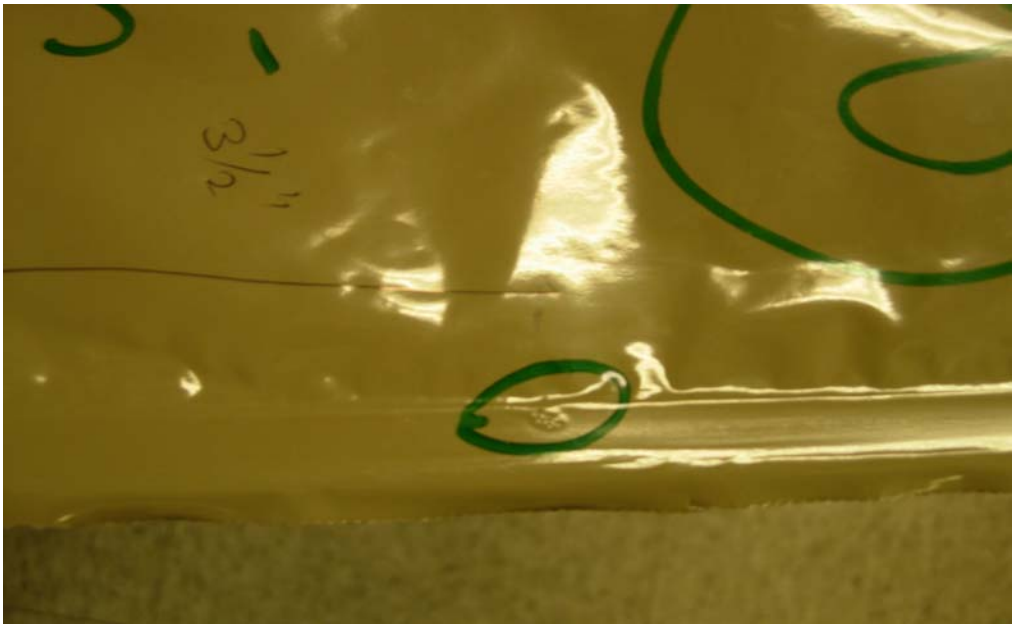

Figure 3.2: A blister in the seal of the food tray.

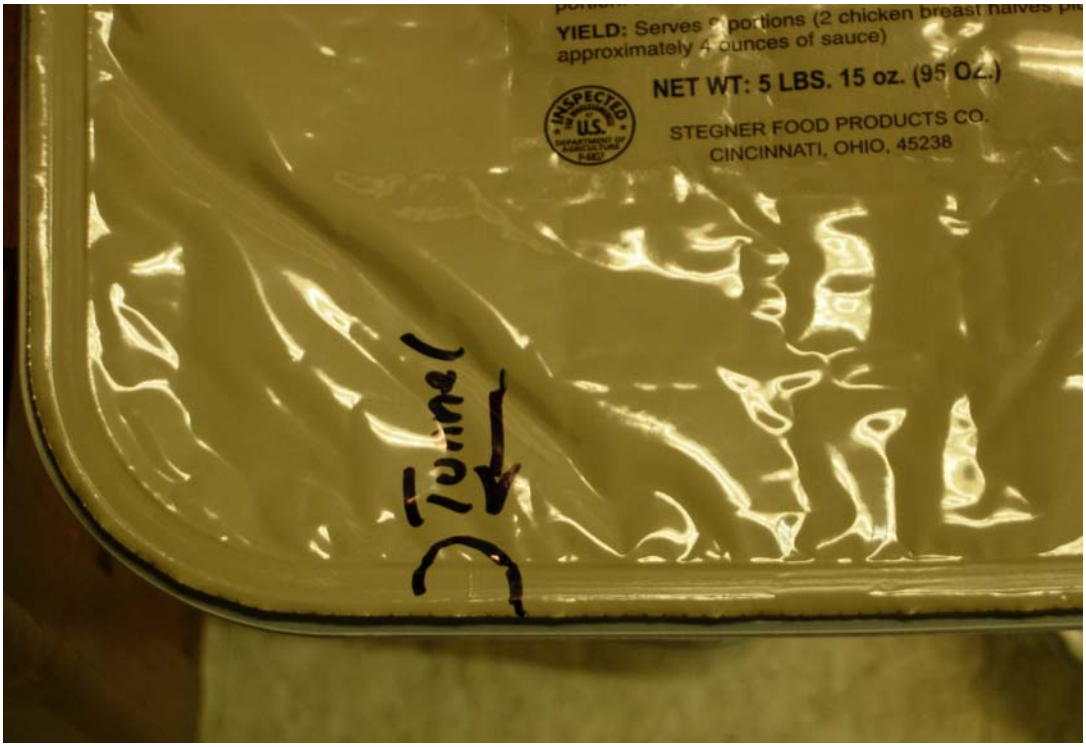

Figure 3.3: Tunneling defect in the seal of a food tray.

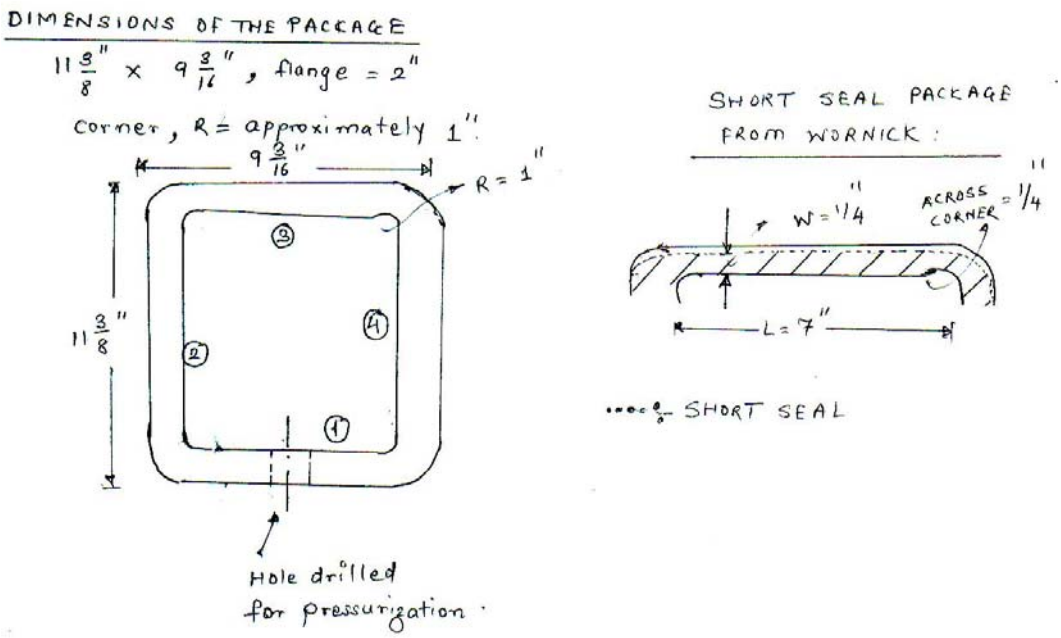

Figure 3.4: Schematic drawing of a defective tray with a short seal from Wornick.

Based on the destructive test, a standard for adequate seal strength can be proposed. This standard can be used to decide which defects, even though present in the seal would not significantly affect the seal strength and food material inside the tray. Such a standard may then reduce the rejection rate and increase revenue. Food inside the tray should remain free from any contamination and be edible for at least 18 months of shelf life. This requirement is met only if seal integrity of a polytray is set to be the highest standard.

3.2.1 Burst Testing:

ASTM standard F 2054 [42] was used as a basis for the design of a burst test system in this project. This standard test method describes burst testing of flexible package seals using internal air pressurization within restraining plates. A burst test (pressurized polytray) was developed to mimic the testing currently being performed at

the manufacturing facilities. The system had to be designed in such a way as to monitor the air flow (leak) and pressure in the package. Earlier work on the development of such a system was done by the colleague of the author at the University of Tennessee, Knoxville [43]. Initial calibration of the system was performed with a relatively simple set-up to monitor the air flow out of the tray as a function of the increasing pressure inside the tray. A computer integrated system monitoring air pressure and flow was then constructed. Figure 3.5 shows the burst chamber designed to hold the package in place while the package is being pressurized. The package to be tested was drilled to make a hole of diameter of 0.75 inch. Plastic tubing of diameter 0.25 inch was used to pressurize the package. A rubber stopper was used to hold the rubber tubing and make the hole airtight. The package would then be inserted inside the burst chamber.

Figure 3.5: Picture of the burst chamber used for the burst testing.

Once the tray was inside the chamber, the rubber tubing was inserted into the drilled hole and was sealed with a rubber stopper. Figure 3.6 shows the schematic diagram of PC-integrated system for burst tests. The PC integrated system consisted of Labview 7.0® in-line with National Instruments® controller (hardware). The air flow and air pressure could be measured and recorded every second. Further, it was noticed that one data point each second was not necessary and the system was modified to record the air flow and pressure every 10 seconds. The maximum flow that could be measured was 20 cc/minute with an accuracy of 0.2 cc/minute. Once the tray was pressurized to an initial value and the controller and system stabilized; the air flow would drop close to zero; and then the experiment would be started. The PC integrated burst system was used for all the polytrays during this project.

This assembly was found to be extremely user-friendly, less tedious as compared to a manual system and did not require much personal attention. All the data was saved to the disk through Labview®7.0. For all the experiments, the initial pressure was set to 10 psi. It would increase in the step of 5 psi every 5 minutes, thus allowing sufficient time for the system to stabilize and flow rate to zero in case there was no leak in the tray. The pressure would rise till the package burst or leak developed in the tray. The pressure at which the package failed was recorded for all the packages. Though the system saved the data every 10 seconds, intermittent pressures and air flow rates were not considered or noted.

The trays that were tested under this project had food inside them. It was initially found that if the tray sustained pressure of 40 psi (which was considered the pressure at which the test could be terminated assuming that the seal was sufficiently strong), the test would be terminated; however because of the pressure inside the package, the food would flow back and clog the entire tubing. Quite often, the pressure was so high that the food would even enter the controller system. Cleaning of the system would then be very difficult and time consuming.

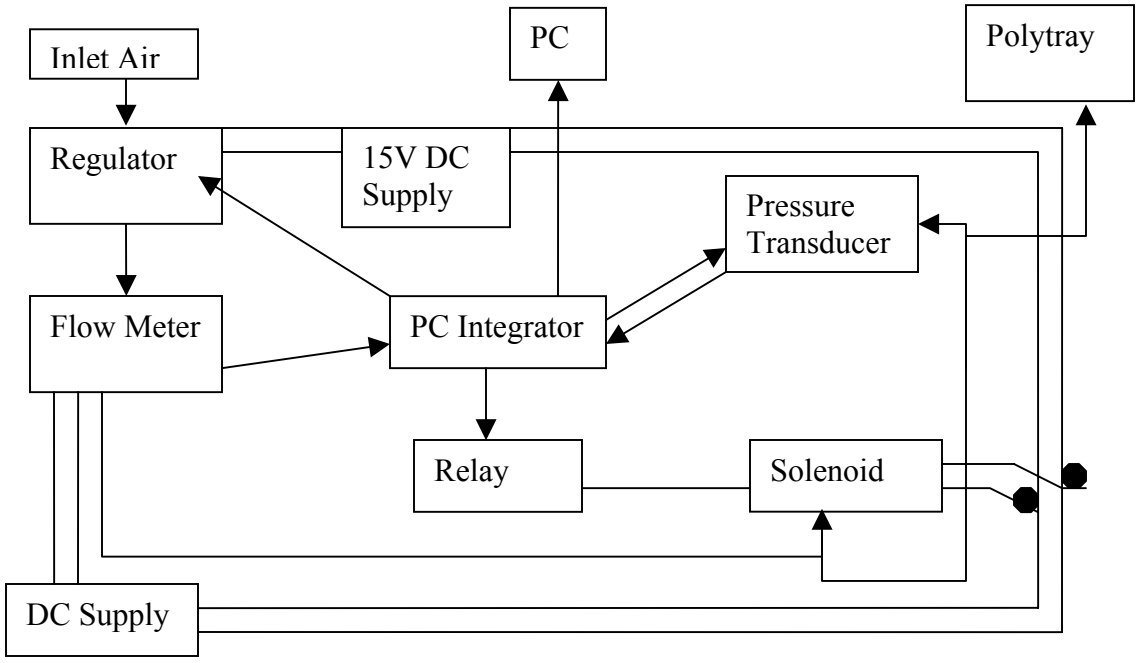

Figure 3.6: Schematic of PC integrated system for burst data analysis.

Therefore, following alternatives were considered as solution to this problem:

1. Tray would be allowed to burst and test would continue till the package burst.
2. The pressure release value would always get clogged. So the release valve would be cleaned before each experiment began.
3. A check valve would be installed in between the controller and pressurized tray.

Having considered all the options, it was decided that letting the tray pressurize would be the best alternative. So the trays were allowed to pressurize till they burst. So the only possible result from the burst test on a tray would be a leak or burst. Therefore whenever the tray sustained the pressure of 40 psi, and burst at higher pressures; the reported pressure would be 40 psi, to maintain consistency with the previous work. The other

perspective of this explanation is, once the tray sustains the pressure of 40 psi, no matter pressure it fails at, the seal will still be considered a good seal.

3.2.2: Post Failure Characterization:

Post failure characterization techniques like Scanning Electron Microscopy (SEM) and FTIR/ATR are extremely useful in understanding the mode of failure. The mode of failure gives information about the stress condition and the mode of propagation of crack. FTIR/ ATR provides direct evidence of presence of one polymer across the boundary. SEM also provides the boundary characteristics and the evidence of delamination across particular layers.

3.2.2.1: Scanning Electron Microscopy:

SEM analysis was done on several seals from the burst food trays. The piece of lid sealed to the tray was cut from the side which burst open. This piece of a lid was essentially sealed to the tray before testing. Samples were chosen after visual inspection in such a way to include most details about fracture. All the samples had two regions separated by a boundary clearly visible on them; one being the sealant PP layer and the other polyester. The dimensions of the samples were such to fit on the aluminum stub in the SEM machine; typically about 8 mm x 5 mm.

The samples used for the SEM analysis were gold-coated first. SPI sputter coater was used for the purpose. This coater has six specimen mounts. The specimen mounts were secured to the holder by the set screws provided. After placing the glass chamber on top, the coating process could start. The Ar pressure was 2 psi, the current passing through the plasma was 20 mA and time required to coat the sufficient amount of gold was 10 seconds. Typically coating thickness depends on cleanliness of sputtering system.

The thickness of gold coating is calculated using the following formula:

$$d = K * i * V * t$$

Where d is the thickness of gold coating; K the constant for Ar-plasma system (0.17); i the plasma current; V the applied voltage; t time in seconds. Thus for our application, the gold coating thickness can be calculated:

d = 0.17*20*10 = 3.4 nm/ kV.

Once the sample is gold-coated, it can be put into Leo 1525® SEM machine. The SEM used for this project was manufactured by Leo, UK. The Leo 1525® workstation utilizes a Gemini field emission column. The imaging was done by secondary electron detectors; SE2 and In-Lens. When the working distance was less than 5 mm and the applied voltage low, In-Lens detector proved to be the best. When the applied voltage is relatively high and working distance greater than 5 mm; SE2 detector was found to work the best. The parameters used while imaging are noted in the Table 3.3. Although 5kX is not very high a magnification if compared to 30kX, (i.e. maximum magnification possible in this microscope) there was always a problem of sample charging above 5kX magnification at relatively low scanning speeds.

Table 3.3: Scanning Electron Microscopy parameters used for imaging the samples.

SEM Parameters	**Value of the Parameter**
Working Distance	5-7 mm
Applied Voltage	3-5 kV
Secondary Electron Detector	SE2 and In-Lens
Magnification	Ranging from 300X to 5 KX

The scanning speed used to capture the images was 4. Once the sample was seen on the screen and in the field of vision, the chromatic aberration and stigmation had to be taken care of by changing the X- and Y-stigmatic correctors and focusing the sample at high magnifications.

To understand the chemical composition of the layers on either side of the fractured boundary, the Energy Dispersive Spectrum (EDS) was collected on the spots across the fracture boundary. The software lets the user select the elements which could be present in the sample based on the prior knowledge. Thus carbon, oxygen and nitrogen were selected to identify the polymer layer on either side of fracture boundary. For EDS to work properly, the voltage in the electron gun was increased to 20 kV.

3.2.2.2 Fourier Transform Infrared (FTIR)/ Attenuated Total Reflectance (ATR):

Infrared spectroscopy was utilized to identify the polymers on either side of the fracture boundary on a lid sample after the burst test on food trays. Each functional group has particular absorption of infrared radiations in the operational range (4000 -700 cm^{-1}). Based on the charts available, each absorption band can be ascribed to a particular bond. An absorption spectrum is obtained by placing the material in between the spectrometer and an energy source which provides an electromagnetic radiation in the frequency range being studied.

Since the samples were not transparent, the Attenuated Total Reflectance (ATR) had to be used on the samples. The internal reflection element used is a germanium crystal. The equipment utilized was the Bio-Rad FTS 6000e spectrometer in conjunction with the WinIR Pro 3.0 software. Table 3.4 lists all the parameters used for the analysis.

Table 3.4: Parameters used for ATR analysis on the samples.

Parameter	**Value of the Parameter**
Speed	5 kHz
Filter	1.2 kHz
Resolution	1 cm^{-1}
Scans to co-add	256
IR Source	Mid-IR
Beam	External
Detector	UMA 500

3.3 Non-destructive Testing:

Non-destructive techniques are used extensively in the industry for the reason that the sample does not have to be destroyed. Examination can be done without physically damaging the sample. Two such techniques were used during this project to non-destructively examine the food trays, namely ultrasonic inspection and infrared thermographic inspection.

3.3.1 Ultrasonic Inspection:

Ultrasonic testing is by far the most popular non-destructive technique and is widely used in the industry. If standardized and all parameters set; ultrasonic technique could really provide a means to reduce the incidence of defective packages reaching the consumer. Ultrasonic techniques do not result in permanent change in the medium under evaluation. Ultrasonic transducers, devices which convert electrical energy to mechanical energy are used to make the measurements. Two general ultrasonic techniques used for flaw detection are transmission and pulse echo techniques. In pulse-echo technique, used

for the experiments, an ultrasonic pulse is propagated into the sample, and the reflected echo produced by the inhomogeneities and flaws is received back by the same transducer. Low frequency transducer (15 MHz) was used for the experiment; their focal length being 3 inches. Figure 3.7 shows the waveform which results from the incidence of the ultrasound wave with the object under examination.

The SONIX® FlexSCAN-C 4.3 System was used for the C-scans of the defective polytrays. Following parameters need consideration while running C-scan; position of various gates, time of flight, and amplitude of signal. These experiments were performed with a colleague of the author and the samples used for the experiment were prepared at Stegner Food Products, Cincinnati, OH with artificial defects in the seals. The food trays tested had channel defects on one side. The wires of different diameters were placed on the flange during sealing process and then subsequently pulled out before the experiment to create tunneling defects on one side of the seal. Such defective packages were tested using ultrasonic inspection.

Polytrays were completely submerged into the water medium and centered in the middle of the tank for the experiment. Parameters were set to optimize resolution of the package as the scanning was done and images of the scans were obtained. Gate locations were set for the area of good seal before the scans were initiated.

3.3.2 Infrared Thermography:

Infrared thermography is another interesting non-destructive method to test the sample. This method utilizes the infrared camera and heating source to capture the images in real time. The infrared camera works on the principle of differential heat loss from a defect in the sample. The heat losses from a uniform, homogeneous and non-uniform, defective surface are not the same. Infrared thermography has the capability to capture this difference.

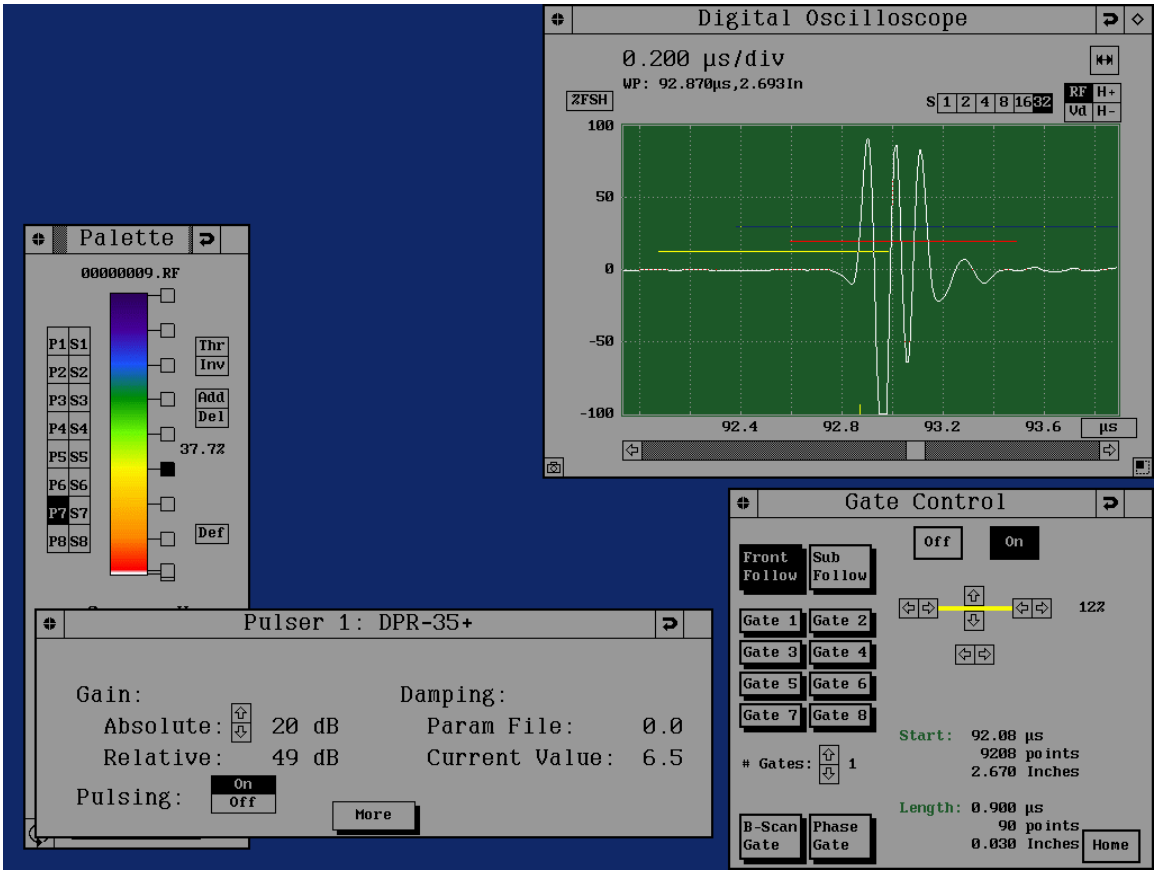

Figure 3.7: The waveform generated by SONIX® in the pulse-echo technique.

The Phoenix® systems with Indigo's real time imaging electronics (RTIE) mid-IR camera was used in conjunction with Talon Ultra 5.2 software to capture and process the images. The camera is as sensitive as 0.2°C change in temperature. Table 3.5 lists some of the specifications of the camera. The experiments were performed by heating the package with a 100 W incandescent bulb. The samples were heated from the tray side, lid facing the camera. The package was clamped and the bulb was placed exactly behind the defect. Then the camera was properly focused to capture the image of defect. Having focused the camera, the tray was heated for 2 minutes and bulb turned off. As soon as the bulb was turned off, the first image was captured on camera, which was to be used as a base image. Each subsequent image was taken at 2 minute intervals. Six such images were captured. To observe the effect of differential heat loss across the defect, the subsequent images were subtracted from the first image. These images were then processed for contrast and resolution using Talon Ultra 5.2 software. The images were then saved into .jpg format. The images captured were two dimensional; which means the depth of the defect could not be ascertained looking at the image. Therefore the superficial defect would create just the same image as a defect which was deep inside the seal would.

Table 3.5: Specifications of the Indigo IR camera.

Parameters	**Specifications of the camera**
Detector	Indium Antimonide (InSb)
Spatial Range	1-5 microns
Digital Resolution	320 X 256 pixels
Integration Time	6 microseconds
Power	35 W

3.4 Finite Element Simulations using Femlab®:

The stresses and deformations developed in the polytray can be modeled using the finite element approach and the software Femlab®. The object under consideration can be drawn using the drawing software such as Solidworks®. The object is then imported into Femlab®.

The real life forces that a tray might experience are then applied to the tray using boundary and subdomain conditions. Once the object is meshed, Femlab® applies the boundary and subdomain conditions in the form of partial differential equations and attempts to find the solution over the nodal points and then integrates the solution over the entire boundary using iterative solver till the solution converges.

Two and three dimensional (2D and 3D) simulations were done in order to understand the stress condition in the polytray. Earlier work showed that Femlab® could be successfully utilized to simulate the conditions in the burst test without any constraints on the displacement of the lid. An attempt was made to simulate the burst test conditions with constraint (in the form of the acrylic plate on top of the tray) in the vertical direction in order to more accurately simulate the actual burst test. When the initial attempts were made to run the simulations, it was found the lid would pass through the acrylic plate under the applied force. The private correspondence with Comsol® experts, made it clear that the equation which would connect the displacement of the lid to that of acrylic plate would be needed if this problem were to be avoided. Therefore an imaginary material with very low stiffness was assumed to be present in between the lid and acrylic plate. This material would itself form a subdomain while specifying the simulation conditions. Thus the connecting equation would be provided by the presence of this subdomain. This material perfectly served the purpose and thus the displacements of lid and acrylic plate were connected. Various simulations with varying distance between the lid and plate were performed and shear and normal stresses across the seal measured.

Figures 3.8 and 3.9 show 2D and 3D drawings of the polytray respectively. The three dimensional drawing was made in Solidworks®.

The gap between the acrylic plate and lid was varied between 6 and 38 mm. In the actual burst tests, the acrylic plate was reinforced with steel bar from top. Therefore, the modulus of acrylic plate was assumed to be 2E11 Pa and that of lid and tray (both being the polymeric materials) to be 1E09 Pa, based on some previous work [30]. The pressure inside the tray was varied from 20000 Pa (3 psi) to 180,000 Pa (27 psi). The modulus of filling material was assumed to be 100,000 Pa. All the sides of the tray except the lid were constrained in x and y-directions. Further simulations were performed with varying gap between the acrylic plate and lid; namely 8 mm, 10 mm, 14 mm, 22 mm, 28 mm, 34 mm and 38 mm to see the variation of stress. Table 3.6 lists all the parameters used for simulations.

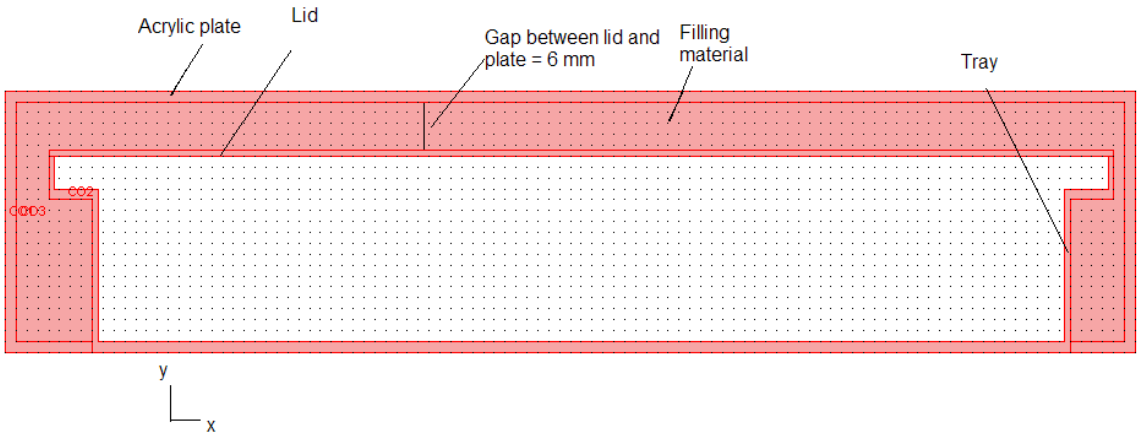

Figure 3.8: 2D drawing of the polytray in Femlab® with a filling material.

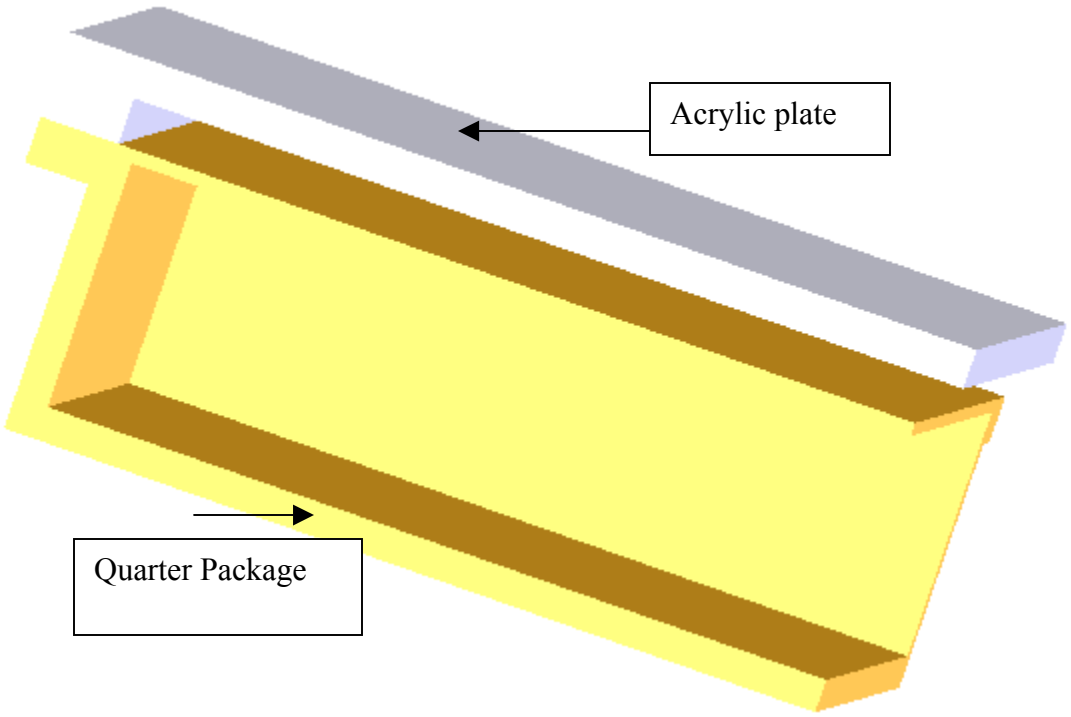

Figure 3.9: Three dimensional drawing of a quarter package with acrylic plate in Solidworks®.

Table 3.6: Some of the parameters specified used for simulations in Femlab®.

Parameters		Value/ Type
Meshing	Predefined Mesh Size	Extremely Coarse
	Number of Degrees of Freedom	143624
	Number of Elements	34992
	Number of Boundary Elements	3128
	Minimum Element Quality	0.5082
Elements	Default Element Type	Lagrange-Quadratic
	Analysis Type	Static
Solver	Solver	Stationary Linear
	Linear System Solver	Direct (SPOOLES)
	Solution Form	Coefficient

Chapter 4: Results and Discussion

4.1 Overview:

The poly trays were examined with destructive and non destructive methods to develop the optimum parameters which would determine whether a tray would be acceptable for long term storage. Results from these tests could help change the inspection criteria which in turn would help reduce the percentage of rejection of trays and thereby increasing profit and capacity. A destructive burst test was used to evaluate the seal integrity of defective and non-defective trays. The results from the defective trays were then compared with those of non-defective ones. The finite element program such as Femlab® was used to simulate the stresses developed in the seal of a tray as a result of the burst test. The destructive test cannot be used to test all the packages, but it certainly gives some basis on which the sample with a specific defect can be accepted or rejected. An effective non-destructive test would identify the defects in the trays without destroying them. Two such methods were evaluated under this project; namely ultrasonic inspection and infrared thermography. Both of these methods, if implemented correctly, would identify the defects right after the tray is sealed and thus provide instantaneous feedback which can be used to alter processing conditions and reduce rejection rate of trays. Feasibility of these techniques will also be discussed.

Post-failure characterization techniques like scanning electron microscopy (SEM) and Fourier transform infrared spectroscopy (FTIR/ ATR) were used to understand the failure in the sample. SEM and ATR provided very valuable information about the mode of failure and delamination between polymeric layers. It was found out that the delamination always took place between PP (tray)/PP (lid) and nylon/PET layers.

4.2 Destructive Testing:

A destructive burst test was performed on defective and non-defective trays to compare the results from the destructive samples with those of non-destructive ones. The burst test was found to be of high utility directly assessing the seal strength of the food trays.

4.2.1 Burst Test:

The burst test gave a direct way of measuring the seal strength qualitatively and quantitatively. The test gave the burst/ leak pressures at which the trays leaked or burst; which could directly relate to whether the seal was strong. The pressure was measured for each food tray. The average burst pressure for each category of defective and non-defective trays was then calculated and used for statistical analysis of the data. At this point, it must be mentioned the basis on which the package was considered to leak. From the previous work, a standard for a leak and burst was set. A tray with air-flow of 20 cc/min would be considered to have developed a leak. A tray which sustained the air pressure of 40 psi without developing a leak would be considered to have adequate seal strength and thus test would be terminated.

4.2.1 Consignment 1:

The first consignment of 13 defective trays and 11 non-defective trays from Stegner and Wornick Food Products, Cincinnati, OH was delivered on July 14, 2004. It was observed that packages from Wornick sustained higher burst pressures than those from Stegner Food Products. The defective trays had air bubbles, short seal, uneven seal, and entrapped matter; or combination of these. Table 4.1 shows the average burst pressure for packages with each of the defects. The results shown in Figure 4.1 shows the average burst pressure plotted against the individual defects. The error bars on each defect are based on the maximum and minimum deviation in burst pressure measured.

Table 4.1: The average burst pressures of trays with different defects.

Defect	**Avg. Pressure (psi)**	**Max/Min Pressure (psi)**	**Number of Packages Tested**
Non-Defective	33.8	40/25	11
Air Bubble	38.3	40/35	5
Entrapped Matter	29.2	40/25	11
Short Seal	34.1	40/25	7
Uneven Seal	29.1	35/25	10

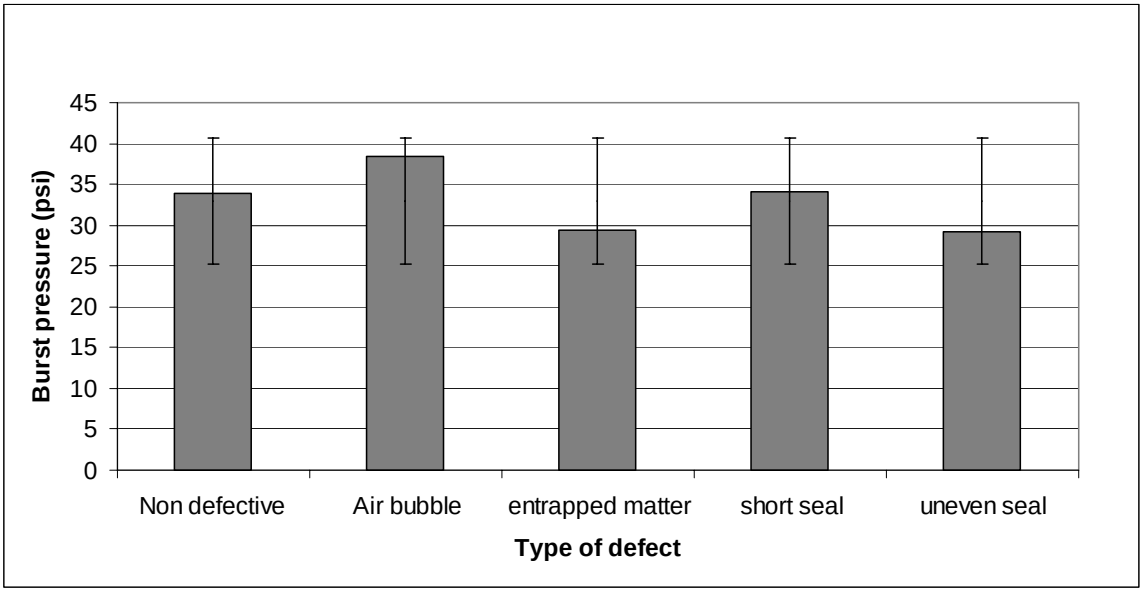

Figure 4.1: Average burst pressure of various kinds of defects in trays (consignment 1).

It can be seen that the average burst pressure for trays with air bubbles in their seals is higher than the average burst pressure of non-defective trays. If the results were shown as those of the trays from two different companies and if those results were compared with non-defective trays from that company, it would be more realistic. However, there were not enough trays to test to give statistically significant results.

4.2.2 Consignment 2:

The second consignment of food trays was received on 29 November, 2004 from Stegner and Wornick Food Products, Cincinnati, OH. The classification of the trays based on the defects can be found in section 3.1.2. Each and every tray was inspected for defects and categorized. The severity of defect was assigned based on the inspection guide provided and sketches were prepared showing the dimensions of defects and defect free length of the seal. Photographs were taken to document how the defects actually appeared before the package was subject to the burst test. One such sketch can be found in Figure 3.2. The consignment received contained trays with the following defects; short seal, entrapped matter, blisters and air bubbles, delamination and tunneling (Refer appendix C for pressures the trays failed at and dimensions of defects). To compare the results from the bust test, non-defective packages were provided and thus the results of the two compared. Figure 4.2 shows the average burst pressure of the trays from Stegner and Wornick Food Products, with and without defects. The error bars seen on the data are based on standard deviation in burst pressure measured for each defect. The function "STDEV" in Excel® was used to calculate standard deviation. Tables 4.2 and 4.3 list the results from burst tests of all the trays from Wornick and Stegner tested respectively.

The consignment from Wornick did not have any trays with tunneling defects. It can be seen that the average burst pressure of the non-defective trays from these two companies is almost the same.

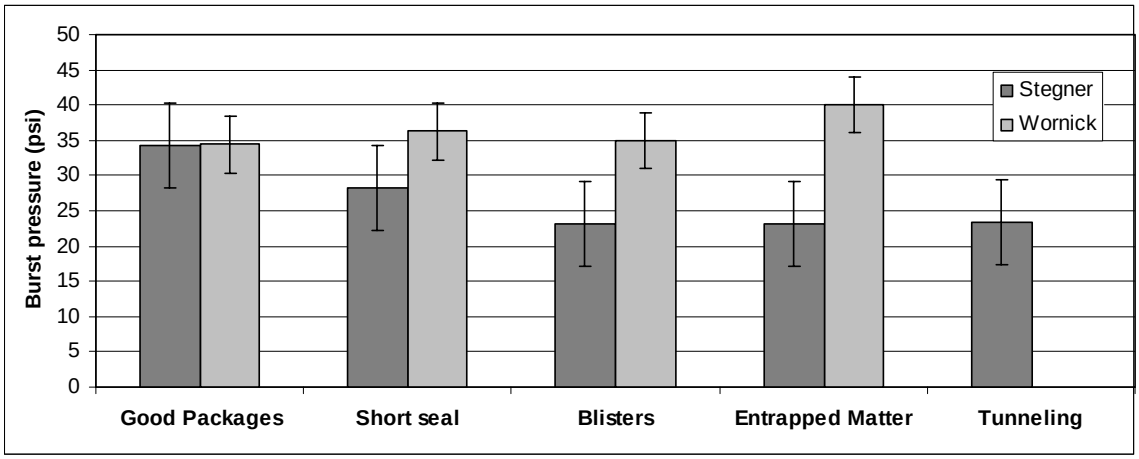

Figure 4.2: The average burst pressure of non-defective and defective packages from Stegner and Wornick Food Products.

Table 4.2: Burst test results for the trays with various defects from Wornick Co.

Defect	**Average Pressure (psi)**	**Max/Min Pressure (psi)**	**No of Trays Tested**	**Standard Deviation**
Non- Defective	34.4	40/25	24	5
Short Seals	36.2	40/35	24	3.8
Blisters	35	40/35	5	3.5
Entrapped Matter	40	40/35	8	4.5

Table 4.3: Burst test results for the trays with various defects from Stegner Co.

Defect	**Average Pressure (psi)**	**Max/Min Pressure (psi)**	**No of Trays Tested**	**Standard Deviation**
Non- Defective	34.3	40/20	14	6.7
Short Seals	28.3	40/25	9	5.5
Blisters	23.1	30/15	27	3.7
Entrapped Matter	23.1	25/20	8	2.6
Tunneling	23.4	30/20	13	3.1

However the trays from Wornick with defects in them sustained higher burst pressures than those from Stegner. Also it seems that the defective packages from Wornick performed as well as the non-defective ones. This probably owes to the high seal width the Wornick trays had. Nine trays from Wornick Co with short seal had seal width of 4/16'', and eleven trays had a seal width of 3/16''. While six trays from Stegner Co had a seal width of 3/16'' and three trays had a seal width of just 1/8''.

Non-defective trays from Wornick Co had seal width close to 5/16''; while those from Stegner had seal width less than 4/16''. The short seal trays from Wornick seemed to perform just as well as the non-defective trays; while those from Stegner had somewhat less burst pressure than the non-defective ones. Figures 4.3 and 4.4 show the relative burst pressures of short seal packages from Stegner and Wornick with different seal widths. Non-defective packages from Stegner showed higher burst pressures than the packages with 2/16'' and 3/16'' of seal width. There was not much difference in the burst pressure of the Wornick short seal trays with seal widths of 3/16'' and 4/16'' compared to that of non-defective ones. This fact should be seen in the perspective that the short seal packages were far less in number than the non-defective ones, and those with 2/16'' seal width were just too few to generate a statistically significant average.

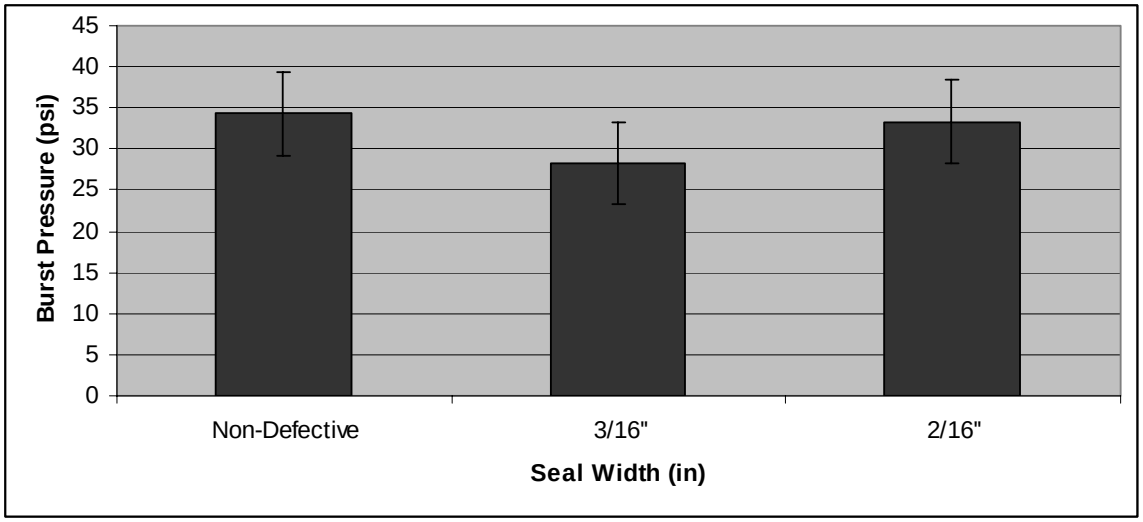

Figure 4.3: Burst Pressure of short seal trays from Stegner.

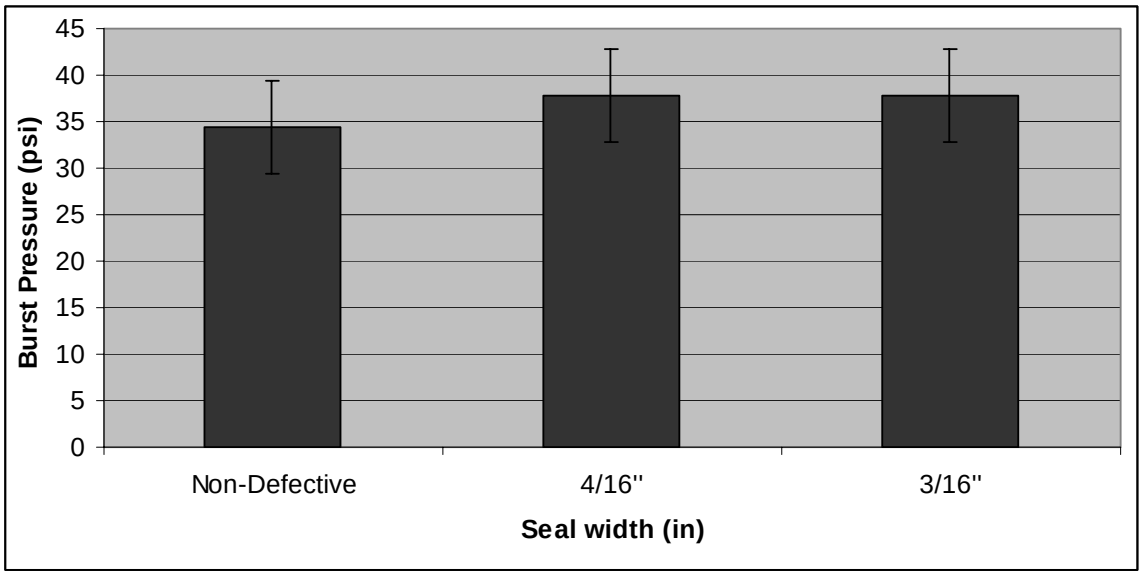

Figure 4.4: Burst Pressure of short seal trays from Wornick.

This result is to be seen as a general trend. There was just one tray from Wornick Co with a seal width of 2/16'' and it sustained 40 psi. This information would not be useful to gain any statistical perspective and hence omitted. Non-defective trays tested had a uniform seal width of 5/16''.

The average burst pressure for the trays from Wornick with entrapped matter and blisters in them had a higher burst pressure than those from Stegner. Entrapped matter does not really seem to affect the seal strength of the Wornick trays; while the trays with blisters in them show a drop in seal strength by some fraction, but not to the extent that the trays would not pass since the average burst pressure was still close to 35 psi. Stegner trays with blisters and entrapped matter have almost the same seal strength, much lower than their Wornick counterparts. According to the inspection guide; the presence of entrapped matter within 1/16 inch of seal would be assigned as a critical defect. Similarly, a blister which would leave less than 1/16 inch of seal width would be scored a critical defect. Even if a defect leaves more than 1/16 inch of defect free seal width, but is on the inner edge of a seal, it is classified as a critical defect [41]. Defect present on the inner edge of a seal would reduce the seal strength of a seal, increases stress concentration on a seal and reduces burst strength.

It would be worthwhile to look at the scattered plots of burst pressures to get the idea of what percentage of trays fail at a particular pressure. Figures 4.5 and 4.6 show the scattered plot of burst pressures with number of trays and percentage of trays failed below 32.5 psi from Wornick and Stegner respectively. Clearly more than 66% of the non-defective trays from Wornick burst higher than 32.5 psi; while close to 50% of those from Stegner burst higher than 32.5 psi. Again, as far as the trays from Wornick are concerned, the short seal does not significantly alter the burst pressure; while it does for the trays from Stegner. Nearly 90% of the short seal trays from Wornick burst at or above 35 psi; while only 30% of those from Stegner burst at or above 35 psi; clearly suggesting that the short seal is not a major factor of reduction in the seal strength for Wornick seals owing to higher seal width.

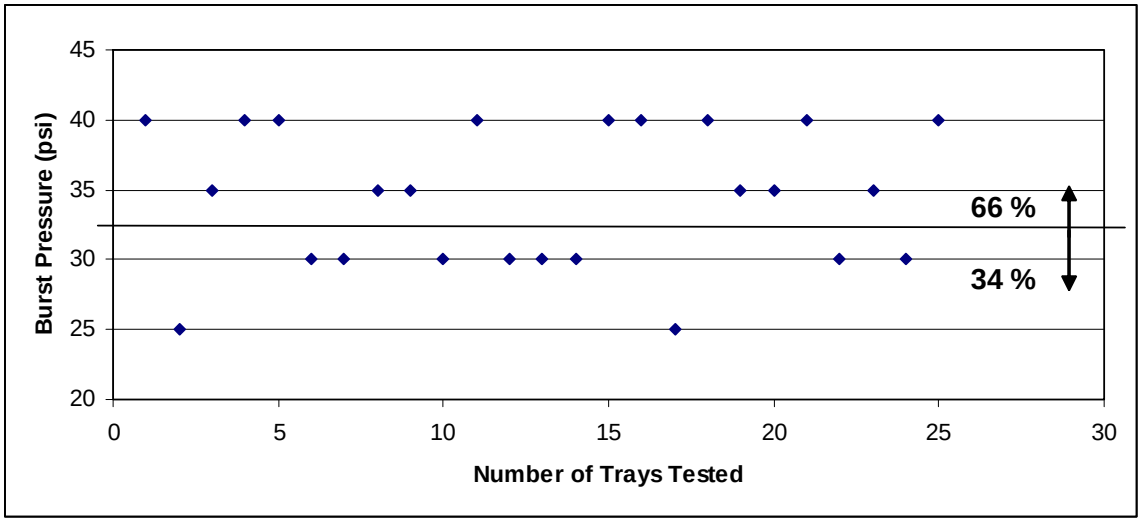

Figure 4.5: The scattered plot of the burst pressure of the non-defective trays from Wornick.

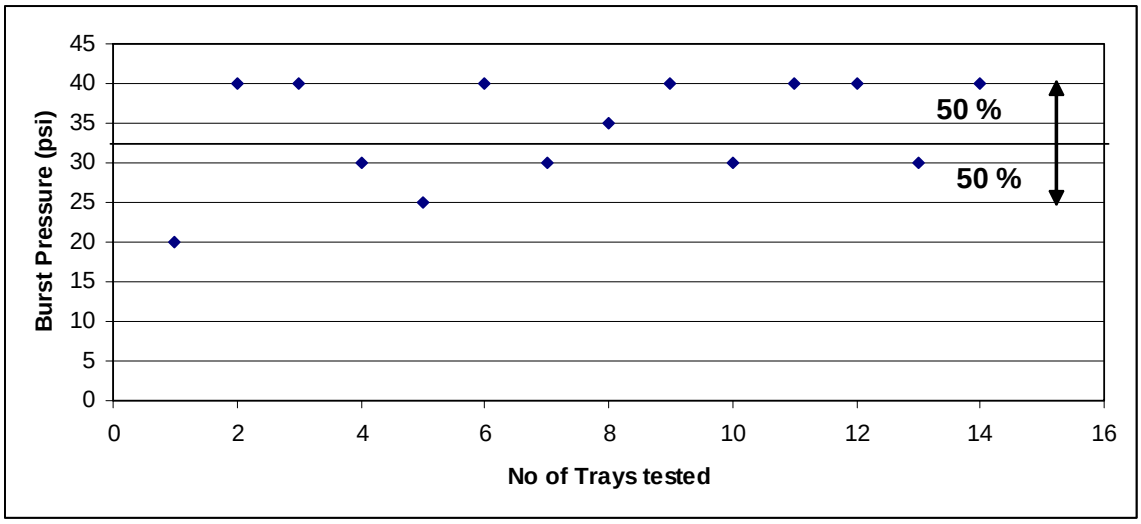

Figure 4.6: The scattered plot of the burst pressure of the non-defective trays from Stegner.

Figure 4.7 shows the percentage of trays, from Stegner with blisters, entrapped matter, tunneling defects, delamination, and short seals failed below particular pressure level. It can be seen that short seal trays from Stegner performed in between the non-defective and other kinds of defective trays. Trays with delamination seemed to perform badly among all other defective trays. The data from the defective Stegner trays is then compared with the non-defective ones to determine the critical pressure level which must be set for a tray to pass the burst test. Figure 4.8 shows the percentage of trays, from Wornick with entrapped matter and short seals failed below particular pressure level. It can be seen that Wornick trays with defects performed just as good or rather slightly better than non-defective trays. This is mainly due to the fact that defective trays tested were really less in number than the non-defective ones. However, it gives the idea that defective trays performed equally well. This data presented in Figure 4.8 can be used to determine the critical pressure level which must be set for a tray to pass the burst test. Figure 4.9 shows the percentage of trays failed below particular pressure level for both Stegner and Wornick. This might be useful to select a particular pressure level which separates a good seal from a bad one. It can be seen from Figure 4.7 that at low pressures more Stegner trays have failed as compared to Wornick trays. Wornick trays seem to perform better at higher pressures. Figures 4.10 and 4.11 show the scattered plots of the burst pressure of short seal trays from Wornick and Stegner respectively. Numbers next to points in Figure 4.10 and 4.11 represent the number of trays burst at that particular pressure. The average seal width for short seal trays from Stegner was close to 3/16'' and that for Wornick trays was close to 4/16''. Figure 4.12 shows the burst pressure of the trays with blisters in their seals. Again the Stegner trays have a very low average burst pressure. This is due to the high percentage of seal area that the blister occupies; leaving a very less non-defective seal area to hold the pressure. The Wornick trays have in general high seal area and so non-defective percentage of seal area is sufficient to hold the pressure inside the tray.

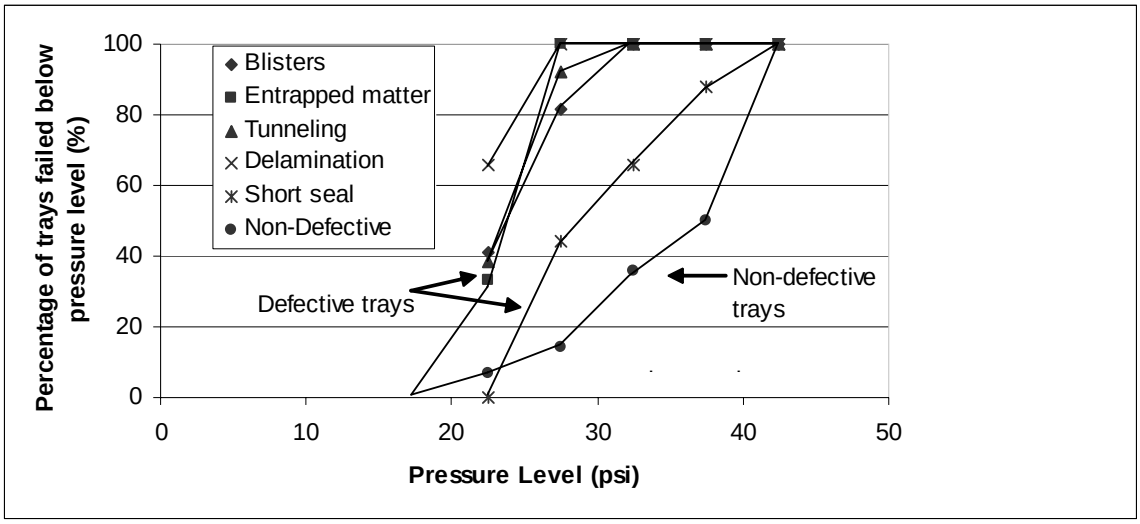

Figure 4.7: Percentage of Stegner trays with defects failed below certain pressure level.

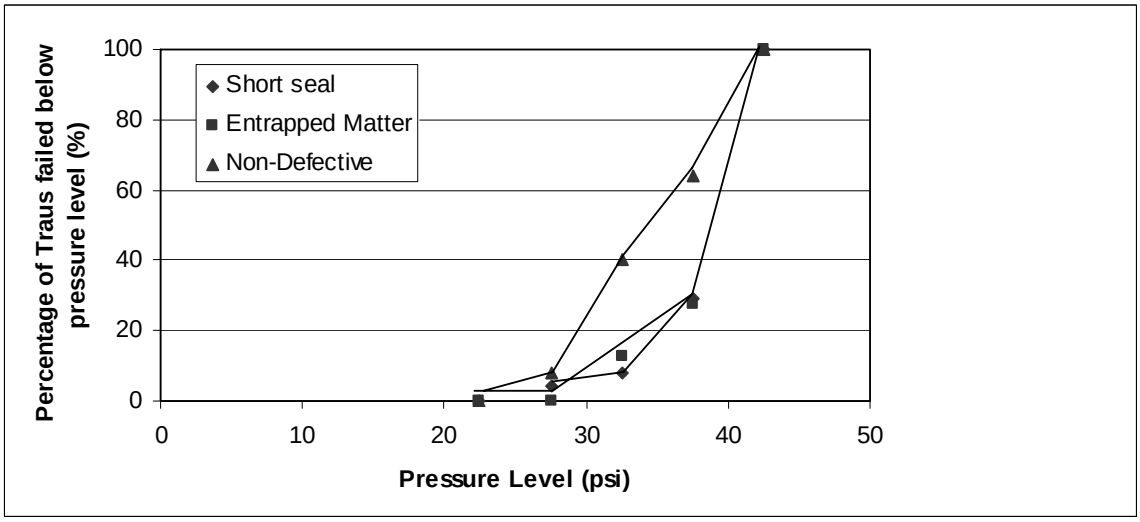

Figure 4.8: Percentage of Wornick trays with defects failed below certain pressure level.

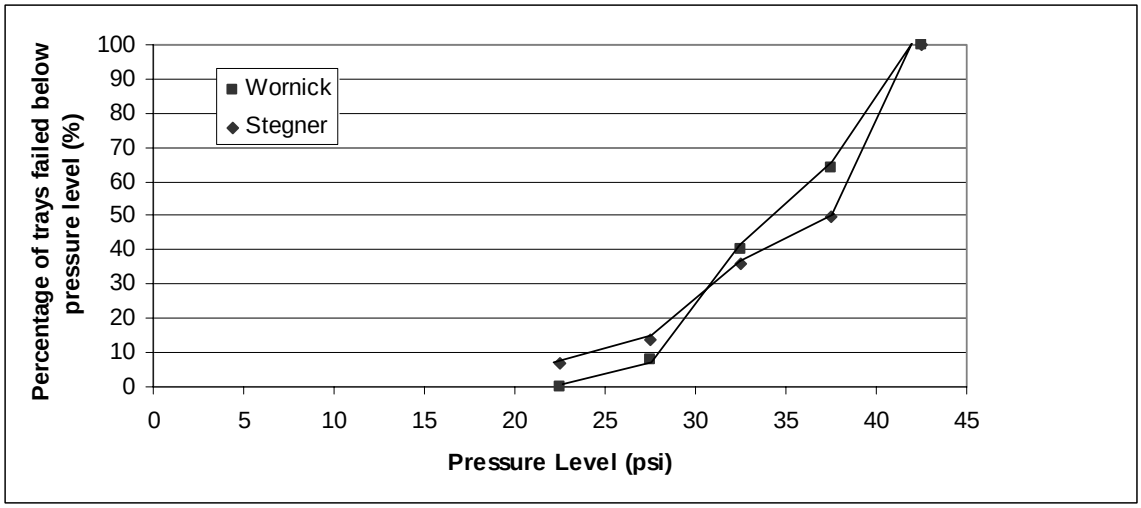

Figure 4.9: Percentage of trays failed below certain pressure level.

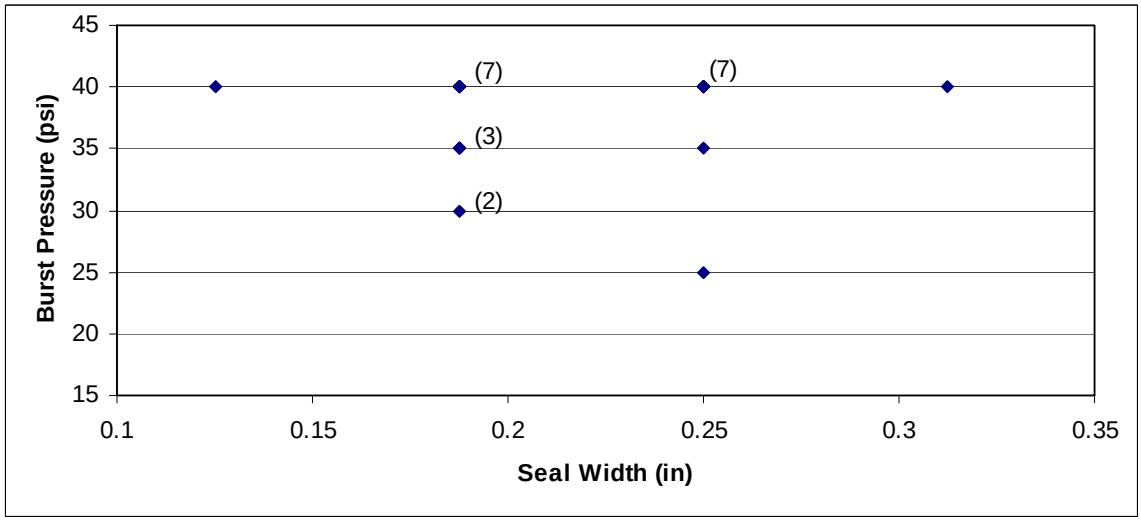

Figure 4.10: Burst pressure of short seal trays from Wornick. Average burst pressure for Wornick trays is 37.6 psi.

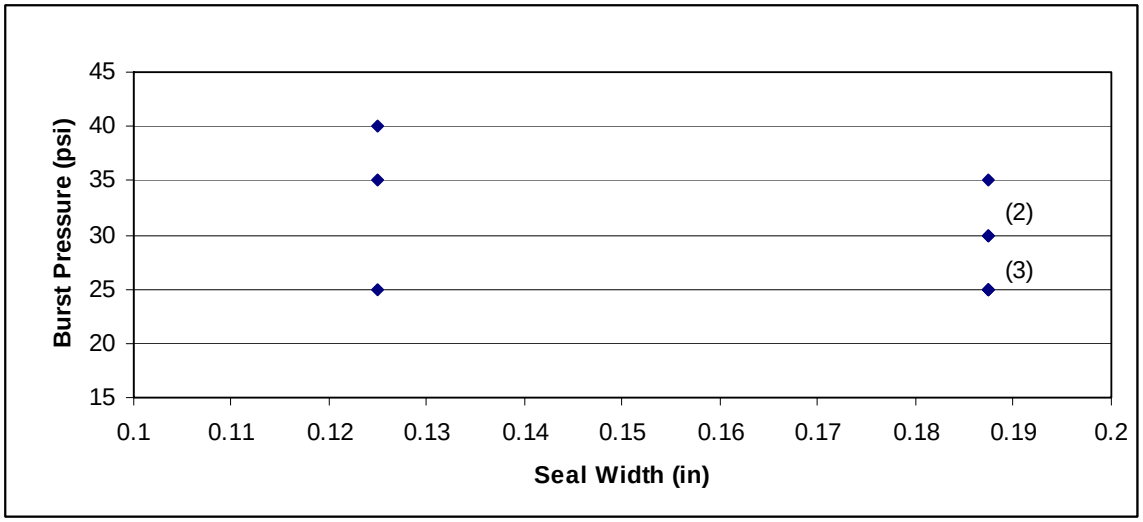

Figure 4.11: Burst pressure of short seal trays from Stegner. Average burst pressure for Stegner trays is 30 psi.

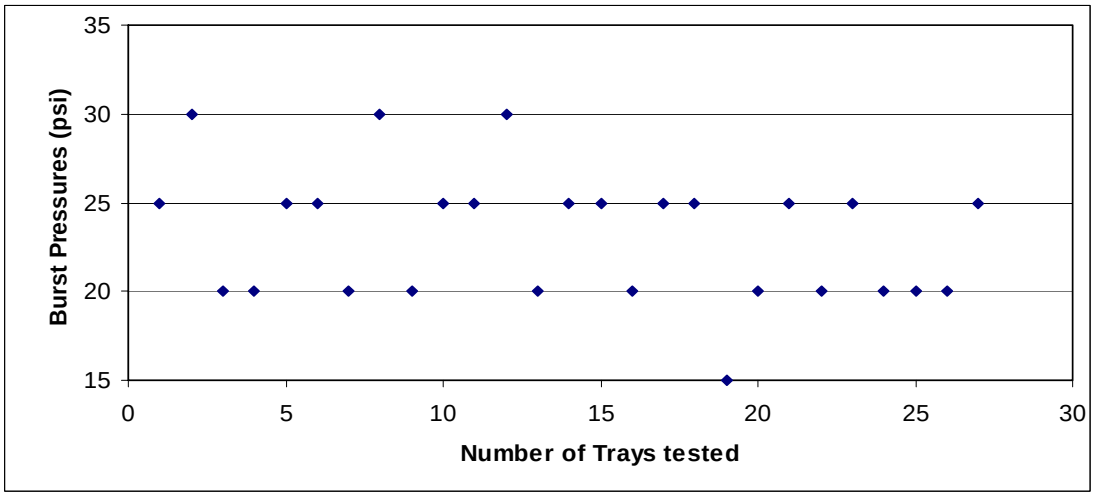

Figure 4.12: Burst Pressure of trays with blisters from Stegner. Average burst pressure for Stegner trays with blisters is 23.2 psi.

The tunneling defect in the seal also has a drastic effect on the seal strength. Just one tray from Stegner withstood the pressure of 30 psi. The remaining 12 trays failed at or low 30 psi. The length of the tunneling defect almost occupied the entire seal width in most of the trays, thus leaving no non-defective area to hold the pressure. Thus most of the trays failed because air started leaking out of the trays at higher pressures. Figure 4.13 shows that all the packages failed at or lower than 30 psi. In general, it can be observed that the burst pressure sustained by food trays manufactured by Wornick Food Products is higher than that by trays manufactured by Stegner Food Products. The main reason for displaying low burst pressures is the lower seal widths of trays by Stegner Food Products. The average seal width of the Stegner trays was about $3/16^{th}$ of an inch; while that of the Wornick trays was close to $4/16^{th}$ of an inch. The trays with tunneling defects were mostly seen to produce leaks at lower pressures; which is expected as the tunneling defect mainly represents a discontinuity in the seal. Food packed inside might have some role to play as far as the seal strength is concerned, but the exact relation could not be established. Food inside the tray is always added with preservatives. Such chemicals might react with either the polymer or the adhesive used in the process of lamination resulting in the deteriorating the seal strength.

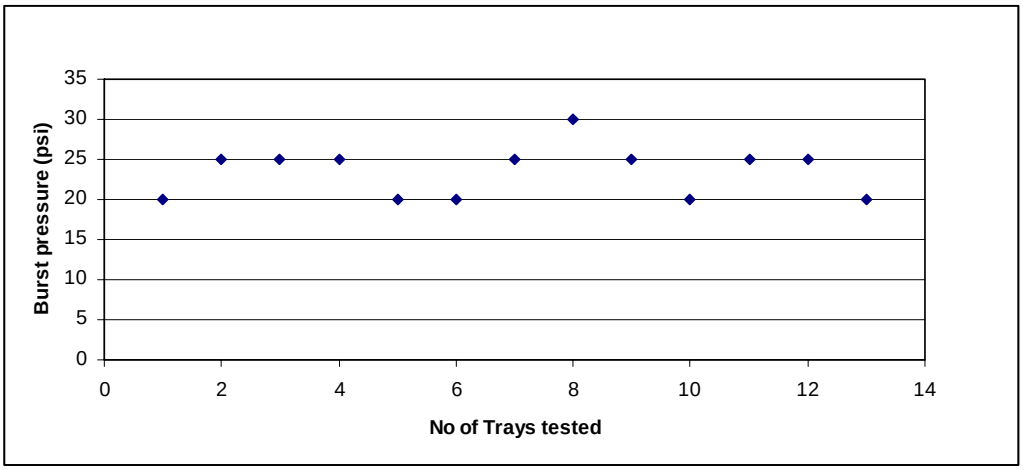

Figure 4.13: Burst pressure of the trays with tunneling defects from Stegner. Average burst pressure for Stegner trays with tunneling defect is 23.5 psi.

4.3 Finite Element Analysis:

The stress condition in the seal as a result of pressurization of the tray can be simulated using a suitable finite element analysis program like Femlab 3.0®. As stated earlier, the software basically divides the object under consideration into small elements through a process called "meshing". Mesh consists of small triangular elements. The software uses equilibrium equations in the global stress components. It solves the Navier's equation of equilibrium expressed in the displacements with the stresses on different domains and subdomains using the boundary conditions specified by the user over the nodes of the triangular elements. The overall solution is obtained by integrating the solution on the nodes to the entire solid surface.

Initial work was done by the colleague of the author using a 3D model to simulate the burst pressure conditions [30]. However the simulations were run without considering the effect of the acrylic plate which prevented the lid from inflating freely. The 3D simulation was first tried with constructing the acrylic plate on the top of the lid with gap of 6 mm. As stated in section 3.4, the displacement of the lid on the tray due to the air pressure inside the tray was not coupled with the displacement of the acrylic plate. As a result, the acrylic plate was seen to be displaced not due to the displacement of the lid, but due to the structural stresses. This is certainly not the true displacement of the plate. And since the displacement of lid was not coupled, the lid would inflate as if the acrylic plate were not present and would "pass through" it. Since the exact coupling equation was not available, the alternative approach of filling the gap with a hypothetical material of a low stiffness was sought after and found useful. The material provides the connecting domain, thus eliminating the need to have a coupling equation. Three-dimensional simulations were highly memory consuming and thus the solution would not converge. Instead 2D simulations would provide similar useful information with fast processing. The 2D simulations were run with constrains Rx = Ry = 0 (displacement in x- and y- direction) on the tray, ensuring that the tray does not move under the internal pressure. Similarly, the tray boundaries were put under same constrains to make sure that

the tray does not move under the force from inside. The tray was meshed using "extremely coarse" mode. The number of elements in the seal area was increased by refining the mesh twice. Thus there were 34,992 mesh elements in the model. It is worthwhile to note the line plot of the stresses in the 2D model. The line/ extrusion plots with shear (Sxy) and normal (Sy) stresses were taken across the seal as shown in Figure 4.14; around where the lid inflated as a result of pressure. The vertical direction was assigned for y-axis; while the horizontal direction was assigned to x-axis. The line plot was taken across x-axis. The effect of increasing distance between the acrylic plate and lid was seen to increase the both the shear and normal stress across the seal. The Figure 4.15 shows the results from the 3D simulation. The lid appears to have gone through the acrylic plate because the displacement of the lid was not connected with displacement of the plate.

Figure 4.16 shows the line plot of shear stress in the seal with the distance between the lid and metal frame 6 mm. The pressure inside the tray was 20,000 Pa. The lid experiences shear stress only where it is bonded with a tray; i.e. the seal of the tray. So the seal is represented by the length between 1-1.65 X 10^{-3} m of arc length. Figure 4.17 shows the line plot of normal stress developed in the seal when the pressure inside the tray was 20,000 Pa with 6 mm separation between the lid and metal plate. In both figures, the linear portion represents the zero stress in the seal. The stress is zero initially then drops, becomes negative and then rises to a maximum. This behavior is represented by that portion of seal which is in bonded with the tray flange. The zero-stress is represented by the remaining portion of the seal which is not in contact with the tray flange.

The simulations were performed with increasing pressure inside the tray. The increase in shear and normal stress in the seal was observed and they followed a linear relationship with the applied pressure. This fact can be seen in Figure 4.18. The pressure inside the tray was varied from 20,000 Pa (3 psi) to 180,000 Pa (27 psi) through 60,000 (9 psi) and 120,000 (18 psi). Figure 4.19 shows the result of 2D simulation with the separation of 6 mm and pressure 20,000 Pa.

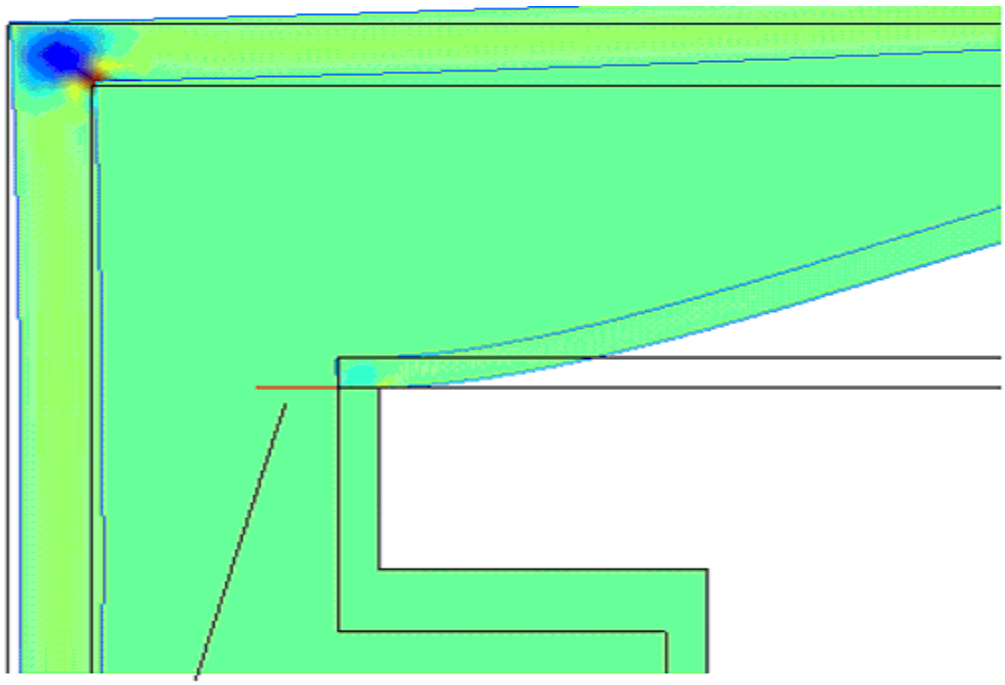

Figure 4.14: The location in the seal where line/ extrusion plot was taken.

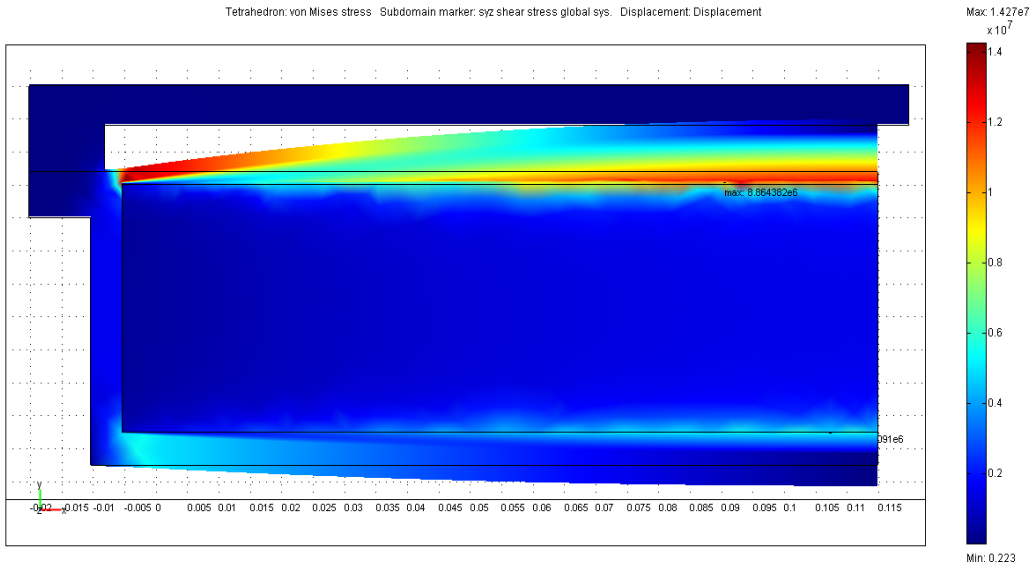

Figure 4.15: 3D Femlab® simulation showing the lid to have gone through the metal.

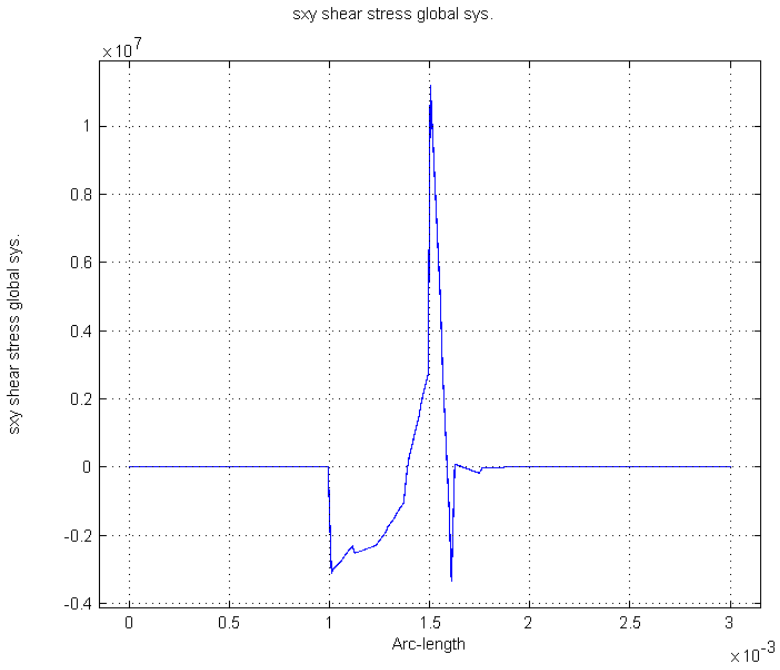

Figure 4.16: The shear stress (Sxy, in Pa) across the seal with 6 mm distance and pressure 20,000 Pa.

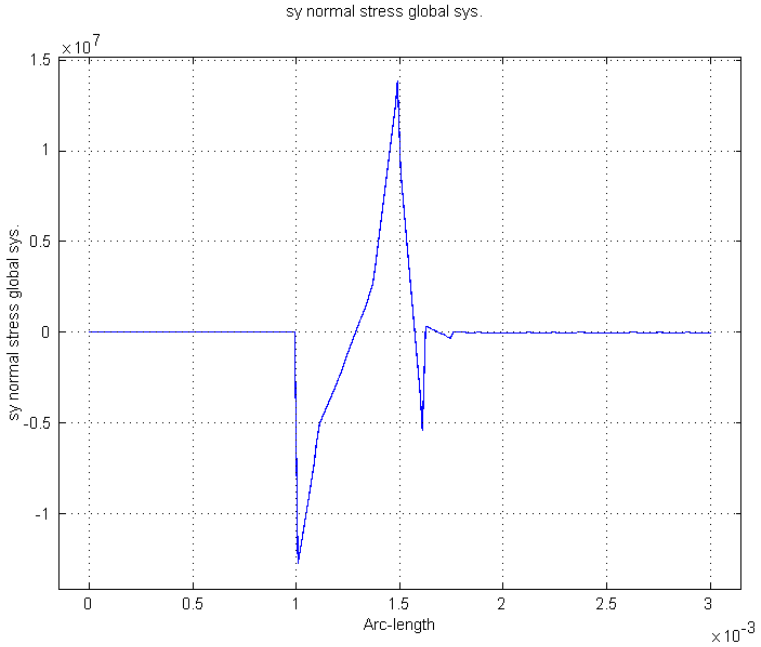

Figure 4.17: The normal stress (Sy, in Pa) across the seal with 6 mm distance and pressure 20,000 Pa.

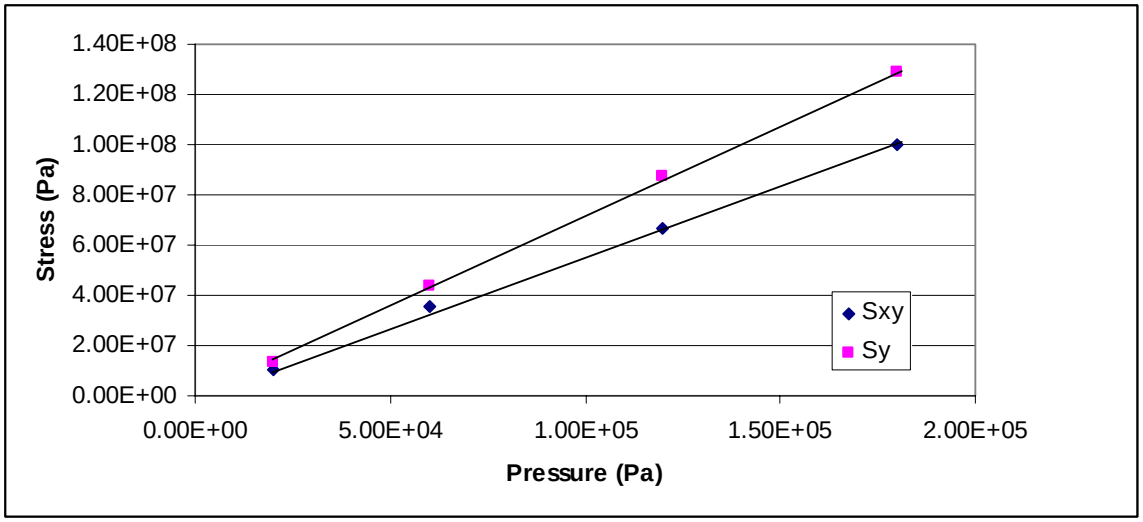

Figure 4.18: Increase in stresses with increase in pressure in the tray. Stress increment follows a linear trend with increase in pressure.

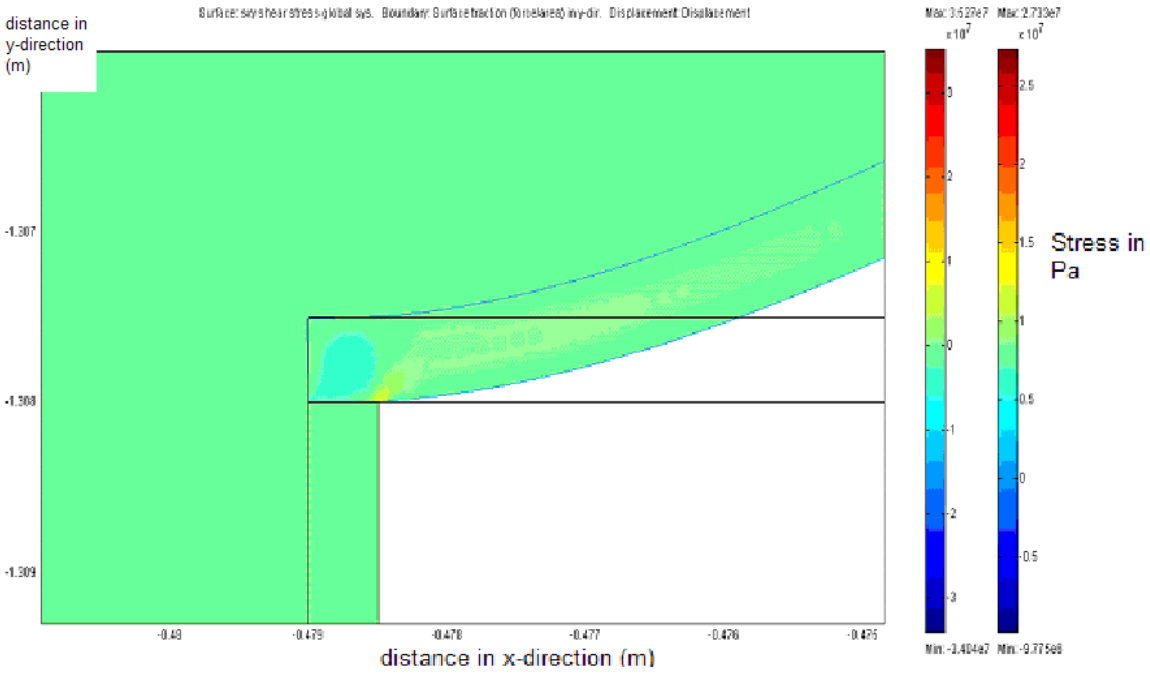

Fig 4.19: The 2D simulation in Femlab® with separation of 6 mm and 20,000 Pa.

The distance between the lid and acrylic plate is 6 mm in the experimental set-up. This is optimum distance of separation between the lid and acrylic plate. This prevents excessive inflation of lid. Current industry standard dictates that the maximum allowable separation of lid and constraining plate should not be more than 6 mm. The simulations were done with increasing the distance between the lid and acrylic plate. The stresses in the seal were expected to increase with increasing separation. The current practice for the burst test in the industry involves pressure of 20 psi for 30 seconds. The minimum separation distance is 3 mm.

Table 4.4 shows the maximum shear and normal stress in the seal with increasing separation between the lid and metal frame. The pressure of 20,000 Pa was used for these simulations. The simulations show that the burst tests that were carried out during this project were more severe than those in current practice. The gap between lid and the acrylic plate was 6 mm for the burst tests carried out during this project. It was also expected that after a certain value of the separation between lid and plate, the stress values would reach plateau values. Figure 4.20 shows the increase in shear and normal stresses in the seal with increase in the distance between lid and the acrylic plate. It can be seen that at higher separation, the stress tapers off and shows the trend of attaining the plateau value.

Table 4.4: Shear and normal stress with increasing separation at 20,000 Pa.

Distance (mm)	Sxy (Pa)	Sy (Pa)
3	8.80E+06	1.07E+07
6	1.06E+07	1.35E+07
8	1.20E+07	1.50E+07
10	1.55E+07	1.98E+07
14	1.78E+07	2.20E+07
22	2.13E+07	2.59E+07
28	2.36E+07	2.93E+07
34	2.51E+07	3.14E+07
38	2.69E+07	3.28E+07

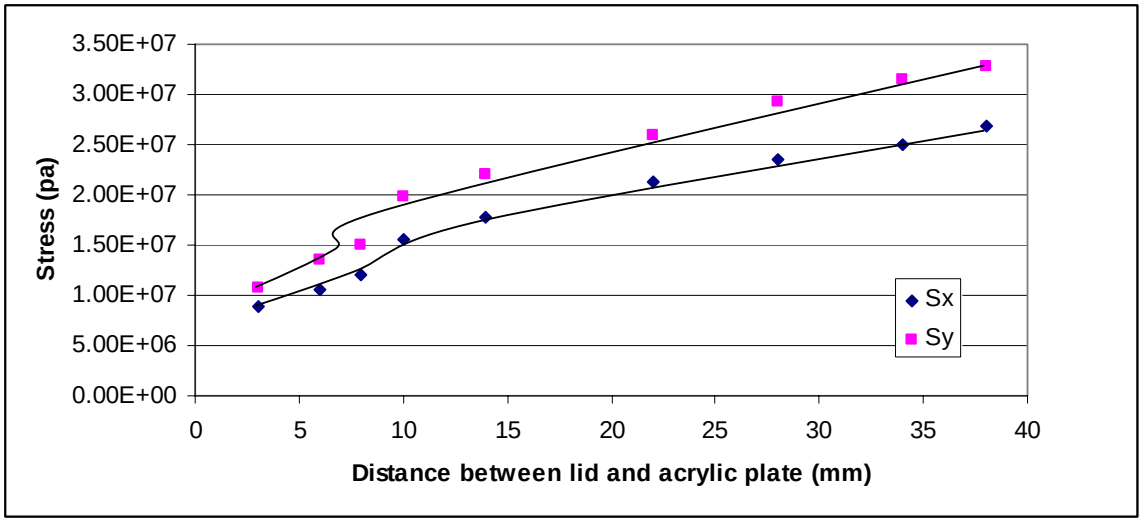

Figure 4.20: The shear and normal stress variation in the seal with increasing separation at 20,000 Pa.

As can be seen here in the Figure 4.20, both, shear and normal stresses keep on increasing as the distance of separation between the acrylic plate and the lid increases. Though the stress appears to taper off at higher separation, for all practical purposes, the stress varies linearly with the increase in the separation. The current standard is 3 mm of separation between the plate and lid. The laboratory burst test setup was designed with 6 mm of gap between the two. It was found that the stresses in the seal in the current laboratory setup exceed those in the industry setup by almost 20 %. Thus the laboratory burst test is much more severe than the industry standard.

Thus, the 2D simulations not only gave the insight of the burst test, but also showed the stress variation across the seal as a result of increase in the separation between the seal and lid. Increase in the pressure inside the tray increased the stresses in the seal.

4.4 Non-Destructive Testing:

4.4.1 Ultrasonic Inspection:

Ultrasonic inspection of food trays was thought to be a useful utility to test the food tray non-destructively. Ultrasonic inspection could be used in-line and thereby provide instantaneous feedback about a defect. Accordingly processing conditions can be altered which will result in the number of defective trays reaching the military. This technique can be used in two modes, namely pulse-echo and through transmission. In pulse-echo technique, the signal generated by a transducer hits the object and returns to be detected by the detector; while in through- transmission technique, the signal passes through the object and detected by the detector at the other end. Pulse-echo technique was used to perform the experiments on the trays. The variation in the signal intensity as a function of time is displayed on the screen in the form of waveform. The important scan parameters which affect the result of the C-scan are gate location, time of flight, and peak amplitude. The ultrasonic testing was performed with a colleague. The trays with artificial defects were produced in the Stegner Food Products. Four aluminum wires of diameters ranging from 50.8 micron were placed on the tray flange during the sealing process. These wires were then drawn out leaving the channel defects behind. These trays were specifically prepared for the ultrasonic testing. Figure 4.21 shows the C-scan of the seal of the tray. The defect with maximum thickness can be identified easily in the center. The other two voids can also been identified with some difficulty. Locating the defects becomes easy if one knows the relative position of the defects. The channel of 50.8 microns is clearly not identifiable, owing to low sensitivity of pulse-echo technique.

Figure 4.22 shows the image from the B-scan. B-scans did provide some information about tunneling defects; but did not prove useful for other defects like short seal. The difference between a B- and a C-scan becomes evident if axes of the images plotted are seen.

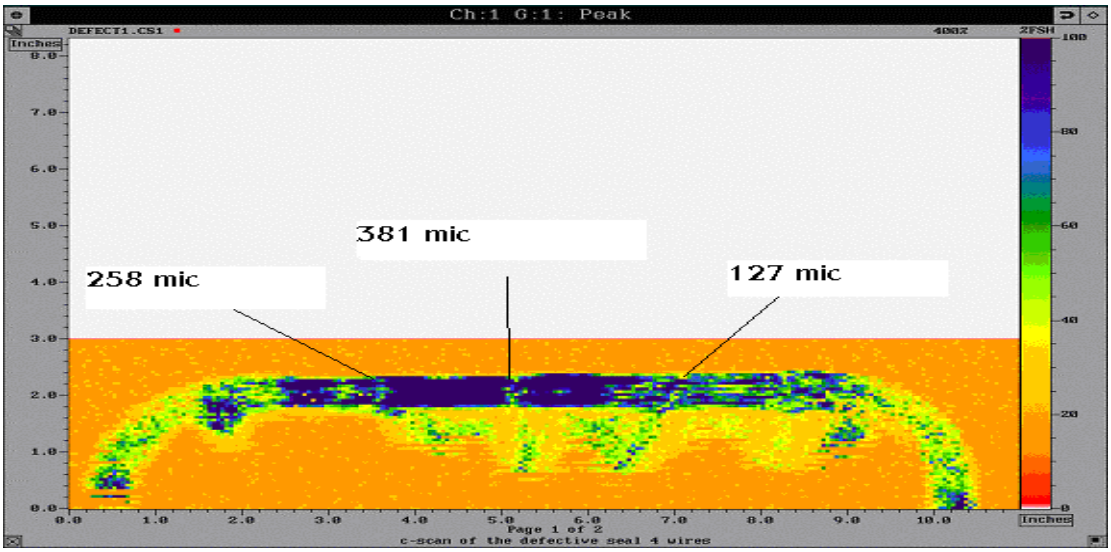

Figure 4.21: C-scan image of the seal with four channel defects.

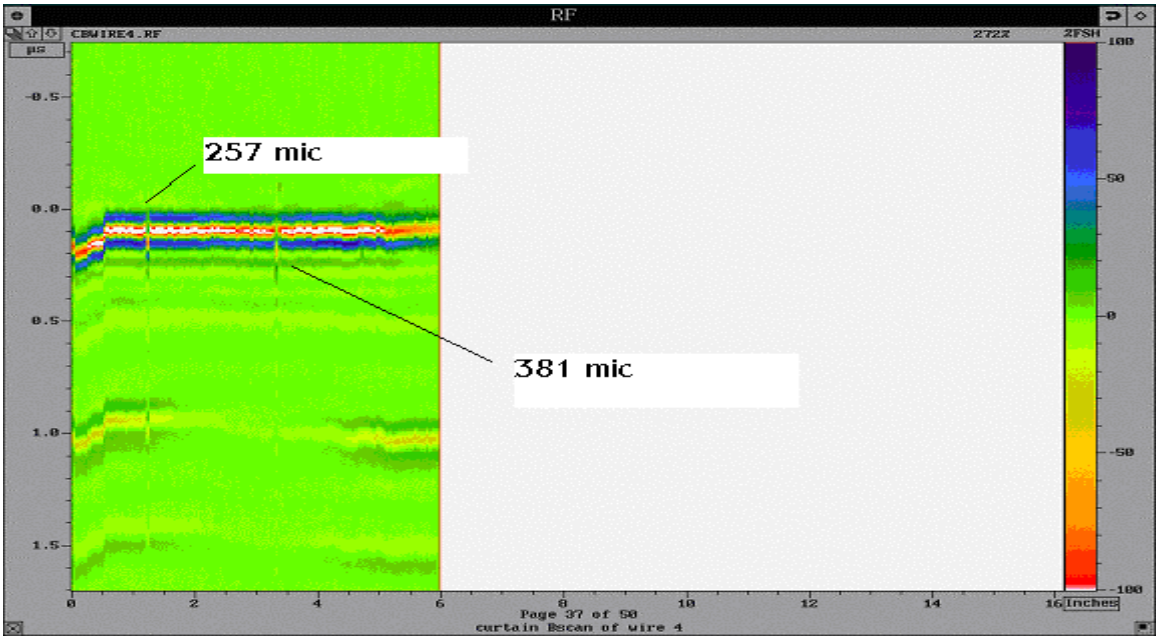

Fig 4.22: The B-scan image of the channel defects 257 and 381 microns.

B-scan is a line scan providing information about a line defect; while on the other hand C-scan provides information about surface under consideration. Images in C-scan are plotted with length both on x- and y- axes (inch in this case); while images in B-scan are plotted with length on x-axis (inch in this case) and time lapsed before signal is recorded (μs in this case). The defects can be identified easily in the image. To get a good B-scan image, it is very important to position B-gate appropriately. But even B-scan is not very promising with other defects as can be seen in Figure 4.23. Figure 4.23 shows the B-scan image of a short seal. The B-scan does not really provide any useful information about short seal. The discontinuities seen in the image might be attributed to short seal. But again it cannot be stated with confidence as against the previous case of tunneling defects. It can be stated that ultrasonic technique is not as sensitive as expected. The resolution is not very good with the images captured. The smaller defects, which are really critical in determining whether the tray is passable, were not captured in the image at all.

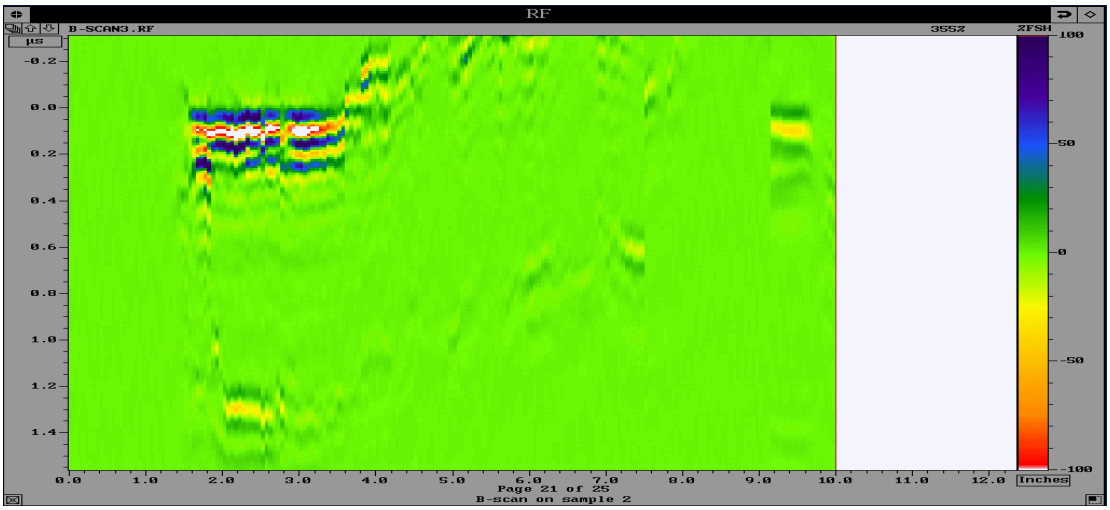

Figure 4.23: The B-scan image of a short seal. It does not give much information about a short seal.

4.4.2 Thermographic Inspection:

Thermographic inspection is another useful non-destructive technique to asses the seal integrity of the food tray. Unlike the ultrasonic method, the IR detectors can be placed in-line. As described in the section 3.3.2, the tray is first heated for two minutes with an ordinary 100 W lamps. As soon as the light is turned off, the first image, also called the base image is captured. Every subsequent image is captured at an interval of 2 minutes. The IR camera used in this experiment is sensitive enough to capture a temperature difference of 0.2 deg C. The IR camera is placed facing the lid and the sample is heated from the other side of the tray. It would be easier to compare the images of defective seal with that of a non-defective seal. Figure 4.24 shows the base image of the seal without any defect. Figures 4.25 and 4.26 show the images of the seal with a tunneling defect in them. These trays were manufactured by Stegner Food Products. These images were captured 2 and 4 minutes respectively after the base image. The image in Figure 4.26 represents the differential heat loss from the seal after 4 minutes which is obviously more than the one with a differential heat loss after 2 minutes. Subsequent images taken were more and more faded. Six such images were taken for each defective sample. The advantage of the thermographic imaging over ultrasonic imaging is the ability to detect the defects which are small in size and still critical. This is illustrated in the Figure 4.27. The figure shows a blister/ air bubble in the seal. The air bubble was of the size of $1/16^{th}$ of an inch in diameter. This particular defect may not be so critical because it is located on the outer edge of the seal. Blister on the inner edge can be easily detected as well. All the images presented in this section are images taken 2 minutes after the base image. Figure 4.28 shows the thermographic image of an uneven seal. The ruffles in the image appear black as compared to the rest of the seal. This is due to the fact that there is a differential heat loss from the defective area of the seal. Therefore, heat loss from this area is less than that from the rest of the seal. The Figure 4.29 shows the image of the seal with entrapped matter. The defect can easily be seen. However, the depth of such a defect cannot possibly be ascertained as thermography is a 2D flaw-detection technique.

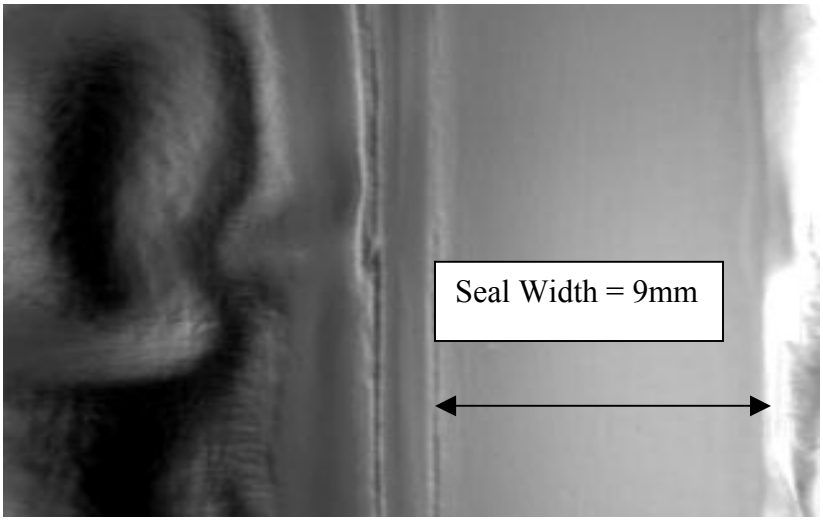

Figure 4.24: Thermographic image of a non-defective seal, no defect is visible.

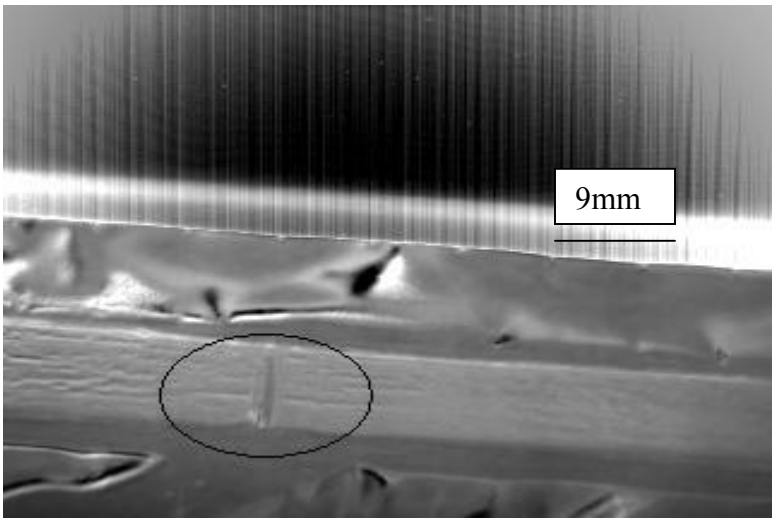

Figure 4.25: Thermographic image of a tunneling defect 2 minutes after the base image.

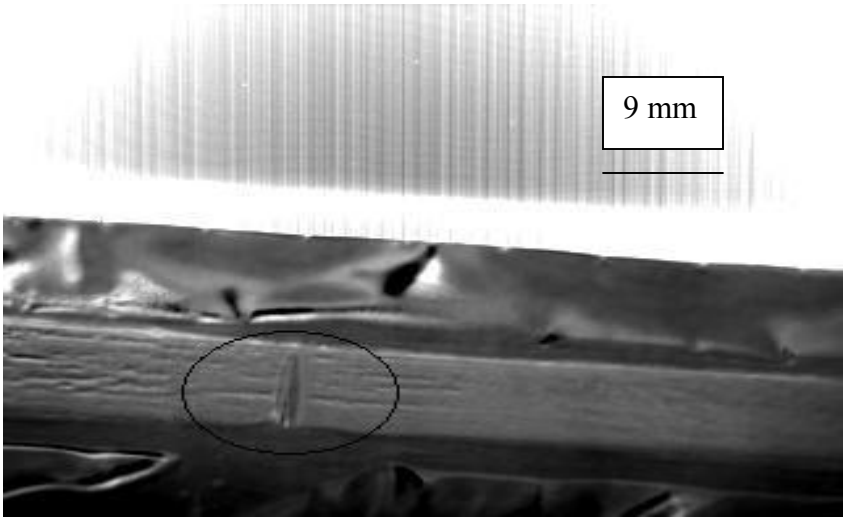

Fig 4.26: The image of the tunneling defect taken 4 minutes after the base image.

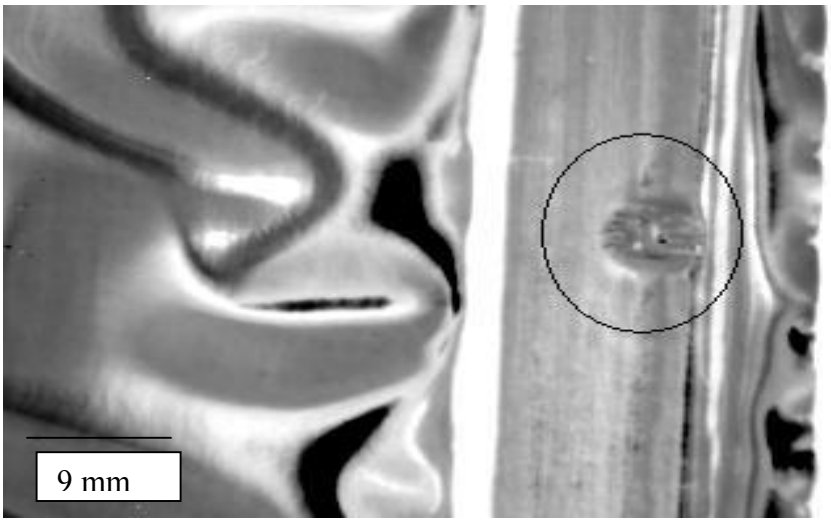

Figure 4.27: The thermographic image of the seal with a blister.

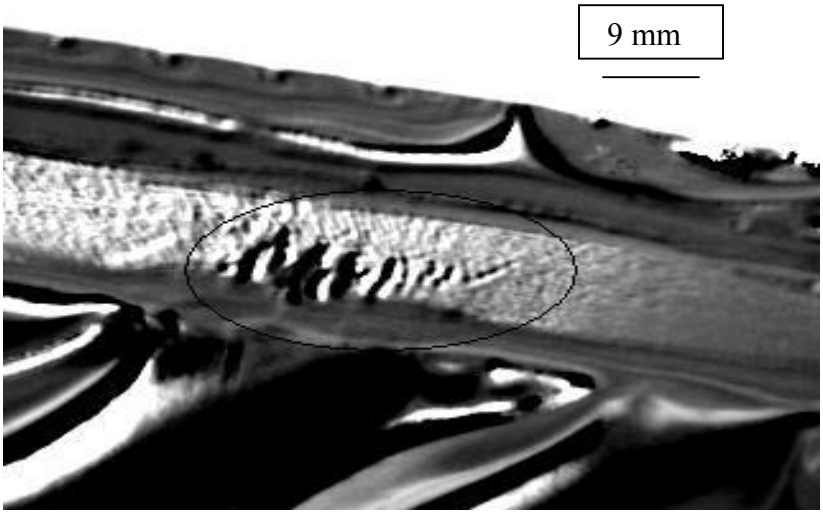

Figure 4.28: The thermographic image of the uneven seal. The defective area appears black as compared to the background.

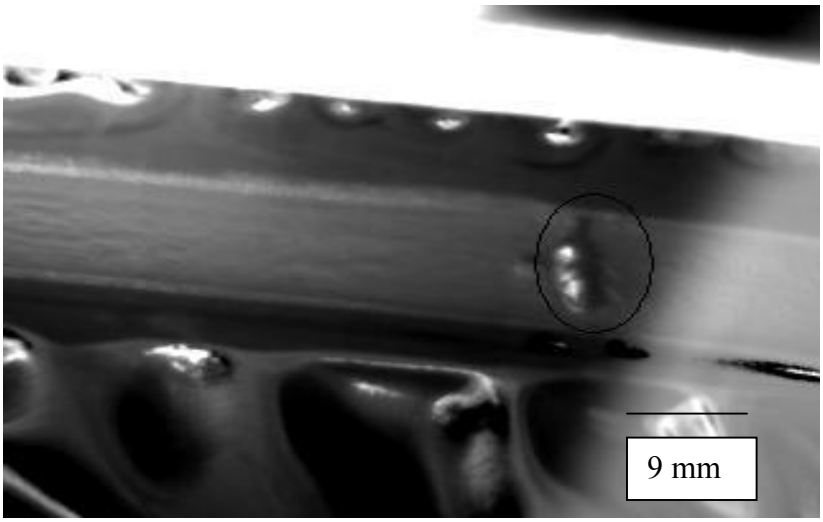

Figure 4.29: The thermographic image of the seal with entrapped matter.

These thermographic images can be compared to the digital images of the defects. Figure 3.2 and 3.3 can be referred to for optical images of blister and tunneling defect respectively. Optical images are highly dependant on contrast and lighting conditions. Glossy films like lid have to be captured with different angles. Thermographic imaging does not pose these problems. Images taken in thermography can easily be identified with the defects they are associated with; which is another advantage of thermography over ultrasonic technique. It is difficult to identify the defects in the ultrasonic imaging with the exception of tunneling defect.

4.5 Scanning Electron Microscopy:

Scanning Electron Microscopy (SEM) is one of the most useful characterization techniques to identify the mode and mechanism of fracture in the polymer films. The SEM was used as a post-failure characterization technique. The samples from the burst test were used for the SEM analysis. They were cut from the seal area of lids of burst empty trays. Empty trays were chosen in order to avoid the problem of contamination. It was assumed that the presence of food would not alter the mode of failure in the samples. Figure 4.30 shows the proposed process of delamination and fracture propagation as a result of pressurization. The process of fracture starts with separation of PP (tray)/ PP (lid). Once initiated, fracture propagates through the lid as shown by the dark lines in Figure 4.30. The fracture propagates across PP/ aluminum, aluminum/ nylon and nylon/ polyester layers. Thus the two layers exposed in the SEM images are PP and PET. These two layers can be seen in Figure 4.31. The main mechanism of failure appears to be crazing. The elongated fibrils can be seen on either side of the fractured surface. This image was taken at 522X with the beam voltage of 3kV. Figure 4.32 shows the magnified image of the PP layer seen in Figure 4.31. The fracture spreads in the path and leaves behind ductile striations and secondary cracks. The paths are separated from each other by fibrillations.

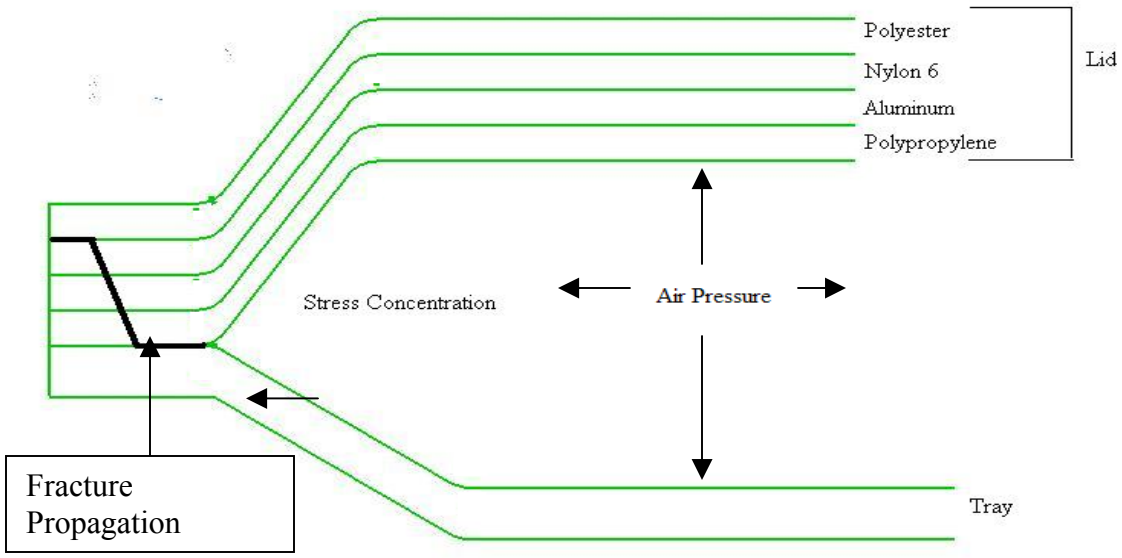

Figure 4.30: Schematic diagram showing the stress concentration and process of delamination.

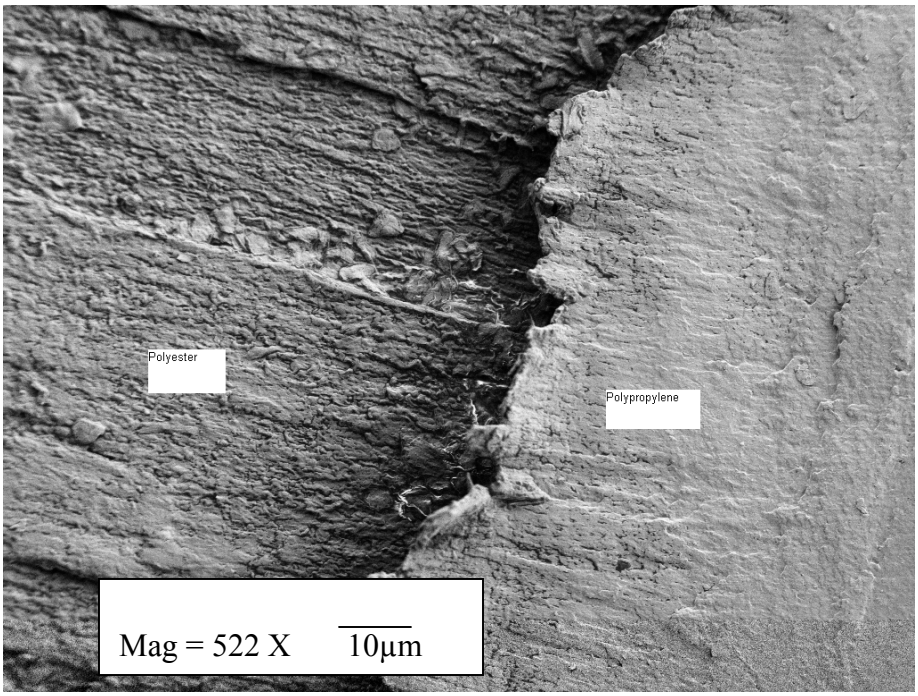

Figure 4.31: The SEM image of the sample showing the PP and polyester surfaces.

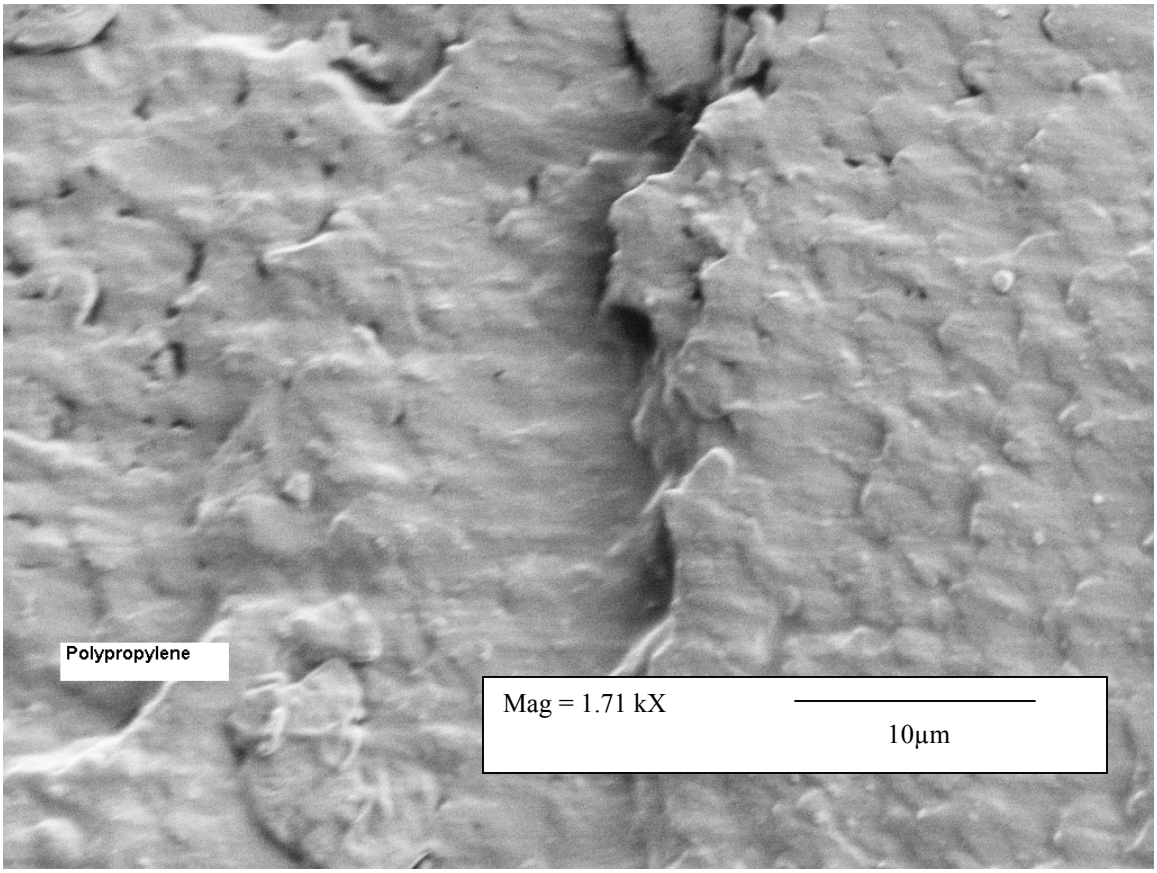

Figure 4.32: The SEM image of the PP layer seen in Figure 4.31.

Figure 4.33 can be compared with Fig 4.32 to see the similarity of fracture mode. The fracture spreads itself in channels and leaves behind ductile striations and cracks. The channels are oriented towards the applied stress, and hence separated from each other. As stated earlier, crazing appears to be the main mechanism of failure. Fibrils and voids can be seen in the Figure 4.34; which are clear indications that the polymer has undergone the crazing. All the samples used for the SEM analysis were seen to be whitened as a result of crazing. Also it is known that crazing occurs as a result of dilative loading, as opposed to compressive loading. So it can be assumed that the conditions encountered during the process of bursting resemble the dilative loading. It would be interesting to look at the similar SEM image from an atlas of polymer damage [44]. Figure 4.35 shows the tear fracture in high density polyethylene (HDPE) with pronounced peak formation.

Energy Dispersive Spectrum (EDS) was run in a point mode on the delaminating layers to confirm the presence of PP and polyester. One problem while analyzing the EDS is the peaks shown by oxygen and nitrogen are very close. The presence of oxygen cannot be possibly ascertained with certainty when there is a possibility of nitrogen being present. However, EDS can certainly show the absence of oxygen/ nitrogen. Techniques like FTIR/ATR were used to ascertain the presence of polyester. Figures 4.36 and 4.37 show the EDS from the two layers seen in the Figure 4.31. Thus, the proposed failure path will be supported by the EDS and FTIR/ATR results presented in Figures 4.36 and 4.37, and section 4.6 respectively.

Clearly the presence of oxygen is seen in the spectrum in Figure 4.36; while it is absent in the spectrum in Figure 4.37. This clearly shows that the separation took place between PP and polyester or nylon 6 layers.

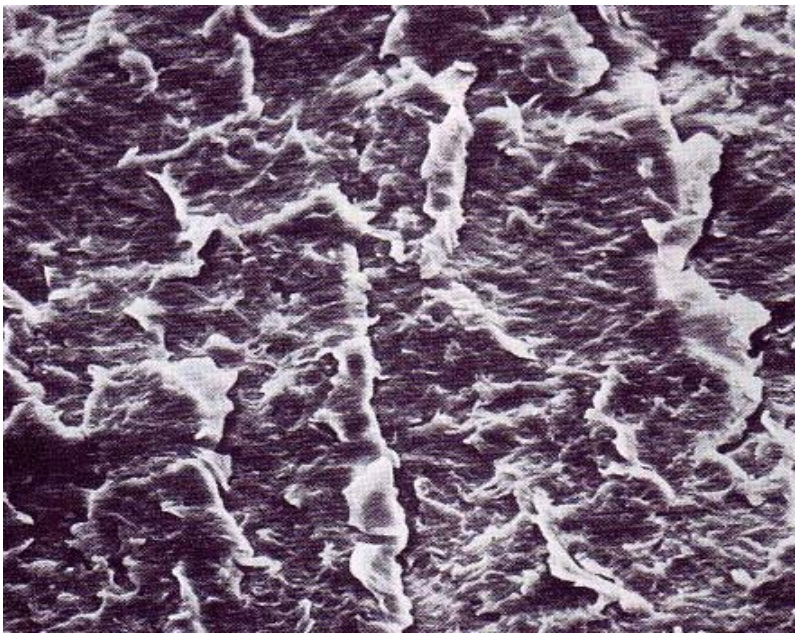

Figure 4.33: Fracture in specimen of high molecular weight HDPE [44].

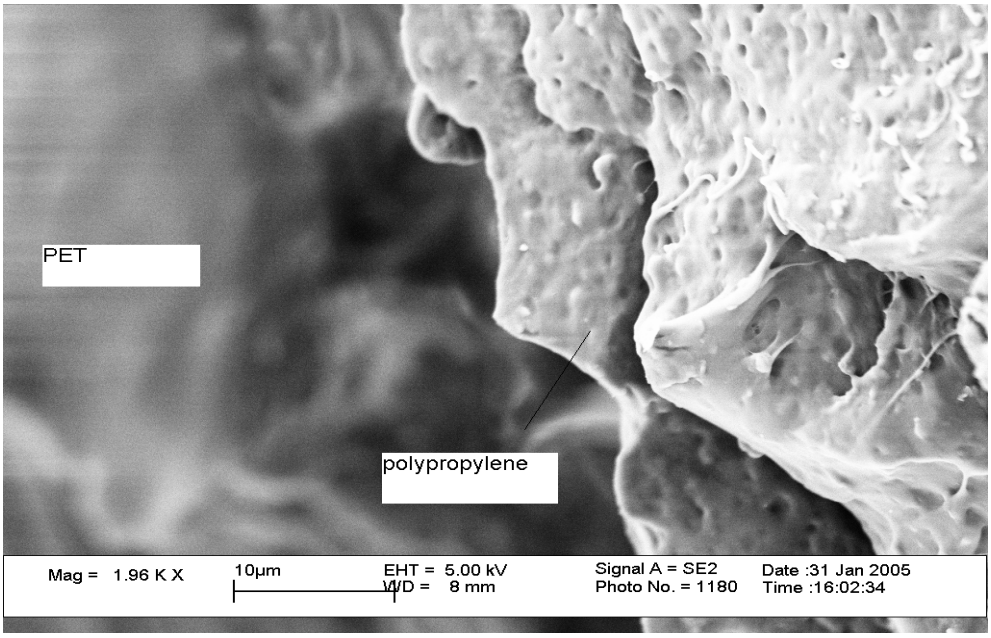

Figure 4.34: SEM image of the burst sample from an empty tray. This shows the fibrillation of the PP layer.

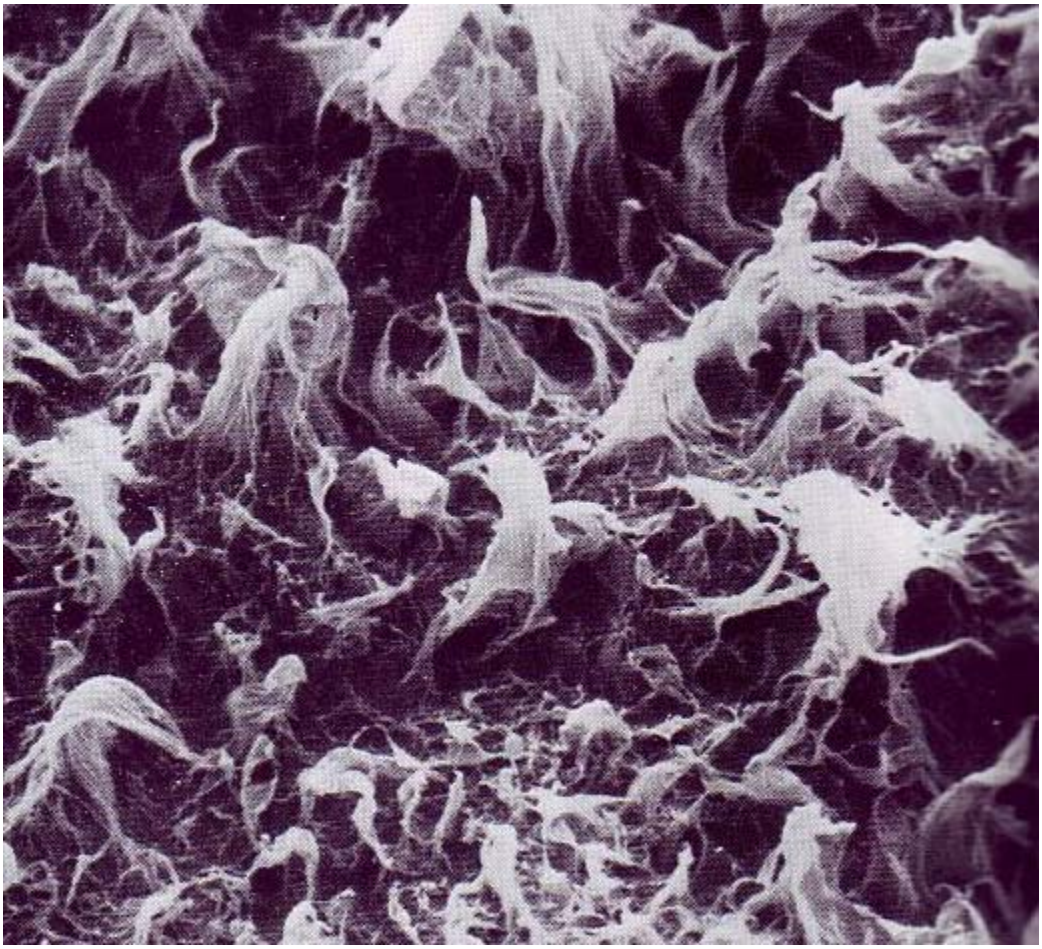

Figure 4.35: Tear fracture in HDPE with peak formation. Fibrils can be seen and compared with Figure 4.34 [44].

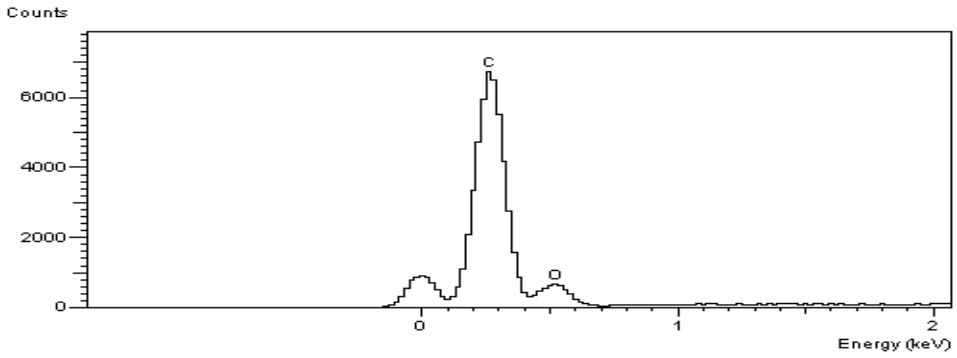

Figure 4.36: EDS from PET of the sample seen in Figure 4.31.

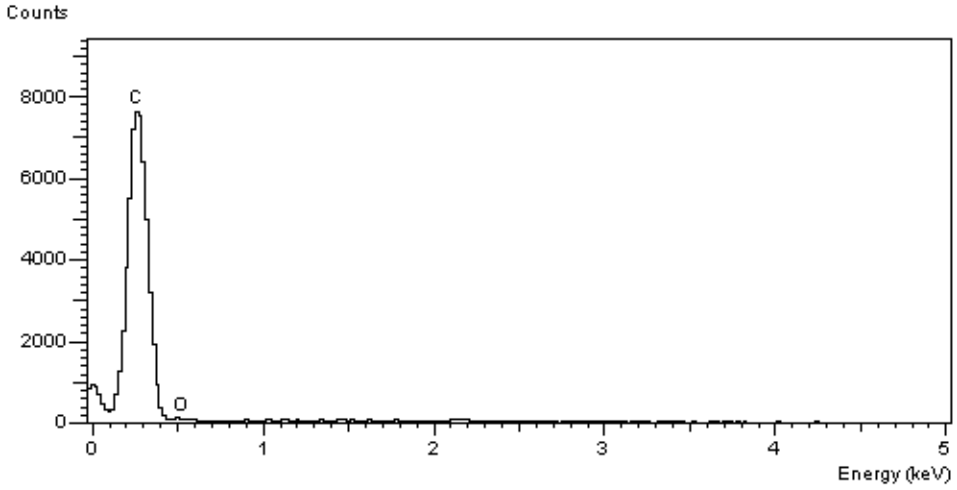

Figure 4.37: The EDS from the PP layer seen in Figure 4.31. Oxygen peak is absent.

As stated earlier in the discussion, all the samples were seen to delaminate between PP and polyester layers. Not in a single scan were layers of nylon or aluminum seen. This led us to believe that the adhesive bonds between the PP/ aluminum and between aluminum/ nylon 6 are strong. Thus if future development is needed or deemed required, the adhesive strength of the bonds between nylon 6/ polyester would require increment.

The SEM analysis not only revealed the mode of failure but clearly shows the two layers which delaminated. For all the samples tested, it was found that the separation took place between polyester and polypropylene layer.

4.6 Fourier Transform Infrared Spectrometry (FTIR)/ Attenuated Total Reflection (ATR):

In order to support the data obtained from EDS, the samples were also run in FTIR/ ATR mode. The samples run in the SEM were used in FTIR/ ATR. It was found that even though the samples were coated with gold for SEM; the gold layer was so thin that it did not interfere with the spectra. The samples were cut from lid portion of failed seal. Samples were run in reflection mode and the spectrum was obtained from either side of the fracture boundary. Each sample tested with SEM showed two distinct regions or layers in it. The ATR analysis was done on those two layers on either side of the fracture boundary. ATR confirmed the results obtained with EDS. For all the samples the layers seen were PP and polyester. Figures 4.38 and 4.39 show the spectra obtained for PP and polyester layers. A peak in Figure 4.38 could be coming from the C=O resulting from the oxidation of C-C bond in PP.

The predominant polyester absorbance bands near 1740 cm^{-1} and near 1275 cm^{-1} corresponding to C=O and C-O-C stretching respectively can be observed in Figure 4.39.

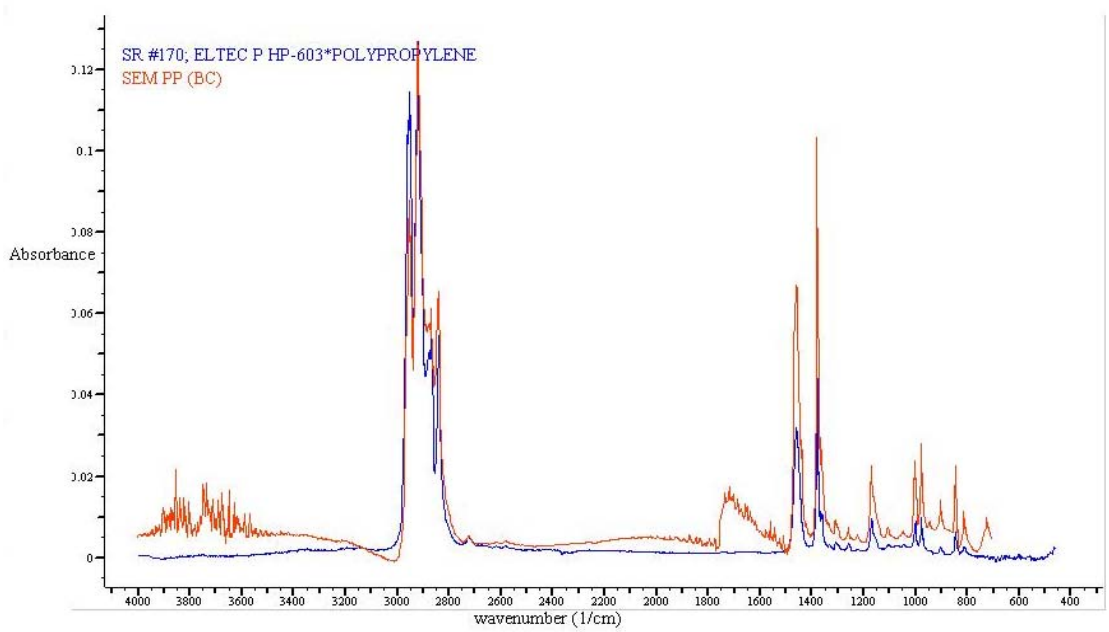

Figure 4.38: The spectrum obtained from PP layer of the sample used for the SEM analysis. The spectrum from the sample is compared with that from the database [45].

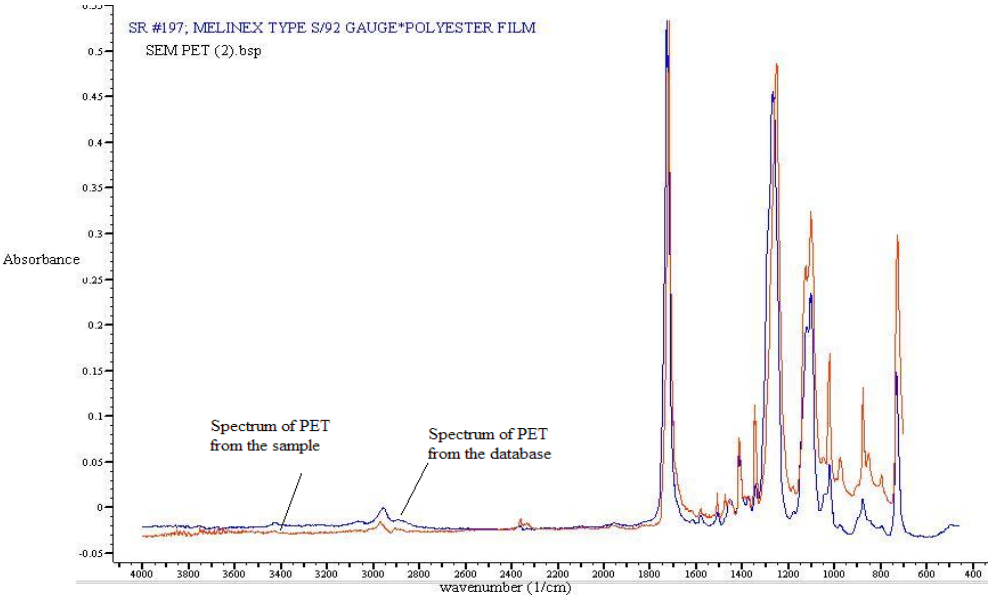

Figure 4.39: The spectrum obtained from polyester layer of the sample used for the SEM.

Absorbance bands for PP (Figure 4.38) closely match with those of standard PP film; namely aliphatic stretch of C-H bond near 2900 cm^{-1} and 1470 cm^{-1}.

The results obtained from EDS scans were supported by the ATR. It is now confirmed that the two layers seen in the SEM pictures were PP and polyester. Thus the delamination as a result of burst test takes place between the PP (tray)/ PP (lid) and nylon/ PET layers.

Chapter 5: Summary and Conclusions

5.1 Summary and Conclusions:

The analysis of seal integrity of military food ration packages was done with the aid of various destructive and non-destructive techniques. Destructive technique like burst testing and non-destructive techniques like Femlab® finite element analysis, ultrasonic B- and C-scan analysis, infrared thermographic inspection of poly trays were used during the project. Characterization techniques such as SEM, EDS, FTIR/ ATR were used to compliment the results obtained from destructive and non-destructive tests.

The burst test provided valuable information about the seal strength of defective and non-defective trays. The trays tested came in two different consignments. The first consignment contained the packages from Stegner and Wornick Co. The average burst pressure for non-defective trays was surprisingly lower than that of trays with air-bubbles entrapped. This owes to the comparatively smaller bubble diameter and higher seal widths. Trays with entrapped matter had low average burst pressure. The second consignment contained 61 trays manufactured by Wornick and 86 trays manufactured by Stegner. On an average, the non-defective trays from Stegner and Wornick performed just as well. However, the defective trays from Wornick performed much better than their Stegner counterparts. The average seal width of trays from Stegner was barely 1/4'', while that of trays from Wornick was close to 5/16''. Thus any defect present in the trays manufactured by Stegner would naturally leave less non-defective seal width to withstand the air-pressure owing to small seal width.

The average burst pressure for trays from Wornick with entrapped matter and blisters was higher than those from Stegner. Wornick trays with entrapped matter did not show much reduction in burst pressure; but trays with blisters did. Stegner trays with entrapped matter and blisters had almost the same seal strength; much less that Wornick counterparts. Tunneling defect had a drastic effect on trays from Stegner. It reduced the

pressure that trays could sustain before bursting or leaking. This behavior is quite obvious as tunneling defect basically represents a void running along the length of the seal. Thus the seal width plays a crucial role in determining the seal strength of a poly tray. The exact interaction of the food inside a tray with the seal strength was not studies during this project. But it can certainly deteriorate the properties of seal and reduce the strength.

The stress conditions that a tray might experience in its service were simulated using finite element analysis software Femlab®. The 3D simulation was tried first with the acrylic plate at the top of the tray. The problems faced during these simulations were discussed in sections 3.4 and 4.3. The lack of the availability of a suitable coupling equation forced us to use 2D simulations with a constraining plate on the top of a tray. The gap between the tray and acrylic plate was filled with a hypothetical material with a low stiffness. The results obtained were practical. The simulations were done with increasing distance between the plate and tray. The initial distance was 6 mm, which was then increased to 38 mm through 8 mm, 10 mm, 14 mm, 22 mm and 28 mm. The other set of simulations was done with keeping the distance of separation 6 mm and increasing the air pressure inside the tray from 3 to 27 psi through 9 and 18 psi. The shear and normal stresses were measured at the seal. Normal stress experienced by the seal was more than shear stress for any given pressure and distance of separation. The normal stress experienced by the seal at 27 psi would be 1.29E08 Pa assuming the seal width to be $5/16^{th}$ of an inch. Thus reducing the seal width would increase the normal as well shear stress in the seal. The shear and normal stress in the seal follow a linear increment with increase in the pressure inside; while a polynomial trend was seen for the increase in stress with increase in the distance between the plate and tray. It is worthwhile to mention here the significance of defects on the stresses in the seal. We assume that the tray has a blister of radius 3mm i.e. $1/3^{rd}$ of the entire seal width. The seal length is assumed to be 30 cm. The calculation is done on one side of the seal. The tray is assumed to be pressurized at 27 psi; thus the normal stress in the seal would be 1.29E08 Pa. The blister in the seal reduces the area on which the normal stress is distributed. The calculation

shows increase in the force on the seal by 1.6 %. Practically a defective tray has multiple defects. Additionally the effect becomes severe near the tensile strength of the seal.

Non-destructive techniques like ultrasonic B- and C-scans and infrared thermography were used in assessment of seal integrity. The popularity and usefulness of non-destructive testing techniques lies in the fact that the sample doesn't have to be destroyed to test its properties. Pulse-echo technique was used with ultrasonic testing. The trays with artificially created tunneling defects were used for testing. Both B- and C-scans could locate and identify the tunneling defects higher than 50.8 microns in diameter. Trays with other defects were also tested with ultrasonic scan. The technique was found useful for identifying tunneling defects. But other smaller defects were not captured in the scans. Blisters and short seals are probably a major concern for the tray manufacturers. Those defects were not captured in the scans. The resolution and clarity of the images scanned were not satisfactory. Ultimately the ultrasonic facility could be of a very limited use. On the other hand, infrared thermography was found really useful and could capture almost all the defects.

As compared to ultrasonic scanning technique, infrared thermography was found much more versatile. With some modifications the IR detectors can be placed in-line and defects can be located in advance. The technique could be used to detect smaller and critical defects like blisters or tunneling. The initial set-up would not be expensive, as the detectors are infrared camera. Thermography was used to identify the defects too small to be identified by ultrasonic technique. Blisters, short seal, uneven seal, tunneling defects were all seen in the images. The resolution and clarity of the images taken were found be satisfactory. The cameras should be sensitive enough to detect a very small difference in the temperature. But on the whole the technique was found to be satisfactory and could be used industrially.

The characterization techniques like Scanning Electron Microscopy (SEM) and Fourier Transform Infrared Spectroscopy/ Attenuated Total Reflection (FTIR/ ATR)

were used to identify the mode of failure and the delaminating surfaces. The samples from the lid of a burst tray were used for the characterization. The SEM analysis not only showed the films which delaminated but revealed the mechanism of fracture. It was found that the failure took place between PP (tray)/PP (lid) and nylon/polyester layers. The presence of PP and polyester was determined by using Energy Dispersive Spectrum (EDS) in a point mode. EDS showed the presence of carbon and oxygen in a polyester layer and carbon in PP layer. The SEM figures also showed that crazing was the main mechanism of failure in PP films. Crazing was believed to occur as a result of dilative loading. Since nylon or aluminum did not appear in EDS analysis, the adhesive bonding between polyester/ nylon and nylon/ aluminum should be really strong. The results from EDS analysis were confirmed by running the samples in ATR mode in FTIR. The scans were run on either side of the fracture boundary and presence of polyester and PP was confirmed.

5.2 Future Work:

The following suggestions should be considered for future work to better understand the quality of seal in military ration polytrays:

- Development of infrared thermography assembly to install it in-line with the production facility.
- Development of 3D simulation in Femlab® with a constraining plate. This could be realized if a coupling equation were developed connecting the displacement of lid with that of an acrylic plate.
- Burst test analysis of more defective polytrays and establish the relation of defect and burst pressure.
- Bacterial challenge tests were not conducted during this project. But if such tests were conducted, it would be really valuable to understand the microbial challenge. Development of a chemical which shows the appearance or growth of bacteria inside a tray; which wouldn't alter the properties of food in any way.

References

1. D. Twede, R.G., *Packaging materials*. 2nd ed. 1998: Pira International, Surrey, UK.
2. Kit, K.M., *Private communication*. 2005: University of Tennessee, Knoxville.
3. Wilmer A. Jenkins, J.P.H., *Packaging Foods with Plastics*. 1991: Technomic Publishing Company, Inc.
4. Antonios E. Goulas, K.A.R., Michael G. Kontominas, *Effect of ionizing radiation on physiochemical and mechanical properties of commercial multilayer coextruded flexible plastics packaging materials.* Radiation physics and chemistry, 2003. **68**(5): p. 865-872.
5. ASTM-D-1709, *Standard test methods for impact resistance of plastic film by the free-falling dart method*. 2004.
6. J.P.Berry. Fracture. 1959: Wliey. 263.
7. I.M.Ward, *Mechanical properties of solid polymers*. 2nd ed. 1971: John Wiley and Sons, Ltd.
8. S.S. Sternstein, L.O., A. Silverman, Applied polymer symposium, 1968. **7**(175).
9. L.E.Nielsen, *Mechanical properties of polymers*. 1962: Reinhold Publishing Corporation.
10. Maugis, D., ed. *Adherence and fracture mechanics*. Adhesive bonding, ed. Leing-Huang Lee. 1991, Plenum Press: New York.
11. Hertzberg, R.W., *Deformation and fracture mechanics of engineering materials*. 3rd ed. 1976: John Wiley and Sons, Inc.
12. J.H.Lamble, ed. *Principles and practice of non-destructive testing*. 1963, John Wiley & Sons.
13. M.A. Pascall, J.R., J.Reimer, B.Farahbaksh, *Non-destructive packaging seal strength analysis and leak detection using ultrasonic imaging.* Packaging technology and science, 2002. **15**: p. 275-285.
14. Pilar Llull, S.S., Antoni Femenia, Jose Benedito, Carmen Rosello, *The use of ultrasound velocity measurement to evaluate textural properties of Sobrassada from Mallorca.* Journal of Food Engineering, 2002. **52**: p. 323-330.

15. Z.Ayhan, Q.H.Zhang, B. Farahbaksh, M. Kneller, *Inspection of seal integrity of food packages using ultrasound and pressure differential techniques.* Applied Engineering in Agriculture, 2001. **17**(2): p. 179-192.
16. Sierra Pacific Corp., *Infrared Theory,* www.x20.org/library/thermal/infrared.htm.
17. J.Hellier, C., *Handbook of non-destructive evaluation*. 2001: McGraw- Hill.
18. A Al-Habaibeh, F.S., N.Brown, D.Kerr, M.Jackson, R.M. Parkin, *A novel approach for quality control system using sensor fusion if infrared and visual image processing for laser sealing of food containers.* Measurement Science and Technology, 2004(15): p. 1995-2000.
19. N. Brown, D.K., M.R.Jackson, R.M.Parkin, *Laser welding of thin polymer films to container substrates for aseptic packaging.* Optics and Laser Technology, 2000(32): p. 139-146.
20. Jones I.A, T.N.S. *High speed laser welding of plastics using lasers*. in *Antec Conference*. 1994. San Francisco, CA.
21. J.P.Coelho, M.A.Abreu, M.C.Pires, *High-speed laser welding of plastic films.* Optics and Lasers in Engineering, 2000(34): p. 385-395.
22. *Infrared cameras*, www.answers.com/infrared%20cameras.
23. Maldague, X.P.V., *Theory and practice of infrared technology for nondestructive testing*. 2001, New York: John Wiley and Sons, Inc.
24. Parker R.S.R, Taylor P., *Adhesion and Adhesives*. 1966: Pergamon Press Ltd.
25. S.S.Voyutskii., *Autohesion and adhesion of high polymers*. 1963, New York: Interscience.
26. Vaseline R.M., Adhesive Age, 1965. **8**(5): p. 21.
27. Campion R.P., *Adhesion*, ed. Allen K.W. 1977, London: Applied Science Publisher.
28. Sealants, SpecialChem Innovation and Solutions in Adhesives and Sealants, *Adhesion Guide*. 2004, www.specialchem4adhesives.com/resources/adhesionguide/index.aspx.
29. Perrins L.E., Pettett K., Plastics and Polymers, 1971. **30**: p. 391.

30. Haines B.M., in *Aspects of Adhesion*, Allner D.J., Editor. 1967, University of London Press. p. 40.
31. D.E. Peckham., in *Aspects of Adhesion*, Allen D.J. and Allen K.W., Editor. 1973: London.
32. J.J Bickerman, *The science of adhesive joint*. 1961: Academic Press.
33. P.Weiss, ed. *Adhesion and Cohesion*. 1962, Elsevier.
34. Ken Booth., ed. *Industrial packaging adhesives*. 1990, CRC Press, Inc.
35. V.N. Kaliakin., *Introduction to approximation and finite element method*. 1992: Department of Civil Engineering, University of Delaware.
36. Femlab 3.0, Modeling Guide, *Structural Mechanics*. 2004.
37. Roduit B., Borgeat.C., Cavin S., Fragniere C., Dudler V., *Application of finite element analysis for the simulation of migration from multilayer packaging*, Swiss Federal Office of Public Health, Division of Food Science.
38. Reed P.E., Breedveld G., Lim B.C., *Simulation of the drop impact test for molded thermoplastic container.* International Journal of Impact Engineering, 2000. **24**: p. 133-153.
39. Travesin M., Magain P., Jodogne P., Dubreuil P., Cochet P. in *Fifth International Tin Plate Conference*. 1992.
40. J. Wang, *Design optimization of rigid metal containers.* Finite Elements in Analysis and Design, 2001. **37**: p. 273-286.
41. Trottier R., *Polymeric tray container defect inspection guide*. 2001.
42. ASTM-F-2054, *Standard test method for burst testing of flexible package seals using internal air pressurization within restraining plates*. 2000.
43. Barlow William James, J., *Evaluation of seal integrity of flexible food polytrays by destructive and non-destructive techniques*, in *Polymer Engineering*. 2004, The University of Tennessee: Knoxville.
44. Engle Lothar et.al. *An atlas of polymer damage: surface examination by scanning electron microscope*. 1981, London: Wolfe Science Books.
45. Bio-Rad WinIR Pro 3.0 software spectra search database.

Appendices

Appendix A: Classification of Trays from Consignment 1

Table A.1: Food trays received in the consignment 1 from Stegner Co. on July 14, 2004.

Packages from Stegner Food Products			
Package Name	Description	Pressure (psi)	Comments
StegnerDefective1	Ruffles in the seal	20	Leaks
StegnerDefective2	Uneven Seal	25	Burst
StegnerDefective3	Channel Defect	30	Burst
StegnerDefective4	Entrapped matter	25	Leaks
StegnerDefective5	Entrapped moisture	25	Burst
StegnerDefective6	Entrapped matter	25	Burst
StegnerDefective7	Uneven Seal	25	Burst
StegnerGood8	Non Defective	40	Didn't burst
StegnerGood9	Non Defective	40	Didn't burst

Table A.2: Food trays received in the consignment 1 from Wornick Co. on July 14, 2004.

Wornick Food Packages			
Def/Non def	Kind of Defect	Pressure (psi)	Comments
ND	"NA"	35	Leaks, steady flow
ND	"NA"	35	Leaks, steady flow
ND	"NA"	40	No leak or burst
ND	"NA"	40	No leak or burst
D	Non uniform seal, air bubble	35	Leaks
D	Non uniform seal	40	Burst
D	Short seal	40	Test terminated
D	Short and Non uniform seal	35	Leaks

D = Defective
ND =Non Defective
NA=Non Applicable

Table A.3: Classification of defective food trays based on defects received in a consignment with mixed trays.

Defective packages	
Kind of defect	pressure (psi) and comment
Air Bubble	40, Leaks
Short Seal	40, Package burst, steady flow
Short Seal	40, No burst, erratic flow
Air Bubble	40, No burst, steady flow
Wrinkles	25, Leak
Entrapped	25, Leak
Wrinkles	25, Leak
Entrapped	25, Leak
Short seal	25, Leak, erratic flow
Entrapped	25, Burst
Short seal	25, Leak
Entrapped	40, No burst
Entrapped	40, No burst

Table A.4: Burst pressures of non-defective trays received in a mixed consignment.

Non-Defective Packages	
pressure	comment
25	Leak
25	Package burst
25	Package burst
30	Leak, burst at 40
25	Leak
40	No burst
25	Leak
40	Package burst
40	Package burst, erratic flow
35	Leak
35	Package burst

Appendix B: Classification of Non-Defective Food Trays in Consignment 2

Table B.1: Non-defective trays from Wornick Co.

Sample Number	**Food**	**Pressure (psi)**	**Comment**
1.1	Blue Berry Desert	40	Smooth flow, test terminated
1.2	Blue Berry Desert	25	Burst early
1.3	Blue Berry Desert	35	Developed leak at 35 psi
1.4	Blue Berry Desert	40	Smooth flow rate
2.1	Mashed Potatoes	40	Test terminated
2.2	Mashed Potatoes	30	Leaked at 30 psi
2.3	Mashed Potatoes	30	Leaked
2.4	Mashed Potatoes	35	Leaked
3.1	Apple Dessert	35	Developed later leaked
3.2	Apple Dessert	30	Smooth flow, later leaked
3.3	Apple Dessert	40	Test terminated
3.4	Apple Dessert	30	Leaked
4.1	Apple Dessert	30	Developed leak at 30 psi
4.2	Apple Dessert	30	Leaked, erratic flow
4.3	Apple Dessert	40	Test terminated
4.4	Apple Dessert	40	Test terminated
5.1	Apple Dessert	25	Developed early leak
5.2	Apple Dessert	40	Smooth flow, test terminated
5.3	Apple Dessert	35	Smooth flow, then leaked
5.4	Apple Dessert	35	Smooth flow, then leaked
5.5	Apple Dessert	40	Smooth flow, test terminated
6.1	Black Berry Dessert	30	Increasing flow rate, leaked
6.2	Black Berry Dessert	35	Developed leak at 35 psi
6.3	Black Berry Dessert	30	Increasing flow rate
6.4	Black Berry Dessert	40	Smooth flow, test terminated

Table B.2: Non-defective trays from Stegner Co.

Sample Number	**Food**	**Pressure (psi)**	**Comment**
1.1	Chicken Breast	20	Early leak
1.2	Chicken Breast	40	Smooth flow, test terminated
1.3	Chicken Breast	40	Smooth flow, test terminated
1.4	Chicken Breast	30	Developed a leak at 30 psi
1.5	Chicken Breast	25	Early leak, burst at 25 psi
2.1	Chicken Breast	40	Smooth flow, test terminated
2.2	Chicken Breast	30	Smooth flow, then burst
2.3	Chicken Breast	35	Burst
2.4	Chicken Breast	40	Smooth flow, test terminated
3.1	Chicken Breast	30	Leaked
3.2	Chicken Breast	40	Test terminated
3.3	Chicken Breast	40	Smooth flow, test terminated
3.4	Chicken Breast	30	Burst
3.5	Chicken Breast	40	Smooth terminated

Appendix C: Classification of Defective Food Trays in Consignment 2

Table C.1: Defective trays with blisters in the seal from Stegner Co. The table contains the description of defects and corresponding burst pressure.

Sample No	Pressure (psi) and Comment
1.1	25,Two blisters, critical L = 1/8'', size = 1/16''
1.2	30, Imperfections on the seal at the corner, a tunneling defect, L = 1/8''
1.3	20, On the corner and on the inner edge
1.4	20, L = 4'', lot of blisters, very small in size, some on the inner edge.
2.1	25, L = 4½'' small blisters, critical on the inner edge; tunneling defect, covering entire seal area
2.2	25, Small size blisters on the inner side; on 4; L = 4'' small blisters
2.3	20, From 4'' from the corner 2 blisters, one major, L = 1/8'' inside the seal,
2.4	30, Two regions, one right next to corner, 1½'' small blisters
3.1	20, Some blisters are critical, inner edge, 2 regions, L = 1'' and 2½''
3.2	25, Lot of small blisters, 5-6 blisters critical, inner edge, L = 3''
3.3	25, Most of the blisters are critical, inner edge L = 2''
4.1	30, Air bubble inside the seal L = 1/2''; One blister on 4; dia = 1/8", 1/16"
4.2	20, one blister, right on the corner, very small, inside 1/8"
4.3	25, Two regions; 5" apart, L = 1½", two of them critical on the inner edge, 2 on the corner
4.4	25, Blisters on all sides of the package
5.1	20, one blister of dia = 1/16"
5.2	25, some bubbles on the side 2; one bubble on corner of side 4; dia = 1/16" and 1/8" inside the seal
5.3	25, L = 4½"; the blisters in this region, almost all are on the inner edge and critical
5.4	15, The region of bubbles on corner, of lengths = 3 and 5"
5.5	20, The bubble of dia = 1/16", on the inner edge, critical

Table C.2: Defective trays with blisters in their seals from Wornick Co.

Sample Number	Pressure (psi)	Comments
1.1	35	L = 3/16", on the corner, seal width = 5/16"
1.2	30	L = 2/16", on the inner edge, 31/2" from the bottom
1.3	35	Diameter = 2/16", right on the edge
1.4	40	on the corner, seal with = 4/16", diameter = 1/16"
1.5	35	The defect is on the corner, dia = 2/16"

Table C.3: Defective trays with delamination from Stegner Co.

Sample No	Pressure (psi) and Comment
1.1	20, Only a wrinkle across the seal, about 3" from the corner
	20, Bubbles + Delam L = 2"; EM on the inner edge L = 2/16" about 3" from bottom corner
1.2	Bubbles + Delamination on bottom corner
	20, Three distinct regions of delamination: L = 3/4", 1/2" and one across the corner.
1.3	Bubbles on 4; L = 2/16" seal = 4/16"
1.4	25, Delamination on the outer edge, L = 1/2"
	25, EM L = 1/4", small; EM L = 1/8" small; Delamination in the form of tunnels
1.1	W = 1/16",L = 1½"
	20, Three Delamination regions: L = 6/16", on the corner; L = 5/16", entire seal width;
1.2	W = 2/16"; L = 2/16"
	20, Delamination in the form in the tunnels; L = 1/2" W = 1/16"; other Delamination;
1.3	4" from bottom corner; L = 1/4"
1.4	20, Negligible width; L = 1/16"; 4½" from bottom corner
	25, 3" of delamination in the form of tunnels, W = 1/16"; some bubbles on
1.1	the inside seal
1.2	20, L = 3/4" of tunnel delamination
1.3	25, two EM defects; L = 2/16" W = negligible; other EM, really small
1.4	20, 2" of delamination, W = 1/16"

All the trays had chicken breast with gravy in them.

Table C.4: Defective trays from Wornick Co. with entrapped matter in their seals.

Sample No	Pressure (psi)	Comment
1.1	35	Air bubble diameter = 2/16" right on the end of the corner
1.2	40	EM + short seal, short seal; L = 7" and W = 3/16"
1.3	45	Diameter = 2/16", seal width = 5/16", defect inside
1.4	40	Diameter = 4/16", almost covers the entire seal width.
2.1	30	Short seal + EM; on 3; seal w = 3/16"; blister on the corner diameter = 1/16"
2.2	40	Short seal + EM; on 3; L = 7"; W = 3/16"; EM on 2; diameter = 2/16",
2.3	40	Wrinkles + Short seal; seal L = 7", W = 3/16"
2.4	35	Wrinkles + Short seal; seal L = 7", W = 3/16", Wrinkles on the corner; entire seal width and other location; L =1/4"; outside

Trays 2.3 and 2.4 had blueberry dessert in them; while the rest had mashed potatoes with chicken in them.

Table C.5: Defective trays from Stegner Co. with entrapped matter in their seals.

Sample No	Pressure (psi)	Comment
1.1	25	Entrapped matter, small bubbles, L = 2" well inside the seal
1.2	25	3 major spots, covering the entire seal width, 1/8",1/2" and 1/8" respectively
1.3	20	various small spots, L = 6"
1.4	25	2 spots, very small in size, one on the corner, and the other 2" from the bottom corner.
2.1	25	on 3 two major voids, entire seal width, on 1, EM, about 2/16"
2.2	20	on 3, EM, L = 1/16"; on 1, EM, L = 2"
2.3	25	on 3,two major defects, 2/16" and 5/16" and short seal on 4;3-4/16"
2.4	20	EM on 3, at the corner L = 3/16",dia = 1/6"; on 4; blisters along the length of 4

All the trays had chicken breast with gravy in them.

Table C.6: Defective trays with short seals from Wornick Co.

Sample No	Pressure (psi)	Comment
1.1	40	runs 7' and seal width 5/16''
1.2	40	L=6¼', extends across corners, width = 1/4''
1.3	35	L = 7', W = 1/4''
1.4	40	L = 7', W = 1/4',
2.1	40	L = 7', W = 3/16''
2.2	40	L = 7', W = 3/16''
2.3	30	L = 7', W = 3/16''
2.4	40	L = 7', W = 3/16'', across corner = ¼''
3.1	35	L = 7', W = 3/16''
3.2	40	L = 6¼'', W = 2/16'', across left and right corner = 3/16''
3.3	40	L = 63/4', W = 3/16'', across left corner = 1/4''
4.1	40	L = 7', W = ¼'', Entrapped moisture on 1st side, Diameter = 1/8''
4.2	25	L = 7', W = 1/4''
4.3	35	L = 7' on either side, on side 3, W = 3/16'', side 1, W = 3/16''
4.4	40	L = 7', W = 3/16'', Entrapped moisture on face 1, Diameter = 1/8''
5.1	40	Not a short seal, wrinkles across side 2.
5.2	40	L = 5½'', W = ¼'', across right corner, W= 3/16''
5.3	35	L = 7', W = 3/16''
5.4	40	L= 7', W = 3/16''
6.1	40	L = 7', W = 1/4'', Entrapped moisture on 1
6.2	40	L = 7', W = 1/4'', Entrapped moisture on 2
6.3	40	L = 4½' for 1/4th of an inch, and 2½'' for 3/16th of an inch.
6.4	40	L = 7' , W = 3-4/16''

Table C.7: Defective trays with short seals from Stegner Co.

Sample No	Pressure (psi)	Comment
1.1	30	L = 7', W = 1/8" across corner 3/16', sort seal on all the side, 3/16"
1.2	40	L = 7', W = 1/8" on side 2, L = 9½" of W = 3/16", on side 4, L = 9', W= 3/16"
1.3	35	L = 7½ and W = 1/8"
1.4	30	Across 1, L = 7½" W = 1/8" and across 4, L = 9½", W = 3/16"
2.1	35	on 1; L = 7', W = 1/4",on 2; L = 2½" and W = 3/16', on 3; L = 4½", W = 3/16"
2.2	25	But critical defect on the inner edge, L = 6½" and W = 1/8''
2.3	25	on 2; L = 6' and W = 3/16", on 3; L = 7', W = 3/16", on 4; for L = 5½", W = 1/8', rest W = 3/16'
2.4	25	Short seal on all the faces, W = 3-4/16'
2.5	25	Short seal on all the faces, W = 3-4/16'

All the trays had chicken breast with gravy in them.

Table C.8: Trays with tunneling defects in their seals from Stegner Co.

Sample No	Pressure (psi)	Comment
1.1	20	One large tunneling defect about 5½" from the corner, and a couple of small
1.2	25	on 1; two tunneling defects (TD), small in size, about 1/16"; and air bubble, diameter = 2/16" separated by about 4½"
1.3	25	on 4, Two TD, one very small on the inner edge; other separated by 1½"; has 2 defects, one 2/16" and other small
1.4	25	Cluster of 3-4 small TD, the bigger one, w = 2/16"
1.5	20	on 2, L = 2/16" other small TD; on the bottom corner of 4; air bubbles, small in diameter
2.1	20	on 2; TD, diameter =1/32",L = 1/16"; from 6" from the corner, on 3; 2 TD; both diameter = 1/32" entire seal width
2.2	25	one TD; entire seal width, really small width
2.3	30	EM, diameter = 1/16" about 5" from the corner; TD, L = 2/16", small width
2.4	25	on 1; 2 TD; both diameter = 1/32", entire seal width; 4/16"; TD on 4; L = 2/16" small in width
3.1	20	One TD, L = 3/16", small width; one EM, outer edge, very small
3.2	25	Scattered bubbles on two sides, near the seal; a bubble on the corner; Diameter = 2/16"; seal = 4/16"
3.3	25	EM: on 2, diameter = 2/16" inner side; on 3 EM of L = 1"; on 4, 4" of bubbles on the seal
3.4	20	on 2; TD outside; diameter = 1/16" seal = 4/16"; on 3; TD, seal = 4/16", diameter = 2/16"

All the trays had chicken breast with gravy in them.

Vita:

The author, Kshitish A. Patankar was born on 10th April, 1981 in Mumbai (formerly known as Bombay), India. He did his undergraduate studies at the University Department of Chemical Technology (well known as UDCT, Mumbai), in the department of Polymer Engineering and graduated in 2002. Having spent one year in the industry, he joined the graduate school in the department of Polymer Engineering at the University of Tennessee, Knoxville in 2003 and graduated in 2005.